Studies on Modified PZT – $CoFe_2O_4$ Magnetoelectric Composites

A Thesis Submitted
For the
Award of the Degree of

Doctor of Philosophy

By

Dipti

(Regn. No: 951112002)

To

School of Physics & Materials Science
Thapar University, Patiala-147004
Punjab, India

September -2015

CERTIFICATE

This is to certify that the thesis entitled **"Studies on Modified PZT-$CoFe_2O_4$ Magnetoelectric composites"** being submitted by **"Ms. Dipti"** in fulfillment of the requirements for the award of degree of Doctor of Philosophy to **Thapar University**, Patiala is a record of bonafide research carried out by her under our supervision and guidance. In our opinion, the work fulfills the requirements for which it is being submitted.

The work included in this thesis has not been submitted elsewhere earlier, in part or in full, for award of any other degree in this or any other institution or university.

Supervisors:

.....

Dr. Chandra Prakash
Scientist G
Solid State Physical Laboratory (SSPL)
New Delhi - 110054

.....

Dr. Sangeeta Singh
Associate Professor
(Electroceramic Research Lab)
G.V.M Girls College
Sonepat -131001

.....

Dr. K.K. Raina
Distinguished Professor
School of Physics and Material Science
Thapar University
Patiala- 147004

Dedicated

To

My

Family

ACKNOWLEDGEMENT

This thesis is based on the research work performed during 2011- 2015 at Electroceramic Research Lab, Physics Department, G.V.M. Girls College, Sonepat, Thapar University, Patiala, Punjab (India) and Solid State Physics Laboratory (SSPL), New Delhi (India).

I am grateful to numerous local and national peers who have contributed towards shaping this thesis. At the outset, I would like to express my deepest gratitude to ***Dr. K.K Raina (Thapar University, Patiala) and Dr. Chandra Prakash (SSPL, New Delhi)*** *for their advice during my doctoral research endeavour for the past four years. As my supervisors, they have constantly forced to me remain focused on achieving my goal. Their guidance and suggestions helped me to establish the overall direction towards research and to move forward with investigation in depth. I thank them for providing me the opportunity to work with a talented team of researchers.*

I would like to thank ***Dr. Sangeeta Singh*** *who helped me to start my research in* ***"Synthesis and Characterization of PZT ceramics by Novel Techniques"*** *in GVMGC, Sonepat. Surprisingly, within six month of my candidature, she advised me to join PhD Programme from Thapar University, Patiala. Her guidance and continuous support helped me all the time during my research work. I am also thankful to her for giving me enough time and attention during my research as well as for writing manuscript and thesis.*

I am grateful to ***Dr. J.K. Juneja,*** *Hindu College, Sonepat for the constant guidance, support and motivation throughout the course of this work. I also thank him for generously sharing his time and immense knowledge. His guidance helped me in all the time of research.*

I must acknowledge ***Dr. Prakash Gopalan,*** *Director, Thapar University , Patiala for academic support and providing research facility to carry out the research work at the university. I also express my gratitude to* ***Dr. Manoj Sharma****, Head, SPMS, Thapar University Patiala for encouragement and support. I also thank* ***Dr. Kulbir Singh*** *for constant support and motivation. Besides my advisor, I would like to thank my thesis committee members,* ***Dr. Puneet Sharma and Dr. B.N. Choorashama,*** *for their insightful comments and encouragement during my research progress meetings, which incented me to widen my research from various perspectives. I would like to thank other faculty members of School of Physics and Material Science (SPMS) and administrative staff for extending their support and encouragement during the course of my work.*

*I would like to express my thank to **Dr. R. P. Pant and Dr. R.K. Kotnala** (NPL, New Delhi) for extending experimental facilities to carry out XRD measurements and magnetic measurements related to the work. I also acknowledge **Dr. Jyoti Shah,** Research Associate and **Anuraag,** NPL, New Delhi for helping me in magnetic measurements.*

*I express my sincere thanks to **Dr. O.P. Pruthi,** President, Managing Committee, G.V.M. Girls College, Sonepat, **Dr. Jyoti Juneja,** Principal, G.V.M. Girls College, Sonepat and members of managing committee for providing me research facilities in Electroceramic Research Lab, GVMGC, Sonepat. Without their help and support, it would not have been possible for me to complete my research work.*

*This thesis could not have been completed without continuous support and stimulating discussions with my seniors and lab members including Dr. Parveen Kumar, Dr. Pratibha Singh, Dr. Renu Rani, Dr. Rekha Rani, Sonam Rai, Jai Kumar and Mrs. Punita Batra. I sincerely thanks **Dr. Parveen Kumar,** DIT University, Dehradun for generously sharing his time and knowledge in research. He has played a major role in making me understand the concepts related to my work. I thank **Dr. Renu Rani** for her comments and suggestions during initial phases of thesis work. She is always ready to help with a smile. I must also acknowledge the contribution of my lab members and friends **including Dr. Ravi shukla, Dr. Supreet, Dr. Rishi Kumar, Ramneek Kaur, Gurpreet Kaur** of Material Research Lab and **Gitanjali** of Nano Lab, Thapar University for their co- operation in every manner throughout the course of my PhD study. I also thank my friends **Preeti Sharma** of Raman Lab, GJUS&T, Hisar, **Mukesh Kumari,** IIT Delhi and **Poonam Pahuja,** Delhi University for valuable discussions and continuous support during the course of my research work.*

I would also like to thank all the support staff at various institutes and College in which I carried out my research work for their help in their respective roles.

*Last, but not the least, I would like to dedicate this thesis to my family, My Mummy **Mrs. Sarvesh goyal** and elder sister **Anjali a**nd my Jiju **Mr. Vikas Jain** for moral support, encouragement and for their love & patience. I would like to acknowledge my younger brothers **Ashwani Goyal & Deepanshu Goyal** for their unconditional support and making this enjoyable.*

Finally, I would like to thank God Almighty who has been giving me Patience, health, wisdom, and blessings to accomplish this thesis.

(Dipti)

ABSTRACT

Advancement in science and technology demands tailor-made materials to satisfy various requirements of the applications in industries. Metallic oxides are an important class of compounds, among which, ferroelectrics and ferrites are most prominent. The main driving force for wide attention in ferroelectric and ferrite materials is their large number of electric and magnetic applications. With the trend towards the device miniaturization, there is ever increasing interest in combining electric and magnetic properties in single materials to perform more than one task and these materials are called magnetoelectric materials. In the last few decades, extensive research work has been carried out on magnetoelectric materials. These materials have attracted much attention from the researchers because they have the properties of their parent compounds (ferrite and ferroelectric phase) and unique property-the magnetoelectric effect.

Magnetoelectric effect is a coupled two field effect in which application of either a magnetic field or an electric field induces an electric polarization and magnetization respectively. These magnetoelectric materials can be categorized into two classes- Single phase magnetoelectric and two phase magnetoelectric materials (composites). The single phase magnetoelectric materials have temperature constraints and they show ME effect at low temperature only. The value of ME coefficient shown by these materials are very low so these materials are not suitable for any technological applications. This difficulty has been overcome by two phase magnetoelectric materials (ferrite-ferroelectric composites). These composites show magnetoelectric coupling depending upon their compositions and properties of constituent phases. Due to presence of ME coupling, these composite materials have various advantages over single phase magnetoelectric materials and they find a lot of technological applications in radio electronics, optoelectronics, microwave electronics and transducers in instrumentation, waveguides, phase inverters, rectifier, modulators, integral optics and fiber communication technology.

Objectives

Objectives of the proposed work were the following:

1) Preparation and optimization of process parameters of PZT- $CoFe_2O_4$ magneto electric composites.
2) To investigate the effect of substitution in PZT- $CoFe_2O_4$ ME composites.
3) To characterize the materials for structural, micro structural, electrical and magnetic properties.

In order to fulfill the objectives of the proposed work, the following ceramic compositional series were synthesized and characterized:

Series I (x) $CoFe_2O_4$ – (1-x) $PbZr_{0.55}Ti_{0.45}O_3$ (x = 0 - 0.15 in step of 0.05)

Series II (x) $Co_{0.8}Ni_{0.2}Fe_2O_4$ – (1-x) $PbZr_{0.55}Ti_{0.45}O_3$ (x = 0 - 0.15 in step of 0.05)

Series III

Series A $Pb_{(1-3y/2)}La_yZr_{0.55}Ti_{0.45}O_3$ (x = 0 - 0.0075 in step of 0.0025)

Series B (x) $Co_{0.8}Ni_{0.2}Fe_2O_4$ - (1-x) $Pb_{0.99625}La_{0.0025}Zr_{0.55}Ti_{0.45}O_3$
(x = 0 - 0.15 in step of 0.05)

Series C (x) $Co_{0.8}Ni_{0.2}Fe_2O_4$ - (1-x) $Pb_{0.9925}La_{0.005}Zr_{0.55}Ti_{0.45}O_3$
(x = 0 - 0.15 in step of 0.05)

Series D (x) $Co_{0.8}Ni_{0.2}Fe_2O_4$ - (1-x) $Pb_{0.9887}La_{0.0075}Zr_{0.55}Ti_{0.45}O_3$
(x = 0 - 0.15 in step of 0.05)

The Research work carried out for PhD thesis titled "Studies on Modified PZT – $CoFe_2O_4$ Magnetoelectric Composites" has been divided into six chapters.

Chapter I- Introduction

Chapter II- Synthesis of Material and their Characterization Techniques

Chapter III- Synthesis and Characterization of PZT: CFO Composites

Chapter IV- Synthesis and Characterization of PZT: CNFO Composites

Chapter V- Synthesis and Characterization of PLZT: CNFO Composites

Chapter VI- Summary and Future Work

In the present work, an attempt has been made to prepare modified PZT-CFO magnetoelectric composites and then characterize for structural, dielectric, ferroelectric, piezoelectric and magnetic properties.

Chapters are summarized below:

Chapter I: In this Chapter, the introduction of ferroelectricity, magnetism and significance of individual phases and magnetoelectric composites are discussed. A brief review of the research and development work that has been carried out till recently in this field has been described. The objectives of the present work including the criteria for selection of constituent phases of the composites and scope of these investigations have also been discussed.

Chapter II: In this chapter, discussion on the method of sample preparation and characterization techniques, used for studying the structural, dielectric, ferroelectric, piezoelectric and magnetic properties of modified composites has been given. Solid state reaction method is opted for synthesis of ferroelectric and ferrite materials. The detailed study of experimental techniques, characterization equipments and their detailed information are also given in this chapter.

Chapter III: This chapter deals with synthesis of individual phases and optimization of sintering temperature of $0.05CoFe_2O_4 – 0.95PbZr_{0.55}Ti_{0.45}O_3$ composite. On the basis of optimum temperature (x) $CoFe_2O_4$ – (1-x) $PbZr_{0.55}Ti_{0.45}O_3$ composites, where x = 0.05, 0.10 and 0.15 are sintered conventionally. Effect of $CoFe_2O_4$ on structural, dielectric, ferroelectric, piezoelectric and magnetic properties of $PbZr_{0.55}Ti_{0.45}O_3$ is discussed.

Chapter IV: In this chapter we discuss the Ni substituted $CoFe_2O_4$ and PZT composites synthesized by conventional solid state reaction method. Effect of $Co_{0.8}Ni_{0.2}Fe_2O_4$ on structural, dielectric, ferroelectric, piezoelectric and magnetic properties of $PbZr_{0.55}Ti_{0.45}O_3$ is discussed here.

Chapter V: This chapter deals with four series, I^{st} series is purely ferroelectric; we discuss the structural, dielectric, ferroelectric, piezoelectric properties of $Pb_{(1-3y/2)}La_yZr_{0.55}Ti_{0.45}O_3$ (series A) for x = 0.0025 to 0.0075 in step of 0.0025. $2^{nd} – 4^{th}$ series (B - D) are composite series in which the effect of ferrite phase $Co_{0.8}Ni_{0.2}Fe_2O_4$ on structural, dielectric, ferroelectric, piezoelectric and magnetic properties of La substituted $PbZr_{0.55}Ti_{0.45}O_3$ is discussed.

Chapter VI: This chapter includes the conclusion and summary of the results. Recommendations for the future work have also been given in this chapter.

LIST OF PUBLICATIONS

I- Research Papers Published/Accepted/Communicated in International Journal

1. Study on structural, dielectric, ferroelectric and piezoelectric properties of Ba doped Lead Zirconate Titanate Ceramics, ***Dipti****, J.K. Juneja, Sangeeta Singh, K.K. Raina and Chandra Prakash,* Physica B **431** (2013) 109–114.

2. Dielectric properties of rare earth (Sm and La) substituted lead zirconate titanate (PZT) ceramics, ***Dipti****, Sangeeta Singh, J. K. Juneja, K. K. Raina, and Chandra Prakash,* AIP Proceedings, **1536** (2013) 1252.

3. Study of (x) CNFO- (1-x) PLZT Magnetoelectric Composites, ***Dipti****, Sangeeta Singh, J. K. Juneja, R.P. Pant, K. K. Raina, and Chandra Prakash,* AIP Proceedings, **1591** (2014) 207.

4. Enhancement in magnetoelectric coupling in PZT based composites**,** ***Dipti****, J.K. Juneja, Sangeeta Singh, K.K. Raina, Chandra Prakash,* Ceramics International, **41** (2015) 6108.

5. Improved dielectric and magnetic properties in modified lithium-ferrites, ***Dipti,*** *Parveen Kumar, J.K Juneja, Sangeeta Singh, K.K. Raina and Chandra Prakash,* Ceramic International, **41** (2015) 3293.

6. Structural, dielectric and magnetoelectric characterization of x $Co_{0.8}Ni_{0.2}$ Fe_2O_4 + (1-x) $PbZr_{0.55}Ti_{0.45}O_3$ composites**,** ***Dipti****, J.K. Juneja, Sangeeta Singh, K.K. Raina, Chandra Prakash,* Ferroelectric letters (Accepted).

7. Multiferroic Properties of Composites of PLZT and Substituted $CoFe_2O_4$, ***Dipti,*** *Parveen Kumar, J.K Juneja, Sangeeta Singh, K.K. Raina and Chandra Prakash,* Journal of Ceramic Processing Research, **16** (2015) 1 .

8. Comparative study of 2mol% Li- and Mn-substituted lead-free potassium sodium niobate ceramics, *Asha Dahiya, O.P. Thakur, J.K. Juneja, Sangeeta Singh, and* ***Dipti,*** International Journal of Minerals, Metallurgy and Materials, **21** (2014) 1241.

9. Study of x $Co_{0.8}Ni_{0.2}Fe_2O_4$ + (1-x) $Pb_{0.99625}$ $La_{0.0025}Zr_{0.55}Ti_{0.45}O_3$ Magnetoelectric Composites, ***Dipti****, J.K. Juneja, Sangeeta Singh, K.K. Raina, R.K. Kotnala, Chandra Prakash, Journal of Magnetism and Magnetic Materials* ***(Accepted).***

10. Study of Structural, Dielectric, Ferroelectric and Magnetic properties of PZT: CF Magnetoelectric Composites, ***Dipti,*** *J.K. Juneja, Sangeeta Singh, K.K. Raina, R.K. Kotnala and Chandra Prakash* **(To be communicated).**

11. Effect of Ni substitution in PLZT- CFO Magnetoelectric Composite, ***Dipti,*** *Parveen Kumar, J.K Juneja, Sangeeta Singh, K.K. Raina and Chandra Prakash* **(To be communicated).**

II – Paper Published in National Conference Proceedings

1. "Study on PZT (60/40) Ferroelectric Ceramics Synthesized by Novel Technique", **Dipti,** *Sangeeta Singh, J.K. Juneja, Chandra Prakash* "National Conference on Recent Advances in Materials Science", 25-26 Feb, 2012, Karnal

2. "Effect of Samarium on Dielectric and Ferroelectric properties of Lead Zirconate Titanate Ceramics", ***Dipti,*** *K.K. Raina, Sangeeta Singh, J.K. Juneja, Chandra Prakash* "National Symposium on Materials and Processing (MAP-2012)", 10-12 Oct, 2012, BARC-Mumbai .

III- Research Papers Presented in International and National Conferences/ Symposium/Seminar

1. "Microwave sintered Pb $Zr_{0.52}Ti_{0.48}O3$ Ferroelectric ceramics", ***Dipti,*** *Sangeeta Singh, J.K. Juneja, Chandra Prakash* "National Conference on Advanced materials and devices", 3-4 July, 2011, Sonepat.

2. "Study on PZT (52/48) Ferrolectric ceramic synthesized by Novel technique", ***Dipti***, *Sangeeta Singh, J.K. Juneja, Chandra Prakash* "National Conference on Futuristic Material", 15-17 Sep, 2011, Sharda University, Greater Noida.

3. "Dielectric and ferroelectric properties of Microwave Processed PZT ceramics", ***Dipti,*** *K.K.Raina, Sangeeta Singh, J.K. Juneja, Chandra Prakash,* "Functional materials for sustainable energy and Advanced Technology", 13-15 Feb, 2012, Thapar University, Patiala.

4. "Study on PZT (60/40) Ferroelectric Ceramics Synthesized by Novel Technique", **Dipti,**

Sangeeta Singh, J.K. Juneja, Chandra Prakash "National Conference on Recent Advances in Materials Science", 25-26 Feb, 2012, Karnal.

5. "Effect of Samarium on Dielectric and Ferroelectric properties of Lead Zirconate Titanate Ceramics", ***Dipti,*** *K.K. Raina, Sangeeta Singh, J.K. Juneja, Chandra Prakash* "National Symposium on Materials and Processing (MAP-2012)", 10-12 Oct, 2012, BARC-Mumbai.

6. "Characterization of Lead Samarium Zirconate Titanate (PSZT) Ceramics Sintered at Various Temperatures", ***Dipti,*** *K.K. Raina, Sangeeta Singh, J.K. Juneja, Chandra Prakash*, " National conference on Functional Materials (NCFM-2012)", 24-25 Sep, 2012, Sonepat

7. "Dielectric properties of rare earth (Sm and La) substituted Lead Zirconate Titanate (PZT) ceramics", ***Dipti,*** *K.K. Raina, Sangeeta Singh, J.K. Juneja, Chandra Prakash* International Conference on Recent Trends in Advanced Materials, (RAM-2013)",1,2 Feb, 2013, Bikaner

8. "Ferroelectric properties of Microwave Sintered $Pb_{(1.02-0.02)}Sm_{0.02}Zr_{0.55}Ti_{0.45}O_3$ Ceramics", ***Dipti,*** *K.K. Raina, Sangeeta Singh, J.K. Juneja, Chandra Prakash ,* National Conference on Advanced Material and Devices, (NCAMD-2013)" , 27-28 Feb, 2013.

9. "Study of x CNFO + (1-x) PLZT Magnetoelectric Composites", ***Dipti,*** *Sangeeta Singh, J.K. Juneja, K. K. Raina and Chandra Prakash,* 58^{th} DAE Solid State Physics Symposium (DAE-SSPS-2013), Thapar University, Patiala, Dec 17-21, 2013.

10. *"Structural and Electrical properties of Calcium doped Lead Zirconate Titanate Ceramics"*, ***Dipti***, *Sangeeta Singh, J.K. Juneja, K. K. Raina and Chandra Prakash,* National Symposium on Electroceramics- Materials and Devices (NSE-MD-2014), G.V.M Girls College, Sonepat, Feb 21-22, 2014.

11. Study of $0.05(Co_{0.80}Ni_{0.20}Fe_2O_4$) - 0.95 ($Pb_{(1.02-3x/2)}La_xZr_{0.55}Ti_{0.45}O_3$ ME Composites, ***Dipti,*** *Sangeeta Singh, J.K. Juneja, K. K. Raina and Chandra Prakash,* International Conference on Electron Microscopy-EMSI-2014, Delhi University, Delhi, July 9-11, 2014.

12. Study of Modified 0.10 CNFO – 0.90 PZT Composites, ***Dipti,*** *Sangeeta Singh, J.K. Juneja, K. K. Raina and Chandra Prakash,* National Conference on Recent Developments in Physics, S.D. College, Panipat, March 29-30, 2014.

13. Dielectric properties of Nb doped ferroelectric BLPZT ceramics, ***Dipti,*** *Parveen Kumar, Sangeeta Singh, J.K. Juneja, K. K. Raina and Chandra Prakash,* 2nd National Conference on Photonics and Material Science, (NCPMS-2014), Guru Jambheshwer University and Technology, March 20-21, 2014.

14. Synthesis and Characterization of Multiferroic Composites, ***Dipti,*** *Sangeeta Singh, J.K. Juneja, K. K. Raina and Chandra Prakash,* National Conference on Advances in Engineering Materials, (NAEM-2015), Dehradun Institute of Technology University (DITU), March 20-21, 2015.

IV- Conferences/ Symposium/Seminar/Workshops Attended

1. *Attended a* International Conference and Workshop on Nanostructured ceramics and Other Nanomaterials (ICWNCN), University of Delhi, *March 13-16,2012.*

2. Attended a "Advanced Workshop on Broadband Dielectric Spectroscopy", University of Delhi, January 17-18, 2014.

3. Attended a "National Seminar on Recent Trends in Physics", Hindu College, Sonepat, March 14-15, 2015.

V- Awards/ Prize/ Achievements

1. Paper entitled "Study on PZT (52/48) Ferrolectric ceramic synthesized by Novel Technique" was selected for **"Best Poster Presentation award"** in National Conference in Futuristic Material held on Sept 15-17, 2011 at Sharda University, Noida.

2. Paper entitled "Synthesis and Characterization of Multiferroic Composites" was selected for **"Best Oral Presentation award"** in National Conference on Advances in Engineering Materials (NAEM-2015), held on March 20-21, 2015 at (DITU), Dehradun.

TABLE OF CONTENTS

Certificate i

Acknowledgement ii

Abstract iv

List of Publications viii

Chapter 1 Introduction 1

1.1 Introduction to Multiferroic Materials 2

1.1.1 Single Phase Magneto-electric Materials 2

1.1.2 Two Phase - Composites 4

1.1.3 Necessary Condition to exhibit good ME Effect in the composites 5

1.1.4 Applications of Magnetoelectric (Ferrite-Ferroelectric) Composites 6

1.2 Ferroelectricity 6

1.2.1 Pervoskite Structure 7

1.2.2 Ferroelectric Curie temperature and Phase Transitions 8

1.2.3 Ferroelectric domains and Hysteresis Loops 9

1.2.4 Introduction to Piezoelectricity and its features 10

1.3. Magnetism in Materials 11

1.3.1 Diamagnetic Materials 11

1.3.2 Paramagnetic Materials 12

1.3.3 Ferromagnetic Materials 12

1.3.4 Antiferromagnetism Materials 13

1.3.5 Ferrimagnetic Material 14

1.3.6 Properties of Ferromagnetic/ Ferrimagnetic materials 16

1.3.6.1 B-H or M-H Hysteresis Loop 16

1.3.6.2 Magnetostriction 17

1.4 Review- Literature Survey 17
1.5 Selection of individual phases 25
1.6 Objectives of the Present work 26
References 27

Chapter 2 Material Synthesis and Characterization Techniques 32
2.1 Material Synthesis 33
2.1.1 Raw Materials and Ball Milling 34
2.1.2 Calcination 36
2.1.3 Shaping 37
2.1.4 Sintering 38
2.1.4.1 Conventional Sintering 39
2.2 Characterizations 40
2.2.1 Density 40
2.2.2 X-Ray Diffraction (XRD) 41
2.2.3 Scanning Electron Microscope 43
2.2.4 Polishing/Electroding 43
2.2.5 Dielectric Measurements 43
2.2.6 AC Conductivity 45
2.2.7 Ferroelectric (P-E) Measurement 46
2.2.8 Poling 48
2.2.9 Piezoelectric coefficients 49
2.2.10 Magnetic hysteresis loop set up- Vibrating Sample Magnetometer (VSM) 50
2.2.11 Magnetoelectric (M-E) Measurement 51
References 53

Chapter 3 Synthesis and Characterization of CFO-PZT Composites 54
3.1 Synthesis of Samples 55

	3.1.1 Synthesis of Individual phases	55
	3.1.2 Synthesis of Composites	55
3.2	Optimization of Sintering Temperature	57
	Synthesis and Characterization of (x) $CoFe_2O_4$ - (1-x) $PbZr_{0.55}Ti_{0.45}O_3$	61
	3.3.1 X-Ray Diffraction	62
	3.3.2 Scanning Electron Microscope	63
	3.3.3 Dielectric Properties	66
	3.3.3.1. Frequency dependence of dielectric properties (ε and tanδ)	66
	3.3.3.2. Temperature dependence of dielectric properties (ε and tanδ)	69
3.3.4	Ferroelectric Properties	73
3.3.5	Ferromagnetic Properties	76
3.3.6	Piezoelectric Properties	77
3.3.7	Magnetoelectric Properties	78
	References	81
Chapter 4	**Synthesis and Characterization of CNFO-PZT Composite**	83
4.1	Synthesis of Composite	84
4.2	Effect of Ni Substitution in Co-Ferrite	85
	4.2.1 Characterization of $CoFe_2O_4$ and $Co_{0.8}Ni_{0.2}Fe_2O_4$	85
	4.2.1.1 X-Ray Diffraction	85
	4.2.1.2 DC Resistivity	86
	4.2.1.3 Magnetic Properties	87
4.3	Characterization of CNFO-PZT Composites	88
	4.3.1 X-Ray Diffraction	88
	4.3.2 Scanning Electron Micrograph (SEM)	91
	4.3.3 Dielectric Properties	92
	4.3.3.1 Frequency dependence of dielectric properties (ε and tanδ)	92
	4.3.3.2 Temperature dependence of dielectric properties (ε and tanδ)	95
	4.3.4 Ferroelectric properties	100

4.3.5 Magnetic Properties 102
4.3.6 Piezoelectric Properties 105
4.3.7 Magnetoelectric Properties 106
References 109

Chapter 5 Synthesis and Characterization of La Substituted PZT- CNFO Composites 112

5.1 Synthesis of Individual phases and Composites 113
5.2 Characterization of (x) $Co_{0.8}Ni_{0.2}Fe_2O_4$ - (1-x) $Pb_{1-3y/2}La_yZr_{0.55}Ti_{0.45}O_3$ 113
5.2.1 X-Ray Diffraction 113
5.2.2 Scanning Electron Microscope 118
5.2.3 Dielectric Properties 121
5.2.3.1 Frequency dependence of dielectric properties (ε and tanδ) 121
5.2.3.2 Temperature dependence of dielectric properties (ε and tanδ) 125
5.2.4 Ferroelectric Properties 134
5.2.5 Piezoelectric Properties 135
5.2.6 Magnetic Properties: M-H Hysteresis loops 139
5.2.7 Magnetoelectric measurement 142
References 145

Chapter 6 Summary and Recommendations for Future Work 147
6.1 Summary of the results 148
6.2 Recommendations for future work 150

LIST OF FIGURES

Page No.

Chapter 1 Introduction

Figure 1.1 Schematic of Multiferroic Materials 2

Figure 1.2 Strain Mediated Magnetoelectric coupling effect 4

Figure 1.4 Schematic of the ferroelectric effect for a perovskite 8
(a) Pervoskite unit cell (b) Ferroelectric polarization of the crystal.

Figure1.5 Ferroelectric (P-E) hysteresis loop 9

Figure 1.6 Diamagnetic Materials 12

Figure 1.7 Paramagnetic Materials 12

Figure 1.8 (a) Ferromagnetic materials (b) Antiferromagnetic 13
(c) Ferrimagnetic materials

Figure 1.9 Unit cell of AB_2O_4 Spinel Structure 15

Figure 1.10 M-H/ B-H Hysteresis loop 16

Figure 1.11 Change in lattice dimension in the direction of applied field 17

Chapter 2 Material Synthesis and their Characterization Technique

Figure 2.1 Synthesis and Processing Steps for Ferroelectric/Ferrite Phase 33

Synthesis and Processing Steps for Composites 34

Figure 2.2 Processing of Powder in Planetary Ball Mill 35

Figure 2.3 Planetary Ball Mill for Mixing Purpose 35

Figure 2.4 Programmable Furnace used for Calcination 36

Figure 2.5 Hydraulic Press for shaping purpose 37

Figure 2.6 Programmable high temperature furnace for sintering with its specification 39

Figure 2.7 Density Measurements by Archimedes Principle 41

Figure 2.8 Geometry for Bragg X-Ray Diffraction 42

Figure 2.9 Hioki 3532-50 LCR Meter 45
Figure 2.10 Diagram of Modified Sawyer-Tawer Circuit 47
Figure 2.11 P-E Hysteresis Loop Tracer 48
Figure 2.12 Electrical Poling Setup with Specifications 49
Figure 2.13 Piezo d- meter for Measuring the Piezoelectric Coefficient 50
Figure 2.14 Schematic for Vibrating Sample Magnetometer 51
Figure 2.15 Magnetoelectric coupling measurement setup 52

Chapter 3 Synthesis and Characterization of CFO-PZT Composites

Figure 3.1 XRD pattern for (a) PZT and (b) CFO 56
Figure 3.2 XRD patterns for (0.05) CFO – (0.95)PZT composite at different sintering temperatures 57
Figure 3.3 Variation of (a) Dielectric constant (ε) with temperature (T (^{o}C)) dielectric Loss (tanδ) with temperature at 100 kHz for (0.05) CFO - (0.95) PZT composite at different sintering temperatures 59
Figure 3.4 P-E Hysteresis loops for (0.05)CFO – (0.95)PZT composite at different sintering Temperatures 60
Figure 3.5 X-Ray Diffraction Pattern for (x) CFO-(1-x) PZT composites; (1) x= 0.00 (2) x = 0.05 (3) x = 0.10 (4) x = 0.15 and (5) x = 1.00 63
Figure 3.6 SEM Micrograph for (x) CFO-(1-x) PZT Composites; (a) x= 0.00 (b) x = 0.05(c) x = 0.10 (d) x = 0.15 and (e) x = 1.00 64
Figure 3.7 Variations of (a) Dielectric Constant and (b) Tangent Loss with Frequency at Room Temperature for (x) CFO-(1-x) PZT Composites; x = 0.00, 0.05, 0.10, 0.15 and 1.00 67
Figure 3.8 Variation of AC Conductivity with Frequency at 100 kHz for (x) CFO - (1-x) PZT Composites (x = 0.00, 0.05, 0.10, 0.15 and 1.00) 68
Figure 3.9 Variations of Dielectric Constant (ε) and Tangent Loss with Temperature at 1 kHz, 10 kHz and100 kHz for (x) CFO - (1-x) PZT Composites (x = 0.00, 0.05, 0.10, 0.15 and 1.00) 71
Figure 3.10 Comparison of Variation of Dielectric Properties ((a) dielectric 73

constant and (b) tangent loss) with temperature at 100 kHz for (x) CFO-(1-x) PZT Composites (x = 0.00, 0.05, 0.10 and 0.15)

Figure 3.11 Ferroelectric P-E Hysteresis loop for all samples at different electric fields (15kV – 25kV) 74

Figure 3.12 Comparisons of P-E Hysteresis Loops at 25^{o}C for (x) CFO-(1-x) PZT Composites (x = 0.00, 0.05, 0.10 and 0.15) 75

Figure 3.13 Ferromagnetic M-H Hysteresis Curve for (x) CFO - (1-x) PZT Composites (a) (x = 0.00, 0.05, 0.10 and 0.15) and (b) x = 1.00 77

Figure 3.14 Variation of ME coupling coefficient with DC magnetic field for (a) x = 0.05 and (b) x = 0.15 79

Chapter 4 Synthesis and Characterization of CNFO-PZT Composite

Figure 4.1 XRD pattern of $CoFe_2O_4$ and Ni doped $CoFe_2O_4$ samples 86

Figure 4.2 Variation of DC resistivity with temperature for $CoFe_2O_4$and Ni doped $CoFe_2O_4$ samples 87

Figure 4.3 M-H Hysteresis loops of $CoFe_2O_4$ and Ni doped $CoFe_2O_4$ samples 88

Figure 4.4 X-Ray diffraction for x CNFO + (1-x) PZT (1) x = 0.00 (PZT) (2) x = 0.05 (3) x = 0.10 (4) x = 0.15 and (5) x = 1.00 (CNFO) 90

Figure 4.5 SEM Micrographs for x CNFO - (1-x) PZT (a) x = 0.00 (PZT) (b) x = 0.05 (c) x = 0.10 (d) x = 0.15 and (f) x = 1.00 (CNFO) 91

Figure 4.6 **(a)** Variation of Dielectric Constant with frequency at room temperature for all samples **(b)** Variation of dielectric loss with frequency for all samples 94

Figure 4.7 Variation of AC Conductivity with Frequency at 100 kHz for x CNFO-(1-x) PZT Composites (x = 0.00, 0.05, 0.10, 0.15 and 1.00) 95

Figure 4.8 Variation of ε and tanδ with temperature for x CNFO + (1-x) PZT composite (a) x = 0.00, (b) x= 0.05, (c) x= 0.10 and (d) x = 0.15 97

	and (e) x = 1.00 at different frequencies (1 kHz, 10 kHz, 100 kHz)	
Figure 4.9	Comparison of Variation of Dielectric Properties ((a) dielectric constant and (b) tangent loss) with temperature at 100 kHz for x CNFO-(1-x) PZT Composites (x = 0.00, 0.05, 0.10 and 0.15)	99
Figure 4.10	P-E hysteresis loop at different electric fields for x CNFO- (1-x) PZT ((a) x = 0.00, (b) 0.05 (c) x = 0.10 (d) x = 0.15	101
Figure 4.11	Comparisons of P-E Loops for all samples at 25 kV	102
Figure 4.12	M-H Hysteresis curve for x CNFO + (1-x) PZT composite (a) x = 0.05, 0.10, 0.15 (b) x = 1.00 measured at room temperature (c) M-H Loops for Electrically Poled Sample and Unpoled Sample for x = 0.05 and (d) x = 0.10	105
Figure 4.13	Variation of ME Coupling Coefficient (α) with a DC magnetic field for x = 0.05 and x = 0.10	107

Chapter 5 Synthesis and Characterization of La Substituted PZT-CNFO Composites

Figure 5.1	XRD Pattern for all samples of (a) Series A (b) Series B (c) Series C and (d) Series D	116
Figure 5.2 (A)	SEM micrograph for **Series A** (a) y = 0.0025 and (b) y = 0.005	118
Figure 5.2 (B)	SEM images for **Series B** (a) x = 0.05 (b) x = 0.10 (c) x = 0.15	119
Figure 5.2 (C)	SEM images for **Series C** (a) x = 0.05 (b) x = 0.10 (c) x = 0.15	120
Figure 5.3 (A)	Frequency dependence of (a) dielectric constant (b) dielectric loss for **Series A**	122
Figure 5.3 (B)	Frequency dependence of (a) dielectric constant (b) dielectric loss for **Series B**	123
Figure 5.3 (C)	Frequency dependence of (a) dielectric constant (b) dielectric loss for **Series C**	124
Figure 5.3 (D)	Frequency dependence of (a) dielectric constant (b) dielectric loss for **Series D**	125

Figure 5.4 (A)	Variation of ε and tanδ with temperature for **Series A** (a) y = 0.0025, (b) y = 0.005, (c) y = 0.0075 at different frequencies (1 kHz, 10 kHz, 100 kHz)	128
Figure 5.4 (B)	Variation of ε and tanδ with temperature for **Series B** (a) x = 0.05 (b) x = 0.10 and (c) x = 0.15 at different frequencies (1 kHz, 10 kHz and 100 kHz)	129
Figure 5.4 (C)	Variation of ε and tanδ with temperature for **Series C** (a) x = 0.05 (b) x = 0.10 and (c) x = 0.15 at different frequencies (1 kHz, 10 kHz and 100 kHz)	130
Figure 5.4 (D)	Variation of ε and tanδ with temperature for **Series D** (a) x = 0.05 (b) x = 0.10 and (c) x = 0.15 at different frequencies (1 kHz, 10 kHz and 100 kHz)	131
Figure 5.5	Comparative study of (a) dielectric constant (ε) and (b) dielectric loss (tanδ) measured at 100 kHz for (a) Series A (b) Series B (c) Series C and (d) Series D	133
Figure 5.6 (a-d)	P-E Hysteresis loops for all Series (a) Series A (b) Series B (c) Series C and (d) Series D	137
Figure 5.7 (a)	M-H Hysteresis loops of **Series B**	141
Figure 5.7 (b)	M-H Hysteresis loops of **Series C**	141
Figure 5.7 (c)	M-H Hysteresis loops of **Series D**	142
Figure 5.8 (a)	Variation of magnetoelectric coupling coefficient (α) with DC magnetic field for x = 0.05, x = 0.10 of **Series B**	143
Figure 5.8 (b)	Variation of magnetoelectric coupling coefficient (α) with DC magnetic field for x = 0.05 of **Series C**	143
Figure 5.8 (c)	Variation of magnetoelectric coupling coefficient (α) with DC magnetic field for (i) x = 0.05 (ii) x = 0.15 of **Series D**	144

List of Tables

Page No.

Chapter 3 Synthesis and Characterization of CFO-PZT Composites

Table 3.1	Lattice parameters of (0.05) CFO – (0.95) PZT composite sample sintered at three different Temperatures	58
Table 3.2	Dielectric parameters of (0.05) CFO- (0.95) PZT sample at 100 kHz for different sintering Temperatures	59
Table 3.3	Ferroelectric Parameters for (0.05) CFO – (0.95) PZT recorded at room temperature	60
Table 3.4	Structural Parameters of (x) CFO - (1-x) PZT composites	65
Table 3.5	Variation of Dielectric Parameters at 100 kHz for all values of x	72
Table 3.6	Ferroelectric Parameters (P_r, E_c and P_s) for all values of x	76
Table 3.7	Magnetic parameters (H_c, M_r and M_s) and Magneto-electric Coefficient (α) for (x) CFO - (1-x) PZT Composites (x = 0.00, 0.05, 0.10 and 0.15)	80

Chapter 4 Synthesis and Characterization of CNFO-PZT Composites

Table 4.1	Structural Parameters of (x) CNFO-(1-x) PZT composites	90
Table 4.2	Variation of Dielectric Parameters (ε_{RT}, T_c (^oC), ε_{max}, $\tan\delta_{RT}$, $\tan\delta_{max}$) at 100 kHz for all values of x	98
Table 4.3	Ferroelectric Parameters (P_r, E_c and P_s) at 25 kV for all values of x	102
Table-4.4	Magnetic parameters (H_c, M_r and M_s) and Magneto-electric Coefficient (α) for x CFO-(1-x) PZT Composites	108

(x = 0.00, 0.05, 0.10 and 0.15)

Chapter 5 Synthesis and Characterization of La Substituted PZT-CNFO Composites

Table 5.1	Lattice Parameters and relative density for (x) $Co_{0.8}Ni_{0.2}Fe_2O_4$ - (1-x) $Pb_{1-3y/2}La_yZr_{0.55}Ti_{0.45}O_3$ for all values of x of all values of y	117
Table 5.2	Variation of dielectric parameters (ε_{RT}, T_c (^oC), ε_{max}, $\tan\delta_{RT}$, $\tan\delta_{max}$) measured at 100 kHz for (x) $Co_{0.8}Ni_{0.2}Fe_2O_4$ - (1-x) $Pb_{1-3y/2}La_yZr_{0.55}Ti_{0.45}O_3$ for all values of x of all values of y	134
Table 5.3	Ferroelectric Parameters (P_r, E_c and P_s) at 30 kV and piezoelectric charge coefficient for (x) $Co_{0.8}Ni_{0.2}Fe_2O_4$ - (1-x) $Pb_{1-3y/2}La_yZr_{0.55}Ti_{0.45}O_3$ for all values of x of all values of y	138
Table 5.4	Magnetic Parameters (M_r, M_s and H_c) and magnetoelectric coupling coefficient (α) for (x) $Co_{0.8}Ni_{0.2}Fe_2O_4$ - (1-x) $Pb_{1-3y/2}La_yZr_{0.55}Ti_{0.45}O_3$ for all values of x of all values of y	140

Chapter – 1

Introduction

Chapter – I

Introduction

Magnetoelectric composite materials are drawing attention of the researchers world over due to their fundamental physics and their potential technological applications in multifunctional devices, like magnetic field sensors, filters, oscillators, phase shifters, multiple state memory elements, transducers and electro-optic devices etc. These materials also show unique property - magnetoelectric effect that is not shown by individuals phases (Ferroelectric and ferromagnetic). Magnetoelectric effect is a effect in which external electric field induces magnetization and vice - versa.

The present work is mainly concentrated on the study of modified PZT-$CoFe_2O_4$ magnetoelectric composites. This chapter includes the brief introduction about the ferroelectricity, ferromagnetism and magnetoelectric composites.

1.1 Multiferroic Materials

Multiferroics are materials which exhibit two or more ferroic properties such as ferroelectricity, ferromagnetism and ferroelasticity [1]. If a material exhibits simultaneously ferroelectricity and ferromagnetism, then material is called magnetoelectric material. Figure 1.1 shows the schematic of multiferroic materials [2]. In such materials external magnetic field produces an electric polarization or external electric field produces magnetization. The magnetoelectric materials are classified into two types: single phase materials and two phase materials [3] (composites).

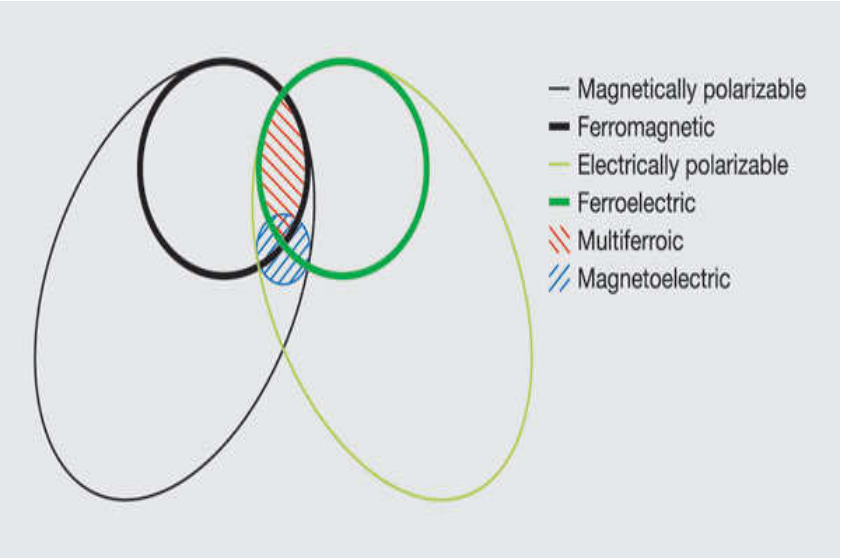

Figure 1.1 Schematic of Multiferroic materials

1.1.1 Single Phase Magneto-electric Materials

In single phase magneto-electric materials, materials exhibit both electric polarization and magnetization in single phase. This can result in the magneto-electric effect due to the coupling of the magnetic and ferroelectric ordering. The magnetoelectric coupling in single crystal is described by Landau free energy theory in terms of applied magnetic field and applied electric field. The free energy can be written as

$$F(E,H) = 1/2\varepsilon_0\,\varepsilon_{ij}\,E_iE_j + 1/2\mu_0\mu_{ij}H_iH_j + \alpha_{ij}E_iH_j + 1/2\beta_{ijk}E_iH_jH_k + 1/2\gamma_{ijk}H_iE_jE_k \quad ..1.1$$

Where the first term corresponds to the contribution of electric field, ε_{ij} is relative permittivity and 2nd term corresponds to the contribution of magnetic field, μ_{ij} is magnetic permeability. The

subscripts i, j and k are the three directions of a Cartesian coordinate system. α_{ij} is linear ME coefficient that corresponds to induction of polarization by a magnetic field or induction of magnetization by an electric field. Other terms represent higher order magnetoelectric coupling coefficients.

The magnetoelectric effect can be determined by derivative of F (E,H) with respect to E_i (H_j) and with respect to H_j (E_i) to determine polarization and magnetization.

$$P_i(Hj) = -\frac{\partial F}{\partial E_i} = \alpha_{ij} H_{j,} \quad \text{.....1.2}$$

$$M_j(Ej) = -\frac{\partial F}{\partial H_j} = \alpha_{ij} E_i \quad \text{.....1.3}$$

In the first half of 19th or 20th century, the ME effect on single phase systems were observed but the single phase materials showing ME coupling were found to be rare. There were some limitations which restrict the coexistence of ferroelectricity and magnetism in single phase as given below:

(i) Symmetry:

There are 122 Shubnikov point groups from which 31 point groups allow spontaneous electric polarization and 31 allow spontaneous magnetization. However, there are only 13 point groups (1, 2, 2', m, m', 3, 3m', 4, 4m'm', m'm2', m'm'2', 6 and 6m'm') that allows both spontaneous electric polarization and spontaneous magnetization simultaneously in single phase [4]. Many materials which are not ferromagnetic and ferroelectric exist in one of the allowed symmetry. Therefore symmetry is responsible for scarcity of ferromagnetic and ferroelectric materials.

(ii) d^0ness

The coexistence of ferromagnetism and electric polarization in single phase is restricted due to the empty d- orbital in B-cation. In ferroelectric materials like PZT, $BaTiO_3$ etc., the ferroelectricity is due to off center displacement of the Ti ion having an empty d-orbital. As there are no d-electrons, creating magnetic moments, then there can be no magnetic ordering. For magnetic ordering, d-orbital should be partially filled. Therefore, different mechanism of ferroelectricity is required to obtain magnetoelectric coupling in single phase [5].

Materials exhibiting magnetoelectric effects are Cr_2O_3, $BiMnO_3$ and $BiFe_2O_3$ etc. are single phase. Experimental confirmation was done by Astrov on Cr_2O_3 who measured the electrically induced ME effect in the temperature range of 80-330K [6]. Since then there has been a lot of papers reporting the observations and measurements of the ME effect in single crystals [7-11]. All exhibit ME effect at low temperature, much below the room temperature and their ME coefficient drops to zero as the transition temperature reaches the Curie temperature. But ME effect is too small to be practically applicable due to temperature constraints. So single phase materials have not yet found any technological applications. However research on suitable single phase magnetoelectric materials is being carried out by number of research groups [12].

1.1.2 Two Phase Magnetoelectric Materials - Composites

To overcome the limitations of single phase magnetoelectric materials and to enhance the magnetoelectric coupling at room temperature, the two phase materials were introduced [13]. In two phase magnetoelectric materials or composites, one phase should be piezoelectric or electrostrictive while other should be magnetic and magnetostrictive. The magnetoelectric coupling between two phases is introduced or induced through indirect coupling. This indirect coupling takes place via stress and results in magnetostriction induced deformation and the generation of piezoelectric charge [14-15]. The strain mediated magnetoelectric coupling is shown in Figure 1.2.

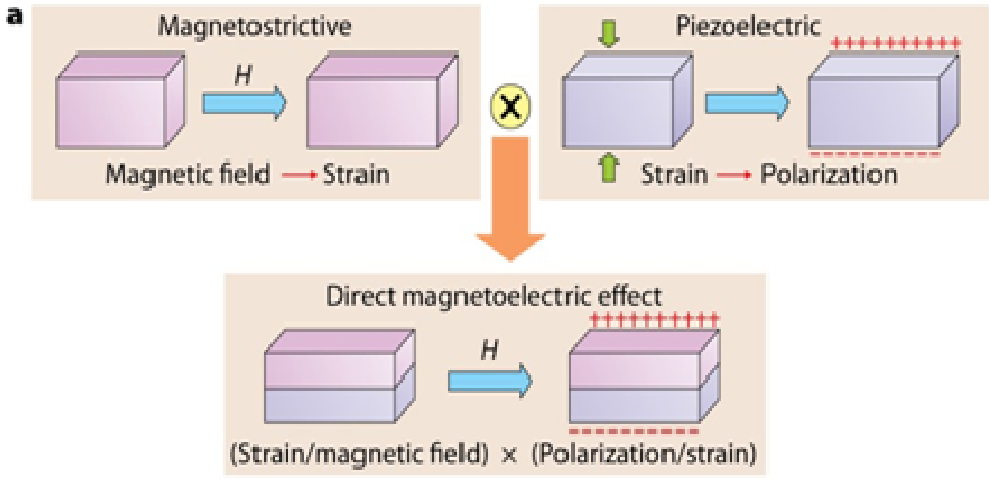

Figure 1.2 Strain Mediated Magnetoelectric coupling effect

The first discussion on synthesized composite materials was proposed by Van Suchtelen in 1972 [16]. When magnetic field is applied to a composite, the ferrite material change their shape because of magnetostriction and this strain is passed to the piezoelectric materials, resulting in an electric polarization. The equation 1.1 shows the schematic representation of ME effect in two phase systems (composites) utilizing the product property [17].

$$\alpha_E = \frac{\delta E}{\delta H} = \left(\frac{\delta E}{\delta z}\right).\left(\frac{\delta z}{\delta H}\right) \qquad \text{……..1.4}$$

Where,

$\alpha_E = \frac{\delta E}{\delta H}$ = ME coefficient

$\frac{\delta E}{\delta z}$ = Piezoelectric field generation

$\frac{\delta z}{\delta H}$ = Magnetostriction deformation

For studying this effect, a combination of ferroelectric and ferrimagnetic materials are been employed. The most widely studied systems that have been reported correspond to substituted $CoFe_2O_4$, $NiFe_2O_4$, $MnFe_2O_4$, $ZnFe_2O_4$ ferrites with substituted $BaTiO_3$, PZT, PMN-PT, BNT, BNT-BT and PVDF [18].

1.1.3 Necessary Condition to exhibit good ME Effect in the composites:

In 1978, Boomgard and Born outlined some requirements to obtain better ME effect in composites [22] which are summarized here:

- Two phases should be in equilibrium and no chemical reaction should take place between the constituent phases.
- Resistivity of the constituent phases should be high to avoid the leakage of charges developed in the piezoelectric phase and possibility to pole at higher fields to get higher magnetoelectric output.
- Magnetostriction coefficient of magnetostrictive phase (ferrite) and piezoelectric coefficient of piezoelectric phase should be high to achieve good ME.
- Sintering temperature should not be too high so as to avoid diffusion between two phases (results in an increase in defect concentrations which leads to lower resistivity of composites and makes the poling more difficult).

1.1.4 Applications of Magnetoelectric (Ferrite-Ferroelectric) Composites

Today is day of device miniaturization, there is ever increasing interest in multifunctional devices which are based on magnetoelectric effect. These magnetoelectric composites are promising candidate for technological applications. These applications are given below:

- Magnetoelectric materials are used for transducers used for converting electric and magnetic fields. These materials can be used as attenuators, filters, data recording devices based on electric control of magnetization and vice-versa [19].
- The coexistence of magnetization and electric polarization in a magnetoelectric material allows the four-state logic states in a single device.
- Magnetoelectric composite materials can be used as micro- sensors in place of magneto resistive read heads.
- Electrically tunable microwave devices such as filters, oscillators and phase shifters in which magnetic resonance is tuned electrically.
- ME composites also find applications in memory devices due to hysteresis nature of composites. ME coupling permits the data to be written electrically and red magnetically in memory technologies.

Dong et al. [20] fabricated a transformer using Lead Zirconate Titanate–Terfenol D composite and predicted the possibility of an extremely high magnetoelectric voltage gain. J. Rhu et al. [21] fabricated magnetoelectric laminated composites of PZT-Terfenol for magnetic field sensing applications.

As magnetoelectric materials are composed of two phases – Ferroelectric and Ferromagnetic materials so it is required to give brief introduction about ferroelectricity and magnetism that are given in following sections.

1.2 Ferroelectricity

Ferroelectricity is a property of certain non conducting crystals, or dielectrics that exhibit spontaneous electric polarization which can be reversed in direction by application of an electric field [23]. Ferroelectricity was reported for the first time by ‘Joseph Valasek’, who worked at the University of Minnesota in Minneapolis, in his work “Piezoelectricity and Allied Phenomenon in Rochelle Salt” in 1920 [24-26]. Rochelle salt and potassium di hydrogen phosphate were two

known ferroelectrics before 1940. In the early 1940's, the discovery of barium titanate ($BaTiO_3$) ceramic, first ferroelectric material has led to the discovery of a large number of similar pervoskites viz. $KNbO_3$, $LiNbO_3$, $PbTiO_3$ etc. A crystal is said to be ferroelectric when it has two or more orientational states in the absence of an electric field and can be shifted from one state to another by the application of an electric field [27]. Ferroelectricity is caused by asymmetries in the lattice structure. So the ferroelectricity in crystals can be explained on the basis of symmetry operations. It is found that symmetry operations can be divided in to 32 different crystal classes. These thirty-two point groups can be further divided into two groups: (a) crystals with a center of symmetry and (b) crystals without center of symmetry.

Crystals with center of symmetry with 11 point groups are known as centrosymmetric. The remaining 21-point groups which do not have a center of symmetry are known as non-centrosymmetric. Out of these, 20 point group give piezoelectric effect i.e., generation of electric charge on application of stress. Further, out of 20 point groups, 10 point groups possess spontaneous polarization and give rise to generation of electric charges on change in temperature and are called pyroelectric materials some of the materials belonging to these 10 point groups show reversible spontaneous polarization on application of electric field are called ferroelectrics.

There has been a continuous succession of new materials and technology developments till now. The main applications of ferroelectric materials are their use in high value capacitors, piezoelectric sensors and actuators, ultrasonic transducers, radio and communication filters, medical diagnostic transducers, stereo, buzzers, positive temperature coefficient (PTC) sensors, switches, ultrasonic motors, thin-film capacitors, and ferroelectric thin film memories etc [28-31].

1.2.1 Pervoskite Structure

The mineral name of pervoskite is calcium titanate ($CaTiO_3$). The simplest structure of perovskite is cubic. A typical ABO_3 unit cell structure is shown in figure 1.4 (a) in which the larger A cations, monovalent or divalent metal (A: Pb^{2+}, Ca^{2+}, Ba^{2+}, La^{3+} etc.) are on the corners of the unit cell. The smaller B cations, tetravalent or pentavalent metal (B: Ti^{4+}, Zr^{4+}, Sn^{4+}, Nb^{5+}, Ta^{5+}etc.) are at the body center of the unit cell. The oxygen atoms are at the face centers of the

cube [27]. The arrows depict the stretching motion due to the electrostatic force. Ferroelectricity is characteristics of compound with distorted Pervoskite structure.

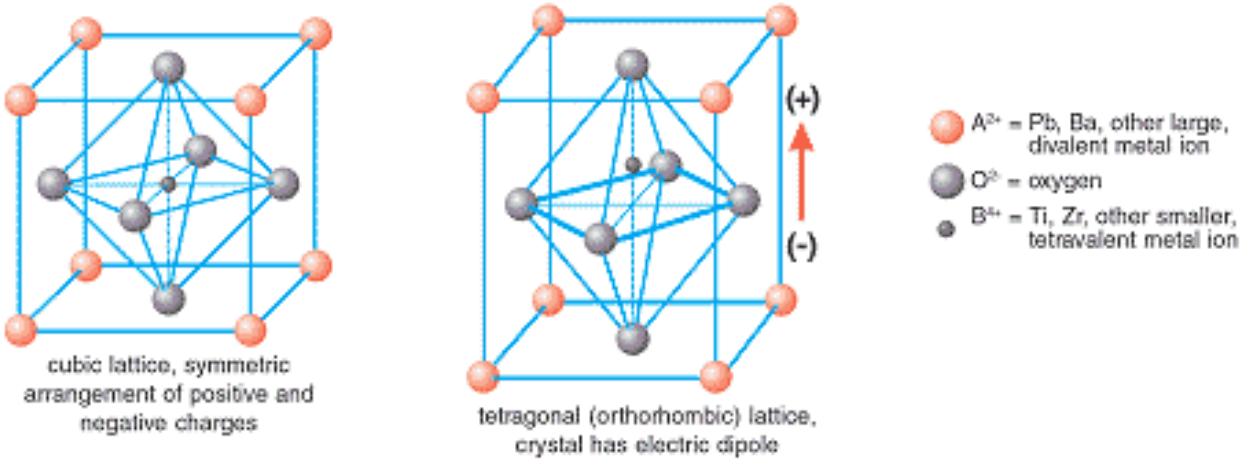

Figure 1.4 Schematic of the ferroelectric effect for a perovskite. (a) Perovskite unit cell. (b) Ferroelectric polarization of the crystal.

1.2.2 Ferroelectric Curie temperature and Phase Transitions

The important characteristics of ferroelectric materials are ferroelectric transition temperature (T_c) or Curie temperature. In general, ferroelectric materials undergo a phase transition on cooling from a paraelectric phase to ferroelectric phase. This would happen when temperature is lower than the Curie temperature. At a temperature above T_c, the crystal does not exhibit ferroelectricity or unit cell becomes symmetric and the material is in paraelectric state; on the other hand, when the temperature is below T_c, the crystal exhibits ferroelectricity or unit cell becomes non-centrosymmetric leading to ferroelectricity.

The ferroelectric behavior in barium titanate ($BaTiO_3$) was observed in 1945, due to its perovskite structure, better ferroelectric properties, chemical and mechanical stability, barium titanate (BT) became one of the most extensively studied ferroelectric materials. After that in 1950, Lead Zirconate Titanate (PZT) having perovskite structure was found to be an attractive ferroelectric. PZT compositions are now the most widely exploited of all piezoelectric ceramics both in research and industry.

If there are more than one ferroelectric phases, the temperature at which the crystal transforms from one ferroelectric phase to another is called the transition temperature. Near the Curie point or phase transition temperatures, properties including dielectric, elastic, optical, and thermal constants show an anomalous behavior. The temperature dependence of the dielectric constant above the Curie point ($T>T_c$) in most ferroelectric crystals is described by the Curie-Weiss law [32-34].

$$\varepsilon = \varepsilon_o + \frac{C}{(T-T_o)} \qquad \text{……...……1.5}$$

Where ε is the permittivity of the material, ε_o is the free space permittivity, C is the Curie constant and T_o is the Curie-Weiss temperature. The Curie-Weiss temperature T_o is, different from the Curie point T_c. For first order transitions, $T_o < T_c$ while for second order phase transitions, $T_o = T_c$ [34].

1.2.3 Ferroelectric domains and Hysteresis Loops

Ferroelectrics possess regions with uniform polarization, known as ferroelectric domains. All the electric dipoles are aligned in the same direction with in a domain. There may be many domains in a crystal separated by interfaces called domain walls [35]. A single domain can be obtained by domain wall motion, by the application of electric field. Strong fields could lead to the reversal of the polarization in the domains known as domain switching. The polarization reversal can be determined by measuring the ferroelectric hysteresis as shown in Figure 1.5.

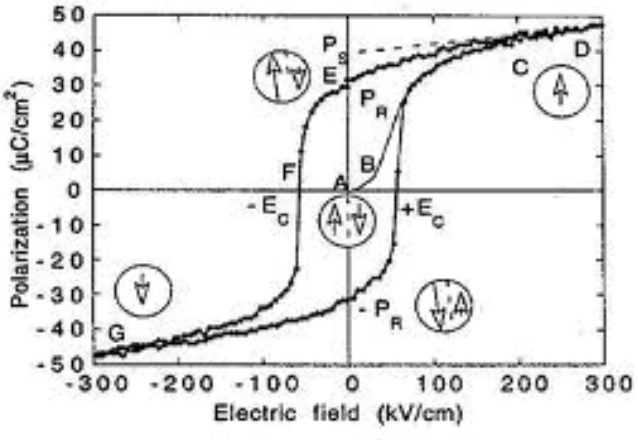

Figure1.5 Ferroelectric (P-E) hysteresis loop

The starting point is assumed to be at A (figure 1.5). As the electric field strength is increased, the domain starts to align in the positive direction, giving rise to rapid increase in the polarization. If the field strength starts to decrease, some domains will reverse but polarization does not fall to zero when the external field is removed. At zero external fields, some of the domains remains aligned in the positive direction and the crystal will show a remnant polarization P_r (AE). The field necessary to bring the polarization to zero is called the coercive field strength, E_c. If the field is increased to more negative value, the direction of polarization flips and hence a hysteresis loop is obtained. The value of spontaneous polarization P_s, is obtained by extrapolating the curve of saturated polarization at point D, onto the polarization axis [36]. The coercive field, spontaneous and saturation polarizations and shape of the loop are affected by a number of factors including thickness, presence of charged defects, mechanical stresses, preparation conditions, pinning centers and measurement temperatures [37,38].

1.2.4 Introduction to Piezoelectricity and its Features:

In 1880, Jacques and Pierre Curie discovered piezoelectricity. They studied the effect of pressure on the generation of electrical charge by crystals such as quartz and tourmaline. Piezoelectricity (piezo means to press) is the generation of electricity as result of a mechanical pressure. A piezoelectric material develops a potential across its boundaries when subjected to a mechanical pressure called direct piezoelectric effect. Conversely, when an electric field is applied to piezoelectric material, a mechanical deformation takes place. This effect is called converse piezoelectric effect. These materials are used to make sensors and actuators. Piezoelectric effect is linear effect which arises due to displacement of ionic charges within a crystal structure. In the absence of the external stress, the charge distribution within the crystal is symmetric and the net electric dipole moment is zero. However, with the application of external stress, the charges are displaced and asymmetric distribution of the charge is observed and a net polarization develops which results in an internal electric field.

When a piezoelectric material is subjected to stress, electric charge generated per unit force is called piezoelectric charge coefficient and is represented by 'd_{33}'. d_{33} indicates the polarization generated in the direction 3 when the stress is applied in the 3rd direction. In addition to piezoelectric coefficient (d), piezoelectric voltage coefficient (g); It is related with

electrical field produced by mechanical stress. It is used to measure the field produced by the stress in piezoelectric ceramics. The 'g' constant is related to the 'd' constant using the relation

$$g = \frac{d}{\varepsilon \varepsilon_o} \qquad \ldots\ldots\ldots\ldots\ldots\ldots 1.6$$

Where ε and ε_o are the dielectric constant of the material and permittivity of the free space respectively. Piezoelectric charge coefficient is measured by pC/N while piezoelectric voltage coefficient (g) is measured in meter volts / Newton.

There is also electromechanical coupling factor 'k' which gives us the measure of the part of the applied electrical energy converted into mechanical energy or vice-versa and measured by resonance method [39]. It is also called efficiency of the material. It is defined as the square root of the ratio of energy output in mechanical form to the total input electrical energy. These electromechanical coupling factors are material constants and they depend on degree of poling for piezoelectric ceramic.

$$k^2 = \frac{\text{Mechanical energy converted into electrical energy}}{\text{input mechanical energy}} \qquad \ldots\ldots\ldots\ldots..1.7$$

1.3 Magnetism in Materials

The magnetic nature of a material is determined by the magnetic moments of the electrons, atoms and ions in the material. The magnetic responses of atoms, electrons and ions can exhibit a variety of behaviors in materials due to the wide range of interactions that can occur between the magnetic moments and their environment. The magnetic moment of an atom has three sources: Electron spin, electron orbital momentum about the nucleus and the change in the spin and orbital momentum induced by an applied magnetic field (**H**). Magnetic moment per unit volume defines the magnetization of the material. Magnetic Materials are classified into different categories depending on the interaction with external magnetic field.

1.3.1 Diamagnetic Materials

Diamagnetic materials are slightly repelled by a magnetic field and the material does not retain the magnetic properties when the external field is removed. In diamagnetic materials, the electrons are paired so there is no permanent net magnetic moment per atom. Diamagnetic properties arise from the re- alignment of the electron paths under the influence of an external

magnetic field as shown in Figure 1.6. Diamagnetic materials have a weak, negative susceptibility (M/H) to magnetic fields and a magnetic permeability (μ/μ_0) less than 0. Alkali earth, Bismuth, superconducting materials and organic compounds are examples of diamagnetic materials.

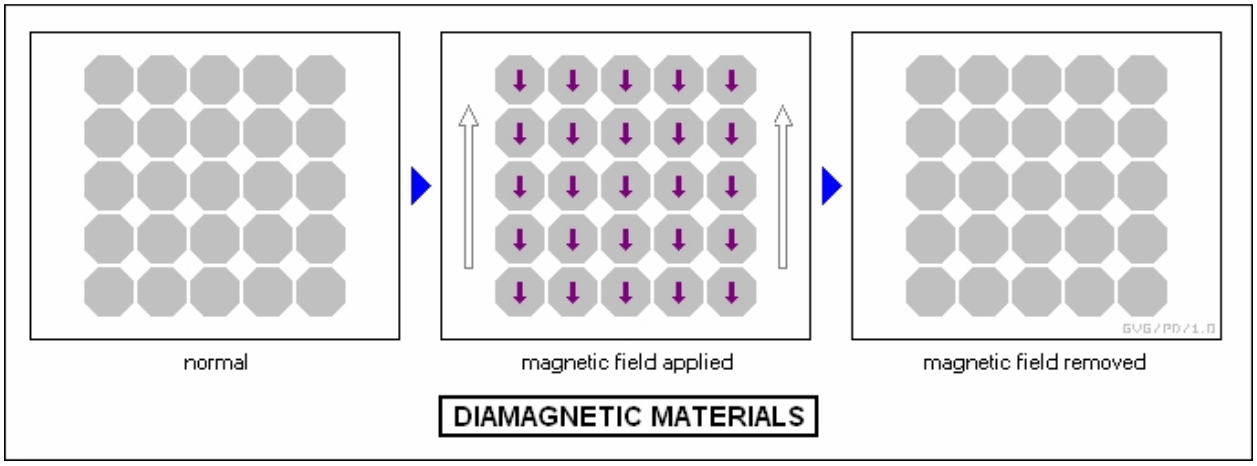

Figure 1.6 Diamagnetic Materials

1.3.2 Paramagnetic Materials

These materials are composed of atoms or molecules having permanent dipole moment which arises from the orbital and spin motion of the electrons. Figure 1.7 shows the paramagnetic material in the absence and presence of magnetic field. Paramagnetic materials are slightly attracted by a magnetic field and the material does not retain the magnetic properties when the external field is removed. They obey Curie's law (i.e. alignment of moments in an external field is opposed by the disordering effects of temperature). Paramagnetic materials have a relative magnetic permeability greater or equal to unity and positive susceptibility. Alkali metals, Transition metals, rare earths are the examples of paramagnetic materials.

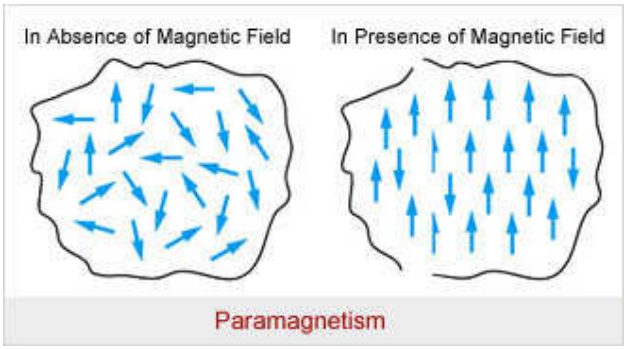

Figure 1.7 Paramagnetic Materials

1.3.3 Ferromagnetic Materials

Ferromagnetic materials exhibit a strong attraction to magnetic fields and are able to retain their magnetic properties after the external field has been removed. Ferromagnetic materials have some unpaired electrons so their atoms have a net magnetic moment. They get their strong magnetic properties due to the presence of magnetic domains. Ferromagnetic ordering occurs when all the moments contribute equally to the spontaneous magnetization**.** It exists below a certain critical temperature called Curie temperature; T_c. The alignment of magnetic moment below the Curie temperature is due to exchange interaction between magnetic ions. It results in the parallel or anti parallel alignment of uncompensated electron spins as shown in Figure 1.8 (a). Above Curie temperature, the thermal effect disturbs the spin alignment and the substance becomes paramagnetic. Ferromagnetic materials have a large, positive susceptibility to an external magnetic field. The examples of ferromagnetic materials are the elements such as Fe, Co, Ni, Gd etc.

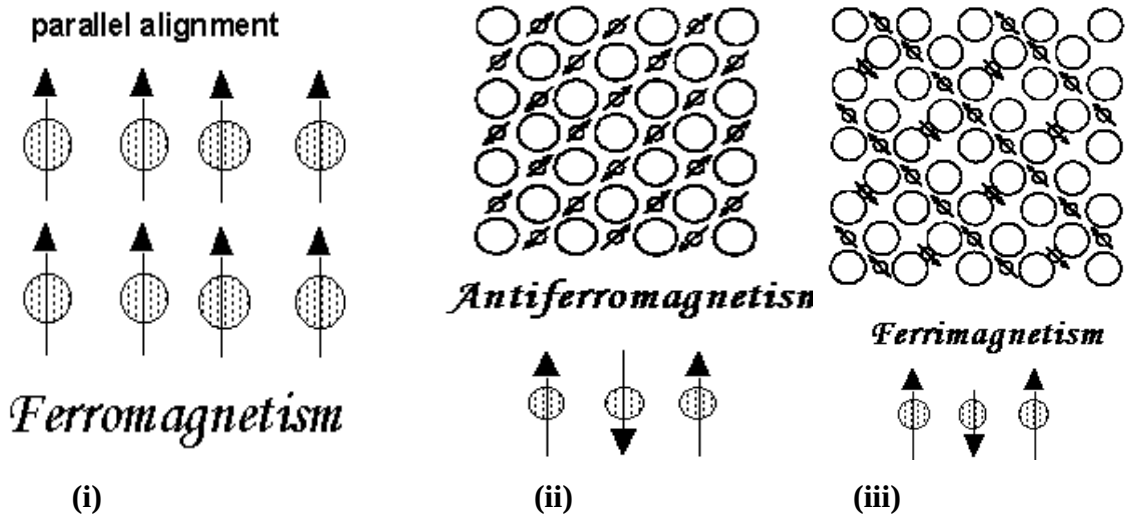

Figure 1.8 (a) Ferromagnetic materials (b) Antiferromagnetic (c) Ferrimagnetic materials

1.3.4 Antiferromagnetic Materials

Antiferromagnetism materials have structures composed of two interpenetrating sub lattices and their ordering is such that there is no net spontaneous magnetization because half of the

dipoles of one sub lattice are aligned in one direction and the other half of the other sub lattice in the opposite direction. Figure 1.8 (b) shows the antiferromagnetism. In the absence of external magnetic field, neighboring magnetic moments cancel each other, therefore no magnetization; however, when field is applied, small magnetization appears in the direction of the field. They have positive susceptibility and susceptibility decreases with further increase in temperature, i. e, antiferromagnetism breaks down and material becomes paramagnetic.

1.3.5 Ferrimagnetic Materials

These materials have structures composed of two sub-lattices (A and B) separated by oxygen's. The magnetic moments of one sub-lattice are antiparallel to that of another sub-lattice and are of unequal magnitude resulting in a net spontaneous magnetization similar to ferromagnetic materials (shown in Figure 1.8(c)). With increase in temperature, the spontaneous magnetization decreases and reaches to zero at a particular temperature called Neel temperature (T_N). Ferrimagnetic materials are like ferromagnetic in which they hold spontaneous magnetization below Curie temperature and become paramagnetic above the Curie temperature.

Ferrites are the well known example of ferromagnetic materials. Ferrites are nonconductive ferrimagnetic ceramic compounds obtained from iron oxide such as hematite Fe_2O_3 or magnetite Fe_3O_4 as well as oxides of other metals. Ferrites are hard and brittle like ceramics. Ferrites crystallize into spinel structure (Soohoo 1960, Smit & Wijin 1959), which is named after mineral spinel $MgAl_2O_4$. Unit cell of AB_2O_4 spinel structure is shown in Figure 1.9. Similar to mineral spinel, magnetic spinel have general formula AB_2O_4, where A and B represent various metal cations including iron (Fe). The spinel lattice is composed of closed packed oxygen arrangement in which 32 oxygen ions from a unit cell. Between the layers of oxygen ions, there are interstitial sites that are occupied by the metal ions. In the unit cell of 32 oxygen ions there are 96 interstitial sites having 64 tetrahedral sites (A) and 32 octahedral sites (B). These sites are occupied by metal ions either by +2 and +3 valance. Out of the 64 tetrahedral sites, only 8 are occupied and out of 32 octahedral sites, only 16 are occupied.

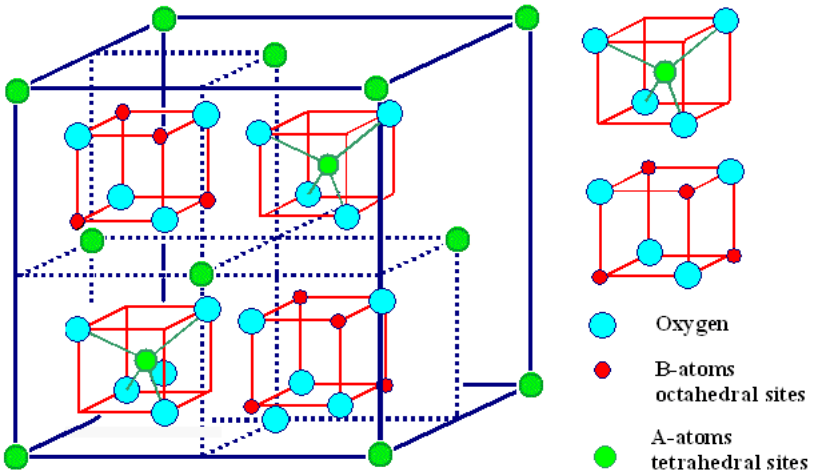

AB_2O_4 spinel The red cubes are also contained in the back half of the unit cell

Figure 1.9 Unit cell of AB_2O_4 Spinel Structure

Depending on the ion position in tetrahedral and octahedral sites, ferrites can be divided into following three categories.

1. Normal Spinel
2. Inverse Spinel
3. Mixed Spinel

Normal Spinel: In Normal spinel ferrites, tetrahedral sites (A-site) are occupied by divalent ions and octahedral sites (B-site) are occupied by trivalent ions. Examples of these ferrites are Zinc Ferrites and Mg-Al ferrites with their formulas are given below: $(Zn^{2+})_A[Fe^{3+}{}_2]_BO_4{}^{2-}$, $(Mg^{2+})_A[Al^{3+}{}_2]_BO_4{}^{2-}$ etc.

Inverse Spinel Structure: The arrangement where divalent metal ions are on the B site (octahedral position) and the trivalent ions are distributed over both A and B site (tetrahedral and octahedral positions) is known as inverse spinel structure. For example: $CoFe_2O_4$ and $NiFe_2O_4$ $(Fe^{2+})_A[Co^{2+}Fe^{3+}]_BO_4{}^{2-}$, $(Fe^{2+})_A[Ni^{2+}Fe^{3+}]_BO_4{}^{2-}$ have inverse spinel structure respectively.

In mixed Ferrites: The arrangement of cations are such that the structure is a combination of both normal and inverse spinel structure, in which divalent ions are distributed partially on both A and B sites. A typical example of mixed ferrite is Nickel Zinc Ferrite having chemical formula $Zn_x\ Ni_{(1-x)}Fe_2O_4$ as $(Zn^{2+}{}_xFe^{3+}{}_{(1-x)})[Ni^{2+}{}_{(1-x)}\ Fe^{3+}{}_{(1-x)}\ ]O^{2-}{}_4$ .In addition to spinal structure, several other structures of ferrimagnetic material such as garnet, hexagonal crystal structure; e.g.: Barium Ferrite ($BaFe_{12}O_{19}$).

The preference of different ions to occupy the two types of sites in the spinel structure is determined by various factors.

1. The ionic radii of the specific ions.
2. The size of interstices
3. Temperature
4. The orbital preference for specific coordination.

1.3.6 Properties of Ferromagnetic/ Ferrimagnetic materials

1.3.6.1 B-H or M-H Hysteresis Loop

Ferromagnetic or ferrimagnetic materials exhibits an important characteristic knows as hysteresis that is usable for memory storage devices. Ferromagnetic material becomes magnetized in the presence of external magnetic field because of alignment of domains in the direction of applied magnetic field. When external magnetic field is removed, domains do not regain their original position and some magnetization is retained by the materials due to hysteresis effect. Typical B–H hysteresis loop is shown in Figure 1.10.

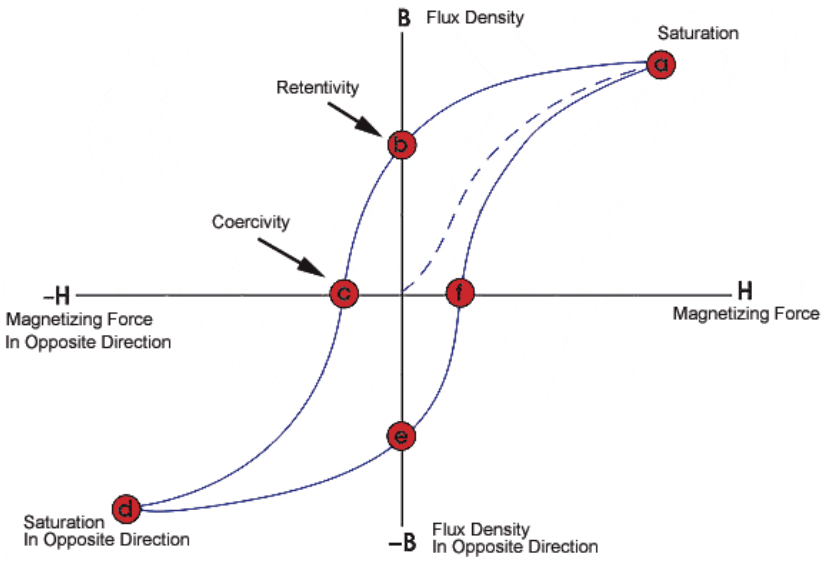

Figure 1.10 M-H/ B-H Hysteresis loop

1.3.6.2 Magnetostriction:

Magnetostriction is just like the electrostriction, property of magnetic materials causing to change their shape and dimension during the process of magnetization. This happens due to spin-orbit lattice coupling. The change in the orbit orientation due to alteration of spin direction causes the change in lattice dimension as shown in Figure 1.11. This effect is known as magnetostriction. The figure shows the magnetostriction effect. The effect was first identified in 1842 by James Joule when observing a sample of iron [40]. Magnetostriction coefficient (λ_m) may be defined as the strain induced by a saturating field. The variation of magnetization of the material by applying magnetic field changes the magnetostrictive strain until it reaches to saturation value (λ). λ_m may be positive or negative. If the field causes the increase in the dimension of the material in the direction of the applied field, then it is taken positive otherwise it is taken as negative. For example: $CoFe_2O_4$ have a magnetostriction coefficient of -110 Parts per million (ppm) while $NiFe_2O_4$ has -26 ppm.

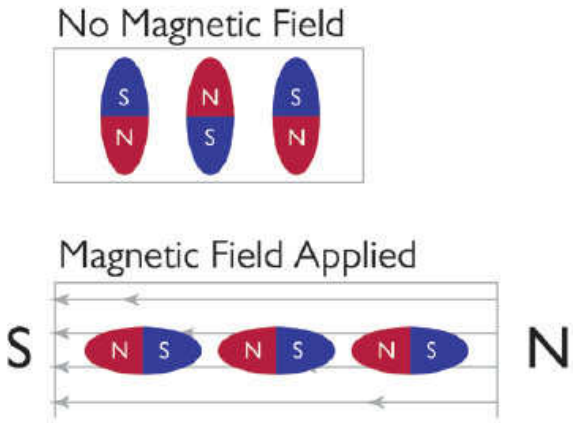

Figure 1.11 Change in lattice dimension in the direction of applied field

1.4 Review- Literature Survey

During last 20-30 years, an enormous research work has been carried out on Multiferroic due to their potential feasibility. A lot of work has been reported on observations and measurements of ME effect in single phase materials [41-50] but all materials exhibited the ME coupling effect at low temperature and weak ME response, because of this it is difficult to use these materials for device applications.

To overcome the limitations of single phase materials, magnetoelectric composites (ME composites) come in to picture. Van Suchtelen in 1972 and other researchers at Philips Laboratories in the Netherlands on the composition of the quinary system Fe–Co–Ti–Ba–O was done first work on ME composites [51-54]. The conceptual points for preparation of good ME composites was given by Boomgard and Born in 1978 [22]. After that a lot of works has been reported on magnetoelectric interaction and their phenomenons. From 2000 onwards, considerable research work has been done on single phase and two phase magnetoelectric materials and reported by number of research groups. The detailed literature survey was collected from internet and INSPEC data base and is summarized in tabular form.

Sr. No.	**Year**	**Authors name**	**Composition studied**	**Properties reported**
1.	1994	M.I. Bichurin et al. [55]	$Y_3Fe_2(FeO_4)_3$-PZT	Comparision of experimental data and theoritocal aspects of magnetoelectric effect.
2.	1997	M.I. Bichurin et al. [56]	Ni-Co Ferrite-PZT	Theortical study on magnetoelectric effect in composites materials.
3.	2000	R.P. Mahajan et al. [57]	$CuFe_2O_4$ - $BaTiO_3$	ε with υ (100Hz-1MHz) and with temperature, α with intensity of magnetic field.
4.	2000	K. Srinivas et al. [58]	$CoFe_2O_4$ – $Pb_{0.96}Sr_{0.04}Ti_{0.47}Zr_{0.53}O_3$	Electromechanical coupling constant
5.	2001	J. Ryu et al. [59]	$CoFe_2O_4$ - $BaTiO_3$	XRD, SEM, ε and tanδ with υ (100Hz-1 MHz) and temperature, α with intensity of magnetic field.

6.	2001	J. Ryu et al. [60]	Laminated composites of PZT and Terfenol-D Disk	magneto-electric voltage coefficient of 4.84V/cm.Oe
7.	2002	M.B. Kothale et al. [61]	$Cu_{0.6}Co_{0.4}Fe_2O_4$ - $Ba_{0.8}Pb_{0.2}TiO_3$	XRD, ε and tanδ with υ (100Hz-1 MHz) and temperature, α with intensity of magnetic field.
8.	2002	Zhi Yu et.al. [62]	$Ni_{0.3}Zn_{0.7}Fe_{2.1}O_3$ - $BaTiO_3$	Maxwell-Wagner polarization
9.	2003	Jun Yi Zhai et al. [63]	$PbZr_{0.57}Ti_{0.43}O_3$ - $CoFe_2O_4$	XRD, ε and tanδ with υ (100Hz-1 MHz), α with intensity of magnetic field.
10.	2003	S.L. Kadam et al. [64]	$Ni_{0.75}Co_{0.25}Fe_2O_4$- $Ba_{0.8}Pb_{0.2}TiO_3$	XRD, ε and tanδ with υ (100Hz-1MHz) and temperature, α with intensity of magnetic field.
11.	2004	B.K. Chougule et al. [65]	$Ni_{0.50}Co_{0.50}Fe_2O_4$ - $Ba_{0.8}Pb_{0.2}TiO_3$	XRD, dc resistivity with temperature and σ_{ac}, α with intensity of magnetic field.
12.	2005	S. Narendra Babu et al. [66]	layered composites of Ni/PZT/Ni and Fe/PZT/Fe.	α with both in the presence of AC and DC magnetic field
13.	2005	B.K. Chougule et al. [67]	$Ni_{0.8}Cu_{0.2}Fe_2O_4$- $Ba_{0.9}Pb_{0.1}Ti_{0.9}Zr_{0.1}O_3$	XRD, ε and tanδ with temperature, α with intensity of magnetic field.
14.	2005	S.R. Kulkarni et al. [68]	$Ni_{0.8}Co_{0.1}Cu_{0.1}Fe_2O_4$- $PbZr_{0.8}Ti_{0.2}O3$	XRD, ε and tanδ with temperature, α with intensity of magnetic field.
15.	2005	G. Srinivasan et al. [69]	$Co_{1-x}Zn_xFe_2O_4$ (CZFO) (x = 0 - 0.6) - PZT	Comparison in ME effect of Laminated and bulk

				composites
16.	2006	Li et al. [70]	Terfenol-D - PZT	α with magnetic field.
17.	2006	N. Ortega et al. [71]	PZT/$CoFe_2O_4$ composite thin films	α was reported by measuring PE hysteresis loops in presence of magnetic field.
18.	2006	R.S. Devan et al. [72]	$BaTiO_3$ - $Ni_{0.92}Co_{0.03}Cu_{0.05}Fe_2O_4$	XRD, dc resistivity and thermo-emf with temperature, σ_{ac} with υ, ε and tanδ with υ, α with intensity of magnetic field.
19.	2006	M.E. Botello et al. [73]	$CuFe_2O_4$ - $BaTiO_3$	XRD, SEM, α with intensity of magnetic field,
20.	2007	Giap.V. Doung et al. [74]	$CoFe_2O_4$ - $BaTiO_3$	XRD, α with intensity of magnetic field
21.	2007	K.K. Patankar et.al. [75]	$Ba_{0.8}Pb_{0.2}TiO_3$ - $CuFe_2O_4$	XRD, SEM, α with intensity of magnetic field, impedence measurement.
22.	2008	P.D. Thang et.al [76]	$CoFe_2O_4$ – PZT nanostructures	decrease in magnetization around the ferroelectric Curie temperature indicates the magnetoelectric coupling between the two phases
23.	2008	B.K. Bammammavar et al. [77]	$Ni_{0.2}Co_{0.8}Fe_2O_4$ - $Ba_{0.8}Pb_{0.2}Zr_{0.8}Ti_{0.2}O_3$	XRD, dc resistivity with temperature, α with intensity of magnetic field, M-H loop
24.	2008	S.R. Kulkarni et al. [78]	$Ni_{0.8}Co_{0.1}Cu_{0.1}Fe_2O_4$ - $PbZr_{0.5}Ti_{0.5}O_3$	XRD, dc resistivity with temperature, α with intensity

				of magnetic field, M-H loop
25.	2008	S.A. Lokare et al. [79]	$BaTiO_3$ - $Ni_{0.92}Co_{0.03}Mn_{0.05}Fe_2O_4$	XRD, dc resistivity with temperature, α with intensity of magnetic field, M-H loop
26.	2008	S.S. Chougule et al. [80]	$Ni_{0.8}Zn_{0.2}Fe_2O_4$ - $PbZr_{0.52}Ti_{0.48}O_3$	XRD, ε and tanδ with υ (100Hz-1 MHz) and temperature, α with intensity of magnetic field.
27.	2008	J.A.Matutes-Aquino. et al. [81]	$NiFe_2O_4$- $BaTiO_3$	XRD, P-E, M-H, M-T, α with magnetic field at room temperature, d_{33}.
28.	2008	S.G. Lu et al. [82]	$CoFe_2O_4$ - PZT	ε and tanδ with υ (100Hz-1 MHz) and temperature, α with intensity of magnetic field. Piezoelectric coefficient and maximum ME coefficient was observed for 0.9PZT-0.1CFO composite. They also reported that the ME coefficient was linearly increased with AC frequency upto 100 kHz.
29.	2008	R.A. Islam et al. [83]	$PbZr_{0.52}Ti_{0.48}O_3$ – $Ni_{(1-x)}Zn_x Fe_2O_4$.	The doping of PZN in PZT affects the resistivity and magnetoelectric coupling of the composite. They reported the maximum

				coefficient 187mV/cm.Oe was observed for 0.85PZT-0.15PZN and NZF composite
30.	2009	B.K. Chougule et al. [84]	$Co_{0.9}Cd_{0.1}Fe_2O_4$ - PZT	XRD, SEM, ε and tanδ with υ (100Hz-1 MHz) and temperature, ac conductivity, dc resistivity, α with magnetic field,
31.	2009	C.M. Kanamadi et al. [85]	$CoFe_2O_4$ and strontium doped $BaTiO_3$	XRD, SEM, ε and tanδ with υ (100Hz-1 MHz) and temperature, α with magnetic field
32.	2009	B.K. Bammannavar et al. [86]	$Ni_{0.2}Co_{0.8}Fe_2O_4$ + $PbZr_{0.8}Ti_{0.2}O_3$	Magnetic properties, magnetoelectric effect,
33.	2009	B.K. Bammammavar et al. [87]	$Ni_{0.2}Co_{0.8}Fe_2O_4$ - $Ba_{0.8}Pb_{0.2}Zr_{0.8}Ti_{0.2}O_3$	XRD, dc resistivity, α with magnetic field.
34.	2009	M.Venkata Ramanaa et al. [88]	$Ni_{0.8}Co_{0.1}Cu_{0.1}Fe_2O_4$ - $PbZr_{0.5}Ti_{0.5}O_3$	XRD, ε and tanδ with υ (100Hz-1 MHz) and temperature. dc resistivity, d_{33}, α with intensity of magnetic field.
35.	2009	Xiaobo Wu et al. [89]	$CuFe_2O_4$-$PbZr_{0.52}Ti_{0.48}O_3$	XRD, SPM, tanδ with temperature, α with intensity of magnetic field, MH loop, P-E Hysteresis loop.
36.	2009	C.M. Kanamadi et al. [90]	$Ni_{0.8}Cu_{0.2}Fe_2O_4$ - $Ba_{0.8}Pb_{0.2}Ti_{0.8}Zr_{0.2}O_3$	AC conductivity and DC conductivity, α with magnetic field at room temp.

37.	2010	C. Miclea et al. [91]	$CoFe_2O_4$ - PZT	XRD, SPM, tanδ with temperature, α with intensity of magnetic field, MH loop, P-E Hysteresis loop.
38.	2010	R.Rani et al. [92]	Ni-$ZnFe_2O_4$ - BST	XRD, SPM, tanδ with temperature, α with intensity of magnetic field, MH loop, P-E Hysteresis loop.
39.	2010	Abdul Samee Fawzi et al. [93]	$Ni_{0.8}Zn_{0.2}Fe_2O_4$ - $Pb_{0.93}La_{0.07}(Zr_{0.60}Ti_{0.4})O_3$	XRD, dielectric properties, P-E, M-H, α with magnetic field at room temp.
40.	2010	A. Gupta et al. [94]	$(x)PbZr_{0.52}Ti_{0.48}O_3-(1-x)Mn_{0.3}Co_{0.6}Zn_{0.4}Fe_{1.7}O_4$	XRD, ε and tanδ with υ (100Hz-1 MHz) and temperature, dc resistivity, α with intensity of magnetic field.
41.	2010	J. Kulawik et al. [95]	$CoFe_2O_4-Pb(Fe_{1/2}Ta_{1/2})O_3$	XRD, SEM, ε and tanδ with υ (100Hz-1 MHz) and temperature, dc resistivity,
42.	2011	X. Chao et al. [96]	$Pb[Zr_{0.23}Ti_{0.36}+0.02(Mg_{1/2}W_{1/2})+0.39(Ni_{1/3}Nb_{2/3})]O_3$ and $Ni_{0.8}Co_{0.1}Cu_{0.1}Fe_2O_4$	XRD, ε and tanδ with υ (100Hz-1 MHz) and temperature, dc resistivity, α with intensity of magnetic field
43.	2011	Hong-fang Zhanga et al. [97]	$Pb(Zr_{0.53}Ti_{0.47})O_3$ - $(Ni_{0.5}Zn_{0.5})Fe_2O_4$	P-E, M-H, α with magnetic field at room temp.
44.	2011	L.M Harib et al. [98]	$CoMn_{0.2}Fe_{0.8}O_4$ - $BaTiO_3$	XRD, SEM, ε and tanδ with υ (100Hz-1 MHz) and temperature, α with dc magnetic field.

45.	2011	Ying Pie et al. [99]	$CoFe_2O_4$ - $Pb(Mg_{1/3}Nb_{2/3})_{0.67}Ti_{0.33}O_3$	XRD, SEM, ε and tanδ with υ (100Hz-1 MHz)and temperature, α with dc magnetic field
46.	2011	Subhasis Roy et al. [100]	$Pb_{0.85}La_{0.15}TiO_3$- $CoFe_2O_4$	XRD, SEM, P-E loop, M-H loop at room temp, ε and tanδ with temperature.
47.	2011	Jiangli Chen et al. [101]	$Ni_{0.93}Co_{0.02}Cu_{0.05}Fe_2O_4$ - $PbZrTiO_3$	XRD, ε and tanδ with υ (100Hz-1 MHz) and temperature, d_{33}, α with dc magnetic field
48.	2012	Sarmistha Basu et al. [102]	$Pb(Zr_{0.53}Ti_{0.47})O_3$- $CoFe_2O_4$	XRD, SEM, ε and tanδ with υ (100Hz-1 MHz) and temperature,ac conductivity.

1.5 Selection of individual phases

As there are a number of ferroelectric and ferrite materials, our first aim is to select a desired composition of ferrite phase and ferroelectric phase that shows novel ferroelectric and ferromagnetic properties and possess good ME effect.

The solid solution of ferroelectric lead titanate ($PbTiO_3$) and antiferroelectric lead zirconate ($PbZrO_3$), known as PZT, with varying Zr/Ti ratio near MPB (PZT : 55:45), exhibits significant behavior [103-106] due to higher resistivity, stronger dielectric and ferroelectric properties, easier to pole, high piezoelectric coefficient, higher electromechanical coupling coefficients as compared to other ferroelectrics. Sm, La, Ca and Ba are well known substituents for PZT ferroelectric ceramics to modify them for desired properties [107-111]. It has been found that La^{+3} substitutions in PZT increases the electrical resistivity and increases the piezoelectric effect. This substituent in PZT results in high dielectric constants, enhanced coupling factors, high remnant polarization and square hysteresis loops [112-113]. $CoFe_2O_4$ is chosen as ferrite phase having high electrical resistivity, low eddy current losses and high magnetocrysatalline anisotropy [114].

From above literature review it was found that a lot of work was done on the PZT-$CoFe_2O_4$ magnetoelectric composites. No study was done on PZT (55:45) - $CoFe_2O_4$ and modified PZT (55:45) - $CoFe_2O_4$ composites. This proposal is an attempt to study and understand the novelty in the CFO-PZT based magneto electric composites and characterize them.

1.6 Objectives of the Present Work

Our aim is to prepare and characterize the ferrite-ferroelectric composites by conventional solid state reaction method. Solid state reaction method is the cheapest, simplest and conventional way to synthesize bulk samples.

The main objectives are as follows:

1. Preparation & optimization of process parameters of PZT- $CoFe_2O_4$ magnetoelectric composites.
2. To investigate the effect of substitution on PZT- $CoFe_2O_4$ composites.
3. To characterize the materials for structural, micro structural, electrical and magnetic properties.

In order to fulfill the objectives of the proposed work, the following ceramic compositional series were synthesized and characterized:

Series I (x) $CoFe_2O_4$ – (1-x) $PbZr_{0.55}Ti_{0.45}O_3$ (x = 0 - 0.15 in step of 0.05)

Series II (x) $Co_{0.8}Ni_{0.2}Fe_2O_4$ – (1-x) $PbZr_{0.55}Ti_{0.45}O_3$ (x = 0 - 0.15 in step of 0.05)

Series III

Series A $P_{(1-3y/2)}La_yZr_{0.55}Ti_{0.45}O_3$ (x = 0 - 0.0075 in step of 0.0025)

Series B (x) $Co_{0.8}Ni_{0.2}Fe_2O_4$ - (1-x) $Pb_{0.99625}La_{0.0025}Zr_{0.55}Ti_{0.45}O_3$ (x = 0 - 0.15 in step of 0.05)

Series C (x) $Co_{0.8}Ni_{0.2}Fe_2O_4$ - (1-x) $Pb_{0.9925}La_{0.005}Zr_{0.55}Ti_{0.45}O_3$ (x = 0 - 0.15 in step of 0.05)

Series D (x) $Co_{0.8}Ni_{0.2}Fe_2O_4$ - (1-x) $Pb_{0.9887}La_{0.0075}Zr_{0.55}Ti_{0.45}O_3$ (x = 0 - 0.15 in step of 0.05)

The structural properties using XRD and SEM, the dielectric properties as a function of temperature and frequency, piezoelectric and ferroelectric properties were studied. Magnetic properties using VSM and Magnetoelectric properties were studied.

References

1. R. Grossinger, G.V. Doung and R. S. Sato- Turtelli, J. Magn. Magn. Mater., **320** (2008) 1972.

2. W. Errenstein, N. D. Mathur, and J. F. Scott, Nature, **442** (2006) 759.

3. C.W. Nan, M.I. Bichurin, S. Dong, D. Viehland and G. Shrinivasan, J. Appl. Phys., **103** (2008) 031101.

4. W. C. Rontgen, Ann. Phys. Chem., **35** (1888) 264.

5. H. Schmid, Ferroelectrics., **162** (1994) 317.

6. D. N. Astrov, Soviet Physics-JETP, **11** (1960) 708.

7. R. M. Hornriech, J. Appl. Phys., **41** (1970) 950.

8. V. J. Folen, G.T. Rado and E. W. Stalder, Phys. Rev. Lett., **6** (1961) 607.

9. S. Foner and M. Hanabusa, J. Appl. Phys., **34** (1964) 1246.

10. R. M. Hornriech, Gordon and Breach Science, New York, USA, 1975.

11. T. J. Martin and J. C. Anderson, Phys. Lett., **11** (1964) 109.

12. N. Pavan Kumar and P. Venugopal Reddy, Mater. Lett., **122** (2014) 292.

13. N. Hill, J. Phys. Chem. B., **104** (2000) 6694.

14. A.M.J.G. Run, D.R. Terrell and J.H. Scholling, J. Mater. Sci., **9** (1974) 1710.

15. J.V. Boomgaard and R.A.J. Born, J. Mater. Sci., **13** (1978) 1538.

16. S.X. Dong, J.F. Li and D. Viehland, J. Appl. Phys., **95** (2004) 2625.

17. F. Cebollada, J.M. Gonzalez, J. de Frutos and A.M. Gonzalez, Bol. Soc. Esp. Ceram. Vidrio **44** (2005) 169.

18. S. Priya and D.J. Inman, Energy Harvesting Technologies, LLC (2009).

19. N. A. Spaldin and M. Fiebig, The Renaissance of Magnetoelectric Multiferroics. Science, **309**, (2005) 391.

20. S. Dong, J.F. Li, D. Viehland, J. Cheng and L.E. Cross, Appl. Phys. Lett., **85** (2004) 3534.

21. J. Rhu, A. V. Carazo, K. Uchino and H. Kim, Jpn. J. Appl. Phys., **40** (2001) 4948.

22. J. Van. Boomgaard and R.A. Born, J. Mater. Sci., **13** (1978) 1538.

23. B. Jaffe, W.R. Cook and H. Jafee, "*Piezoelectric Ceramic*", Ch. 1. Academic Press London 1971.

24. W.G. Cady, Piezoelectricity, McGraw Hill, New York, Revised Edition by Dover Publications, New York (1964).

25. J. Valasek, Ferroelectrics, **2** (1971) 239.

26. J. Fousak, Proceedings of ISAF'9, University Park, PA (1994).

27. M.E. Lines and A.M.Glass, *Principles and applications of ferroelectrics and related materials,* Oxford university press, New York, 2001.

28. G. Busch, Ferroelectrics, **74** (1987) 267.

29. W. Kanzig, Ferroelectrics, **74** (1987) 285.

30. L.E. Cross and R.E. Newnham, History of Ferroelectrics, Am. Ceram. Soc., Westerville, OH (1986).

31. G. Busch, Ferroelectrics, **71** (1987) 43.

32. R. E. Nettleton, Ferroelectrics, **1, 3, 87, 93, 121, 127, 221** (1970).

33. R. E. Nettleton, Ferroelectrics, **2, 5, 77, 93** (1971).

34. A. Safari, R. K. Panda, and V. F. Janas, Key Eng. Mater. **35** (1996) 122.

35. D. Damjanovic, Rep. Prog. Phys., **61** (1998) 1267.

36. B.T. Batthais and A.Von. Hippel, Phy. Rev., **73** (1998) 1378.

37. R. Ramesh, S. Aggarwal and O. Auciello, Mater. Sci. Engg. B., **32** (2001) 191.

38. B. Jaffe, W. Cook and H. Jaffe, Piezoelectric Ceramics, Academic Press, London (1971).

39. P. R. Chowdhary and S. B. Deshpande, Ind. J. Pure. Appl. Phys., **17** (1979) 571.

40. J. P Joules, " On the effects of Magnetism upon the dimensions of iron and steel bars"

41. R. M. Hornreich, Solid State Commun., **7** (1969)1081.

42. R. M. Hornreich, J. App. Phys., **41**(1970) 950.

43. E. Fischer, G. Gorodetsky and R. M. Hornreich, Solid State Commun., **10** (1972) 1127.

44. S. Foner and M. Hanabusa, J. Appl. Phys., **34** (1963) 1246.

45. L. M. Holmes, L. G. Van Uitert, and G.W. Hull, Solid State Commun., **9** (1971) 1373.

46. R. M. Hornreich, IEEE Transactions on Magn. **8** (1972) 584.

47. S. R. Das, R. N. P. Choudhary, P. Bhattacharya, R. S. Katiyar, P. Dutta, A. Manivannan and M. S. Seehra, J. Appl. Phys., **101** (2007) 034104.

48. R. Hornreich and S. Shtrikman, Phys. Rev., **161** (1967) 506.

49. T. J. Martin and J. C. Anderson, IEEE Transactions on Magn., **2** (1966) 446.

50. M. Mercier, in Proceedings of the Symposium on Magnetoelectric Interaction Phenomena in Crystals, Seattle, Wash, USA (1973).

51. J. Van Suchtelen, Philips Research Report, **27** (1972) 28.

52. J. Van Den Boomgaard, A. M. J. G. van Run, and J. Van Suchtelen, Ferroelectrics, **10** (1976) 295.

53. J. Van Den Boomgaard, D. R. Terrell, R. A. J. Born, and H. F. J. I. Giller, J. Mater. Sci., **9** (1974) 1705.

54. A. M. J. G. Van Run, D. R. Terrell, and J. H. Scholing, J. Mater. Sci., **9** (1974) 1710.

55. M. I. Bichurin and V. M. Petrov, Ferroelectrics, **162** (1994) 33.

56. M. I. Bichurin, **161** (1994) 53.

57. K. K. Patankar, S. A. Patil, K. V. Sivakumar, R. P. Mahajan, Y. D. Kolekar and M. B. Kothale, Mat. Chem. Phys., **65** (2000) 97.

58. K. Srinivas, G. Prasad, T. Bhimashankaram and S. V. Suryanaryana, Mod. Phys. Lett. B., **14** (2000) 663.

59. J. Ryu, A.V. Carazo, K. Uchino and H. E. Kim, J. Electroceram., 7 (2001) 17.

60. J. Ryu, A.V. Carazo, K. Uchino and H. E. Kim, J. Electroceram., 40 (2001) 4948.

61. M. B. Kothale, K. K. Patankar, V. L. Mathe and B. K. Chougule, Mat. Chem. Phys., 77 (2002) 691.

62. Z. Yui and C. Ang, J. Appl. Phys. **91** (2002) 794.

63. J. Y. Zhai, N. Cai, L. Liu, Y. H. Lin and C. W. Nan, Mat. Sci. Eng. B **99** (2003) 329.

64. S. R. Kulkarni, C. M. Kanamadi and B. K. Chougule, Mat. Res. Bull.**40** (2005) 2064.

65. S. L. Kadam, K. K. Patankar, V. L. Mathe, M. B. Kothale, R. B. Kale and B. K. Chougule, Mater. Chem. Phys., 78 (2003) 684.

66. S. N. Babu, T. Bhimasankaram and S. V. Suryanarayana, Bull. Mater. Sci., **28** (2005) 419.

67. B. K. Chougule, C. M. Kanamadi and L. B. Pujari, J. Mag. Mater., **295** (2005) 139.

68. S. R. Kulkarni, B. K. Chougule and C. M. Kanamadi, Mater. Res. Bull., **40** (2005) 2064.

69. G. Srinivasan, R. Hayes and C.P. Devreugd, Appl. Phys. A., **80** (2005) 891.

70. T. Li, S.W. Or, H. Lai and W. Chan, J. Magn. Magn. Mater., **304** (2006) e442.

71. N. Ortega, P. Bhattacharya and R. S. Katiyar, J. Appl. Phys., **100** (2006) 126105.

72. R. S. Devan, S. A. Lokare, B. K. Chougule, S. S. Chougule and Y. D. Kolekar, J. Phys. Chem., **67** (2006) 1524.

73. M. E. Botello -Zubiate, D. Bueno- Baques, J. de. Frutos V Aquerizo, L.E. Fuentes Cobas and J. A. Matutes- Aquino, Ferroelectrics, **338** (2006) 247.

74. Giap V. Duong and R. Groessinger, J. Mag. Mat., **316** (2007) 624.

75. K. K. Patankar, S. A. Kanade, D. S. Padalkar and B. K. Chougule, Phys. Lett. A **361** (2007) 472.

76. P. D. Thang, M. T.N. Pham, G. Rijnders, D. H. A Blank, N. H. Duc, J. C. P Klaasse and E. Bruck, J. Korean. Phys. Soc. **52** (2008) 1406**.**

77. B. K. Bammannavar, L. R. Naik, R. B. Pujar and B. K. Chougule, J. Alloys. Compd., **477** (2008) 24.

78. S. R. Kulkarni, R. S. Devan and B. K. Chougule, J. Alloys Compd. **455** (2008) 336.

79. S. A. Lokare, R. S. Devan and B. K. Chougule, J. Alloys Compd. **454** (2008) 471.

80. S. S. Chougule and B. K. Chougule, Mater. Chem. Phys., **108** (2008) 408.

81. J. A. Matutes-Aqiuno, M. E. Botello-Zubiate, V. Corral-Flores, J. de Frutos, F. Cebollaba, E. Menendez, F. J. Junenez and A. M. Gonzalez, Integr. Ferrolectr., **101** (2008) 22

82. S.G. Lu, Z.K. Xu, Y.P Wang, S.S. Guo, H. Chen, T.L. Li and S.W. Or, J. Electroceram., **21** (2008) 398.

83. R. A. Islam, D. Viehland and S. Priya, J. Mater. Sci., **43** (2008) 1497.

84. B. K. Chougule, Y. B. Kambale and S. S. Chougule, J. Alloys Compd. **476** (2009) 733.

85. C. M. Kanamadi, B. K. Das, C. W. Kim, D. I. Kang, H. G. Cha, E.S. Ji, A. P. Jadhav, B-Eog Jun, J. H. Jeong, B. Chun, Choi, B. K. Chougule and Y. S. Kong, Mater. Chem. Phys., **116** (2009) 6.

86. B. K. Bammannavar, G. N. Chavan, L. R. Naik and B. K. Chougule, Mater. Chem. Phys., **117** (2009) 46.

87. B. K. Bammannavar, L. R. Naik, R. B. Pujar and B. K. Chougule, J. Alloys Compd., **477** (2009) 4.

88. M. V. Ramanna, N. R. Reddy, G. Shreenivasulu, K. V. Shiva Kumar, B.S. Murty and V.R.K. Murthy, Current Appl. Phys., **9** (2009) 1134.

89. X. Wu, W. Cai, Y. Kan, P. Yang, Y. Lui, H. Bo, X. Lu and J. Zhu, Ferroelectrics., **380** (2009) 48.

90. C. M. Kanamadi, G. Seeta Rama Raju, H. K. Yang, B. C. Choi and J. H. Jeong, J. Alloys Compd., **479** (2009) 807.

91. C. Miclea, C. Tanasoiu, L. Amarande, C.F. Miclea, C. Plavitu, M. Cioangher, L. Tripuna, C.T. Miclea, T. Tanasoiu, M. Susu, I. Voicu, V. Malczanek, A. Ivanov and C. David., J. Optelect. Ad. Mater., **12** (2010) 272.

92. R. Rani, P. Kumar, S. Singh, J.K. Juneja, K.K. Raina, R.K. Kotnala and C. Prakash, Integr. Ferroelectr., 122 (2010) 38.

93. A.S. Fawzi, A.D. Shiekh and V.L. Mathe, Mater. Res. Bull., **45** (2010) 1000.

94. A. Gupta and R. Chatterjee, J. Magn. Magn. Mater., **322** (2010) 1020.

95. J. Kulawik, P. Guzdek, D. Szwagierczak and A. Stoch, Compos. Struct., **92** (2010) 2153.

96. X. Chao, Z. Yang, M. Dong and Y. Zhang, J. Magn. Magn. Mater., **323** (2011) 2012.

97. H.F. Zhang, S. W. Or and H.L. Wa.Chan, J. Alloys Compd., **509** (2011) 6311.

98. L.M. Harib and O.F. Katun, J. Alloys Compd. **509** (2011) 6644.

99. Y. Pei, Q. Li, W. Shi, B. Zhang, Q. Chen, X. Yue, D. Xiao and J. Zhu, Ferroelectrics, **410** (2011) 82.

100. S. Roy and S.B. Mujumdar, Phys. Lett. A., **375** (2011) 1538.

101. J. Chen, Z. Xu and X. Lu, Ferroelectrics, **410** (2011) 29

102. S. Basu, K. Ramesh Babu and R.N.P Choudhary, Mater. Chem. Phys., **132** (2012) 570.

103. B. Noheda, J. A. Gonzalo, L.E. Cross, R. Guo, S-E park, D.E. Cox, G. Shirane, Phys. Rev. B., **61** (2000) 8687.

104. O.P. Thakur and Chandra Prakash, Integr. Ferroelectr., **122** (2010) 100.

105. J.K. Juneja, Chandra Prakash, O.P. Thakur and T.P. Sharma, Ferroelectric Lett., **29** (2002)

106. R. Guo. L.E Cross, S.E. Park, B. Noheda, D.E. Cox, G. Shirane, Phys. Rev. Lett., **84** (2000) 5423.

107. G.H. Haretling, C.E. Land, J. Am. Ceram. Soc., **54** (1971) 1.

108. Chandra Prakash, O.P. Thakur and P. Kishan, Ferroelectrics, **263** (2001) 61.

109. S.K. Pandey, O.P. Thakur, A. Goyal, D.S. Rawal, Chandra Prakash. R. Chatterjee and T.C. Goyal, Mod. Phys. Lett. B **20** (2006) 1883.

110. K. Kakegawa, K. Arai, Y. Sasaki and Y. Tomizawa, J. Am. Ceram. Soc.**71** (1988) 49.

111. Y. Tomita, K. Lijima, R. Takayama and I. Ueda, J. Appl. Phys.**60** (1986)361.

112. M. Okyama and Y. Hamakawa, Ferroelectrics, **63** (1985) 243.

113. M. Einat, D. Shur, E. Jerby and G. Roseman, J. Appl. Phys. **89** (2001) 548.

114. A. Gupta and R. Chatterjee, J. Euro. Ceram. Soc., **33** (2013) 1017.

Chapter – 2

Material Synthesis And Characterization Techniques

Chapter – II

Material Synthesis and Characterization Techniques

Sample preparation methodology and their characterization techniques for magnetoelectric composites (Ferrite- Ferroelectric) are described in this chapter. The performance of ME composites depends on the processing methodology therefore, it is necessary to understand the various processing methods for sample preparation. Here, processing of samples using conventional solid state reaction method is described in detail. The details of characterization techniques such as structural, electrical, ferroelectric, piezoelectric and magnetic properties used for this study of various properties of samples are discussed here.

2.1 Material Synthesis

The method of synthesis and various processing parameters plays a key role to attain desired properties. Different processing techniques have been developed to synthesize the ceramics, conventional solid state route, co-precipitation, sol-gel processing, hydrothermal synthesis, spray and freeze drying [1-4] etc. In the present study, conventional solid state reaction route was opted for synthesis of magnetoelectric composites and their constituent phases such as ferrite and ferroelectric. This method is better to fabricate bulk samples due to their cost effectiveness, ease of fabrication and better control of processing parameters. The steps used in the processing of ferroelectric, ferrite and composites of the above mentioned process are given in Figure 2.1 (a) and 2.1 (b) respectively.

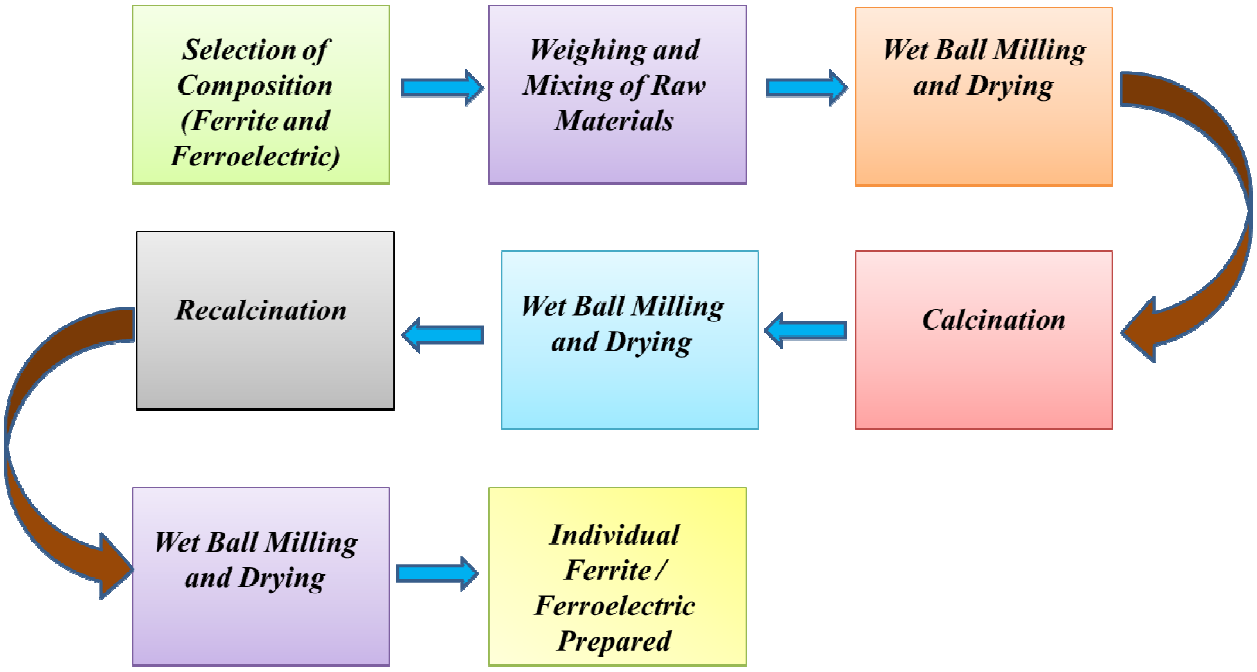

Figure 2.1 (a) Synthesis and Processing Steps for Ferroelectric/Ferrite Phase.

Synthesis of Composites

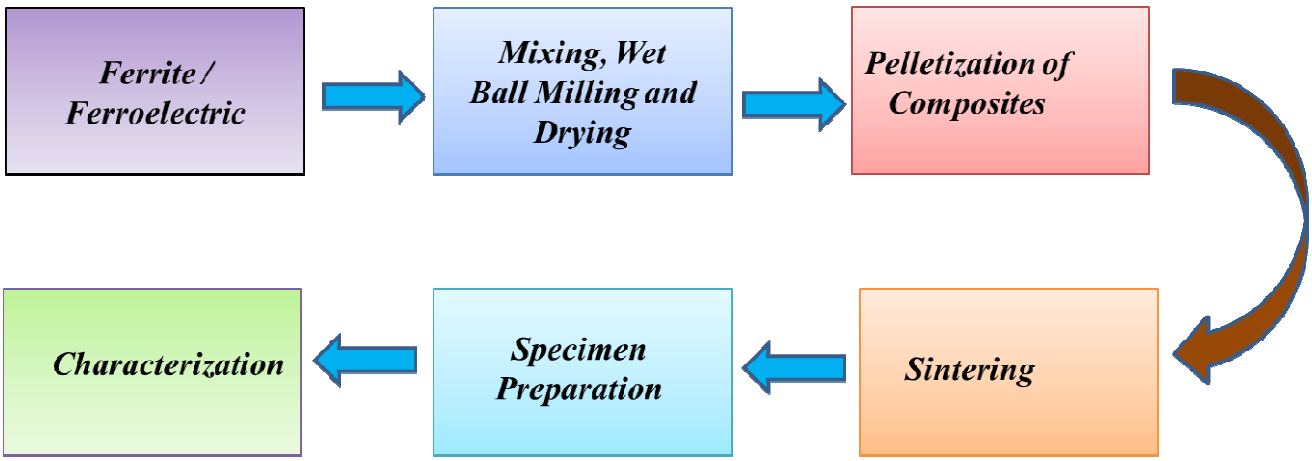

Figure 2.1 (b) Synthesis and Processing Steps for Composites.

2.1.1 Raw Materials and Ball Milling

Weighing of raw material is the first step of material synthesis. In the solid state method, the raw material is weighed according to the stoichiometry of the compound. Firstly, raw materials are mixed mechanically using pestle mortar to get the homogenous mixture. After that, mixing is done by Ball milling. Figure 2.2 shows the processing of planetary ball milling. The ball mill consists of grinding bowls and rotating plate. The direction of movement of the plate is opposite to that of the bowls. The centrifugal forces, created by the rotation of the bowl around its own axis together with the rotation of the rotating plate, are applied to the powder mixture and milling balls in the grinding bowl. The difference in the speeds of the grinding balls and bowl releases high dynamic energies resulting in better homogeneity and fine particle size of the mixture. The ball milling process helps in reducing particle size (1-10 µm) and eliminating aggregates by means of mechanical force. Distilled water (non-toxic, inflammable) is used as ball milling media and hard zirconia balls are used as grinding medium. Water reduces the heat produces by frictional force of zirconia balls.

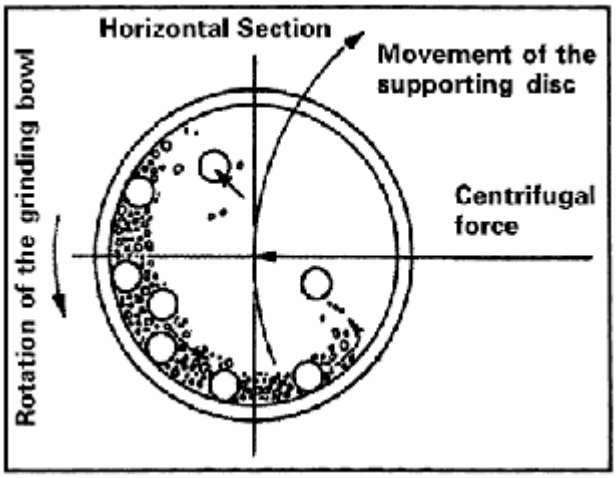

Figure 2.2 Processing of Powder in Planetary Ball Mill

The raw materials used for the present work were PbO, ZrO_2, TiO_2 , La_2O_3, for modified ferroelectric phase and $Co(CO_3)$ (Cobaltus Carbonate), NiO, Fe_2O_3 for modified ferrimagnetic phase and all were analytical grade (AR grade, 99.9 % Purity). The ball mill used in the present work with its various specifications is shown in Figure 2.3. These starting raw materials were weighed in desired stoichiometric ratio and ball milled in the planetary ball mill. High density zirconia balls and distilled water were used as milling media. The ball milling was done for 3 hrs for all the samples. The wet slurry was then kept in an oven at 120^oC for drying purpose.

Specifications:

- Type: Mini Ball Mill (Two Bowls)
- Purpose: For grinding raw materials for synthesis of ceramics
- Plate speed: 40 to 500 r.p.m.
- Bowl speed: Maximum 1000 r.p.m.

Figure 2.3 Planetary Ball Mill for Mixing Purpose

2.1.2 Calcination

Raw materials for the compound formation were in the form of oxides or carbonates. But oxides and carbonates do not react at room temperature so for a reaction to occur, preheat treatment of raw materials in the presence of air or oxygen is required. This preheating process is known as Calcination. Calcination causes the interaction of constituents by interdiffusion of their ions. This process reduces the extent of diffusion that must occur during sintering and results in homogenous body, hence it can be considered as a part of the mixing process. Calcination is done at a temperature lower by 200 – 300^{o}C than final sintering temperature.

For the present study, both Ferroelectric and ferrimagnetic powder mixture were calcined in alumina crucible in a programmable furnace with heating rate of 5^{o}/minute. The programmable furnace used in the present work with its specifications is shown in Figure 2.4. Calcination and recalcination temperature of ferroelectric phase were 800^{o}C and 850^{o}C for 4 hrs and for ferrimagnetic phase, the calcination and recalcination temperature were 900^{o}C and 950^{o}C for 4 hours.

Specifications:

- Heating elements: Silicon carbide
- Working area (inside heating zone): 12" Depth x 6" Height x 6" Width
- Maximum operating temperature:1550^{o}C
- Thermocouple used: R-type
- Accuracy: ±1 ^{o}C
- Heating rate and soaking period are programmable

Figure 2.4 Programmable Furnace used for Calcination

2.1.3 Shaping

The dried powder (individual ferroelectric, ferrite and mixture of both) obtained after ball milling and drying requires a particular shape. There are a number of molding methods which include Uniaxial Pressing, Isostatic Pressing, Extrusion, Injection molding, Tape Casting, Slip Casting, Gel Casting [5].

For shaping, firstly we have to increase the strength of powder sample. Now to increase the strength of powder, an organic binder is added to the powder before compaction. For the present work, dilute solution of polyvinyl alcohol (PVA) was used as a binder. Added binder should be such that it would be able to remove it from the compacted shapes without any disruptive effect.

The dried powder was mixed with a few drops of diluted polyvinyl alcohol (PVA) binder (3% by weight). The Uniaxial pressing method was used for shaping the powder into green body. The hydraulic press used in the present work with its various specifications is shown in Figure 2.5. The dimensions of the pressed circular discs were 15 mm diameter and 1-2 mm thickness after applying the pressure of 10 Ton (200 kg/cm^2) for 2 min.

Specification:

- Maximum Pressure -10 Ton
- Dies are available for pressing circular discs of various sizes and ring shape

Figure 2.5 Hydraulic Press for shaping purpose

2.1.4 Sintering

Sintering is the heat treatment process by which the green body is transformed to a strong, dense body. Driving forces and atomic mechanism is responsible for solid state sintering. Due to driving force, there is reduction in the excess energy associated with the surfaces. This may be occurring either by coarsening or by densification. Reduction of total surface area by an increase in the average size of the particle is responsible for the occurrence of coarsening or by eliminating solid/ vapour interfaces and creation of grain growth leads to densification. Sintering temperature, heating/cooling rate and soaking time does have considerable effect on the density and properties of the material. In sintering at appropriate temperature, the atomic motion is more violent and the area between grains in contact increases due to the thermal expansion and finally only one interface between two grains remains. This corresponds to a state with much lower surface energy. In this state, the atoms on the grain surfaces are affected by neighboring atoms in all directions, which results in densified ceramic [6]. During grinding and shaping process, internal strains in the form of lattice distortion exist in the grains. The lattice distortion and internal stress are reduced by atomic diffusion. The changes, which occur due to grain growth and secondary recrystallizations, are related to the grain size and shape. Grain growth is a process where the average grain size (which can be strain-free or nearly strain free) in the material increases continuously during the heat treatment without change in grain size distribution. As average grain size increases, some grains must shrink and disappear. Then the driving force for the process is the difference between the fine-grained and larger grain size product resulting from grain boundary area and the total boundary energy. Secondary recrystallizations is the process in which some large grains get nucleated which grow at the expense of fine-grained but essentially strain free matrix. These occur when the continuous grain growth is inhibited by the presence of some impurities or pores. This commonly happens in the case of oxides, titanates and ferrites ceramics. The free energy changes by the elimination of the solid vapor interfaces. This takes place with the coincidental formation of new but lower energy solid interfaces. On a microscopic scale, material transfer is affected by the pressure difference and the change in free energy across a curved surface. Higher sintering temperature and larger soaking time would result in larger grains resulting in highly dense ceramics [7]. There are many factors that affect the sintering process; some of them are:

- Time and temperature
- Composition
- Geometrical structure
- Density

2.1.4.1 Conventional Sintering

In conventional sintering, energy is transferred to the material from the surface of the material through conduction, convection and radiation process. In the present work, the green bodies were placed in closed alumina crucible for lead based samples; extra lead was taken to compensate the lead loss during sintering. The pallets were sintered at suitable temperatures according to composition of the samples (ferroelectric, ferrite and composite) in a programmable furnace with silicon carbide heating elements (Figure 2.6). The heating rate was kept at 5 ^{o}C/min and soaking period of 4 hrs.

Specification:

- Heating elements : Silicon Carbide
- The working area (inside heating zone) : 12″ Depth × 6″ Height × 6″ Width
- Maximum operating temperature: 1550 ^{o}C.
- Thermocouple Used: R-type thermocouple.
- Heating rate and soaking time are programmable
- Temperature accuracy: ± 1 ^{o}C

Figure 2.6 Programmable high temperature furnace for sintering with its specification

2.2 Characterizations

The samples prepared by solid state method were studied for various properties such as structural (XRD and SEM), dielectric, ferroelectric, piezoelectric, ferromagnetic and magnetoelectric properties. The various techniques used for different characterizations for the present work are discussed here below.

2.2.1 Density

For bulk samples, experimental density was measured by the method based on Archimedes's Principle. Density measurement setup based on Archimedes Principle is shown in Figure. 2.7. The ratio of W_a and the difference between W_a and W_w gives the experimental density of sintered samples as given in equation 2.1.

$$d_{exp} = \frac{W_a}{W_a - W_w} \times d_w \qquad \text{……2.1}$$

In this equation, W_a is weight of the sample and W_w is weight of the sample taken in water. dw is water density taken at room temperature (which is 1.00 gm/cc).

Theoretical density d_{th} (gm/cc) was calculated using lattice parameters (for both phases individually) using the relation

$$d_{th} = (1 - x)d_{th}(\text{Ferroelectric}) + x\, d_{th}(\text{Ferrite}) \qquad \text{..……..2.2}$$

Where x is the concentration of ferrite phase. d_{th} (ferroelectric) and d_{th} (ferrite) are the theoretical densities of ferroelectric and ferrite phase respectively [9].

$$d_{th} = \frac{Z \times M}{N a^3} \qquad \text{…… 2.3}$$

Where Z is the number of molecules per unit cell and its value is different for both phases (ferroelectric and ferrite phases)

Z = 8 for ferrite phase and

Z = 1 for ferroelectric phase

M is the molecular weight, N is the Avogadro's number (6.023×10^{23}) and $V = a^3$ is the volume of the unit cell.

Relative density (%) was calculated by

$$d_{rel} = \frac{d_{exp}}{d_{th}} \times 100 \quad \text{…...……..2.4}$$

Relative density is represented by d_{rel} Porosity (%) was calculated using relation

$$Porosity\ (\%) = 1 - d_{rel} \quad \text{……2.5}$$

For good properties, sample should have higher density and lower porosity.

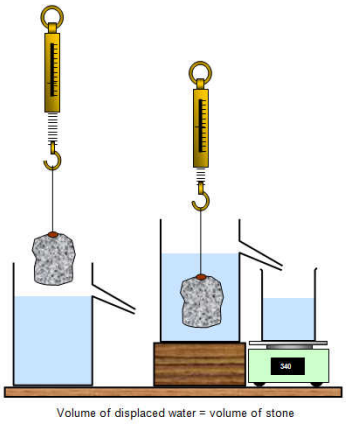

Figure 2.7 Density Measurements by Archimedes Principle

2.2.2 X-Ray Diffraction (XRD)

The X-ray diffraction is characterization technique for structure analysis in solid state chemistry and material science. It provides the qualitative as well as quantative analysis of XRD data. XRD data can be used to determine the crystal structure, lattice parameters and fingerprint characteristics of crystalline materials [8]. X-rays are electromagnetic radiation having energy greater than 100 keV and wavelength of the order of 0.1Å. For the X-ray diffraction analysis, wavelength of X-ray should be comparable to interplanar spacing which would be suitable for probing the structural arrangement of atoms and molecules in wide range of materials [9, 10].

The basic principle for X-ray diffraction analysis is that for a fixed wavelength (λ), the constructive interference occurs for a fixed set of an interplanar spacing (d) and incidence angle (θ) as shown in Figure 2.8. According to Bragg's condition of diffraction

$$2d\sin\theta = n\,\lambda \quad \text{…….2.6}$$

Where n is the order of the diffraction (normally in XRD, only 1st order (n = 1) is observed).

From the θ values, one can calculate the interplaner spacing (d).

For cubic system, the interplaner spacing (d) is given by

$$\frac{1}{d^2} = (h^2 + k^2 + l^2)/\, a^2 \qquad \text{……..….2.7}$$

Where (h, k, l) are miller indices and are obtained at a particular angle.

By combining the equation 2.6 and 2.7, we get

$$sin^2\theta = \frac{\lambda^2}{4a^2}(h^2 + k^2 + l^2) \qquad \text{…….2.8}$$

Similarly, the relation for a tetragonal and rhombohedral system is given by the relation

$$sin^2\theta = \frac{\lambda^2}{4}\left(\frac{h^2+k^2}{a^2} + \frac{l^2}{c^2}\right) \qquad \text{…..…….2.9}$$

$$sin^2\theta = \frac{\lambda^2}{4}\left(\frac{h^2}{a^2} + \frac{k^2}{b^2} + \frac{l^2}{c^2}\right) \qquad \text{…….2.10}$$

For any set of planes, for a given 'λ' if the above condition is satisfied, we can calculate the d-values for different values of θ and also we can find out the unit cell parameter.

For the present work, the structural analysis of the constituent phases and for the composite was done by XRD using Bruker, D-8 Advance model with Cu-K_α (λ = 1.54056 Å) radiations for capturing the diffraction pattern. The diffraction angle, 2θ was taken from 20^o to 70^o for both calcined powder as well as for sintered pallet. All the lattice parameters were calculated using equation 2.6 and Powder X software with an accuracy of ±0.002 degrees in 2θ value. An XRD instrument measures the intensity of diffracted radiation as a function of θ.

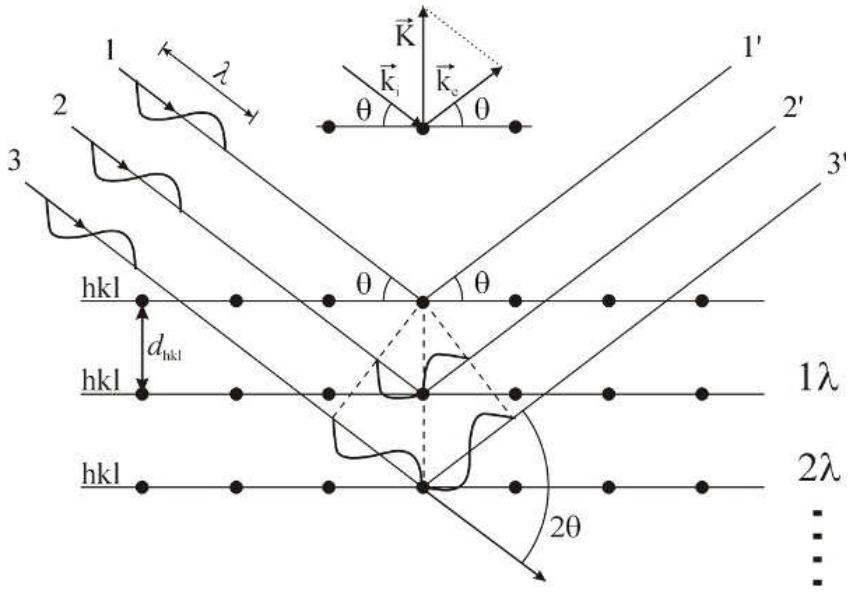

Figure 2.8 Geometry for Bragg X-Ray Diffraction

2.2.3 Scanning Electron Microscope

The scanning electron microscope is a vital technique used to determine the crystalline size and surface morphology of sintered pallet. It provides the knowledge of distribution of grains and average grain size. SEM measurements are based on the principle of irradiating the sintered sample with a finely focused electron beam. Secondary electrons, backscattered electrons, characteristic x-rays, auger electrons and several other radiations are released from the specimen. Generally, SEM uses secondary electrons for image formation with smaller wavelength in comparison to light photons. This generates high resolution information.

For the present study, freshly broken pieces of sintered pallet were used for SEM micrograph. The broken pieces were placed in stub and thin coating of gold was done with the help of gold sputtering technique. The SEM images of samples were obtained by Scanning Electron Microscope (JEOL JSM 6510LV, Japan). Observed secondary image were taken to observe the grains and grain growth. This helps to understand the porosity and uniformity of the grain. Linear intercept method was used to determine the average grain size of the samples.

2.2.4 Polishing/Electroding

As ceramic samples are insulators. For studying various properties, it is necessary to make parallel plate capacitor. This can be possible only by polishing the sample on both side of the surface.

For the present work, electrical contacts were made by applying the silver paste on both sides of sintered pallets. The polished pallets were annealed in conventional furnace at 400 ^{o}C - 500^{o}C for 1 hour to get good electrical contacts.

2.2.5 Dielectric Measurements

As ferroelectric and composite materials are good dielectrics, so these materials are suitable for various applications which is based on the dielectric measurements. Study of dielectric measurements provides essential information about the suitability of these materials for capacitor applications. For this, dielectric constant (ε) and tangent loss ($\tan\delta$) are most prominent

parameters. Dielectric properties depend on the frequency, temperature, moisture and other external factors [11].

The dielectric constant (ε) is the ratio of the capacity of a capacitor containing dielectric to the capacitor capacity in free space. The capacitance (C) of a parallel plate capacitor separated by vacuum is given by [12]

$$C = \varepsilon_0 . A/t \quad \ldots\ldots\ldots\ldots\ldots\ldots 2.11$$

Where ε_o is the permittivity of free space and is equal to 8.85 x 10^{-12} F/m, A is the area of the plates and t is the separation between two parallel plates. If a dielectric material is introduced between the plates of the capacitor, then the capacitance of the capacitor increases by a factor έ (έ is called the dielectric constant of the dielectric material). Therefore, for a parallel plate capacitor with a dielectric between the capacitor plates, the capacitance (C) is given by:

$$C = \varepsilon\varepsilon_0 . A/t \quad \ldots\ldots\ldots\ldots\ldots\ldots\ldots 2.12$$

When alternating field is applied, the dielectric constant can be expressed in terms of real and imaginary quantities as

$$\varepsilon_r = \varepsilon' - i\,\varepsilon'' \quad \ldots\ldots\ldots\ldots\ldots\ldots 2.13$$

Where ε' is the real part of dielectric constant and with in phase with applied electric field. ε" is the imaginary part of dielectric constant and 90^0 out of phase with respect to electric field. The ratio of imaginary part of dielectric constant to the real part is known as dielectric loss (tanδ).

$$tan\delta = \varepsilon''/\varepsilon' \quad \ldots\ldots\ldots\ldots\ldots\ldots 2.14$$

Dielectric loss is also known as dissipation factor. When the dielectric material between the plates of capacitor is ideal (loss free), the current leads the voltage by 90^o. However, in real dielectric materials (non-ideal), there exists a loss current in addition to the charging current associated with the storage of electric charge by the dipoles which arises due to DC ohmic conduction and the dissipation of energy related with the rotation or oscillation of dipoles [13]. So, the total current in the real dielectrics is a complex quantity and leads the voltage by 90-δ, where δ is called loss angle.

For the present study, measurement of dielectric properties such as capacitance (dielectric constant) and loss tangent (tanδ) of the samples (ferroelectric, ferrite and composites) were measured as a function of AC frequency (100Hz to 1MHz) at room temperature and as a function

of temperature (30^{o}C to 500^{o}C) at discrete frequencies carried out using Impedance analyzer (HIOKI, RS-3532-50) interfaced with a PC and programmable temperature controller shown in Figure 2.9.

Specification:

- Supplier : HIOKI 3532-50
- LCR HiTESTER
- High Speed Measurement of 5 ms LCR meter
- Source Frequency: 42 Hz to 5 MHz
- Help in determining piezoelectric parameters (k_p)
- Give good physics about k_p, d_{33} and other parameters
- From impedance analyzer we can get a continuous spectra with different resonance and anti-resonance peaks which helps in calculating k_p and $k_t$and thus gives more physics about piezoelectricity

Figure 2.9 Hioki 3532-50 LCR Meter

The dielectric constant (ε) of the materials at different frequencies were calculated using the relation

……..2.15

Where required parameters used are mentioned above. C_p is the capacitance measured in parallel mode.

2.2.6 AC Conductivity

The AC conductivity is used to understand the performance of the dielectric material. It supports the information about the defects and loss mechanisms in the dielectric materials. Most of the earlier investigations on ceramic materials describe the contribution of electrons (holes),

polarons, impurity ions, oxygen vacancies and impurities in electrical conductivity [14]. Conductivity of the ceramic samples may be given as [15]:

$$\sigma_{ac} = \sigma_0 + A\omega \quad \ldots\ldots\ldots\ldots\ldots 2.16$$

Where σ_0 term represents the contribution of dc conductivity, A is constant and σ_{ac} is the ac conductivity. The term $A\omega$ is frequency dependent and characterizes all the dispersion phenomena in the materials.

For the present work, the Ac conductivity of the samples was calculated from the dielectric parameters using the standard relation [16]:

$$\sigma_{ac} = \omega\varepsilon\varepsilon_o \tan\delta \quad \ldots\ldots\ldots\ldots\ldots 2.17$$

Where ω is the angular frequency, ε_o (8.85E-12 F/m) is the permittivity of the free space, ε is the dielectric constant and tanδ is the loss tangent.

2.2.7 Ferroelectric (P-E) Measurement

The main feature of ferroelectricity is the polarization reversal (switching) with electric field. This can be observed by measuring the polarization vs electric field hysteresis loop (P-E hysteresis loop). This is usually done by using Sawyer-Tower circuit [17] as shown in Figure 2.10. An alternating voltage *V* is applied across the electrodes on the ferroelectric material and a capacitor C_o with high value of capacitance is connected in series with the test sample (C_x) and then studying the relationship between the stored charge and the instantaneous voltage for test sample. The voltage across this capacitor measures the charge stored in the test sample.

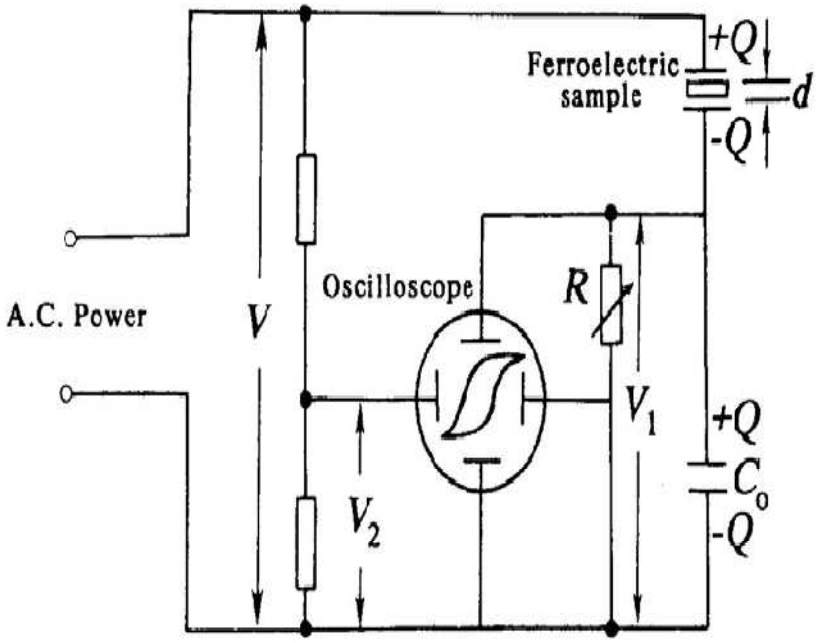

Figure 2.10 Diagram of Modified Sawyer-Tawer Circuit

For the present work, the ferroelectric nature (P-E) of the ferroelectric and composite samples was analyzed using an automatic PE loop tracer system shown in Figure 2.11. The P-E loop tracer was based on Sawyer –Tower circuit and can be operated at discrete frequencies ranging 50 Hz to 100 Hz. The system consists of PC, software, programmable voltage source (up to 3 kV). For measurement, the sample was kept in a spring-loaded jig and immersed in a silicon oil bath (to avoid any sparking or breakdown) at high voltage. The PE loop was recorded by the system at different applied electric field values and at room temperature. All the ferroelectric parameters like saturation polarization (P_s), remnant polarization (P_r), coercive field (E_c) and maximum field (E_{max}) were determined from P-E Loop.

Figure 2.11 P-E Hysteresis Loop Tracer

2.2.8 Poling

Poling is a process in which application of large dc electric field on the sample forces the domains of piezoelectric material to reorient in the direction of the applied electric field. The ferroelectric ceramic material does not possess any piezoelectric properties owing to the random orientation of the domains in the ceramics so to exhibit the piezoelectric properties poling is necessary for sample. A field higher than coercive field (E_c) must be applied to the sample at higher temperature during poling for obtaining good piezoelectric properties. The poling set-up used for the present work is shown in Figure 2.12.

For the present work, electroded sample was kept in silicon oil and then was heated to 150^{o}C and DC electric field (~15 KV/cm) was applied for 1 hour. After that the sample was cooled to room temperature in the presence of electric field and then electric field was removed.

Specifications:

- High DC voltage power supply (2500V)

Figure 2.12 Electrical Poling Setup with Specifications

2.2.9 Piezoelectric coefficients

The electrically poled samples are used to measure piezoelectric charge coefficient and electromechanical coupling factor. The piezoelectric coefficient is defined by charge generated per unit force both in the direction of polarization of piezoelectric material. The piezoelectric charge coefficient is given using relation:

$$d_{33} = Q/F = CV/F \quad \text{……..2.18}$$

Where $Q = CV$ is the charge developed per unit electrode area of piezoelectric material, C is the capacitance, V is the Voltage and F is the force applied in Newton (N).

Piezoelectric coefficient can be measured by different methods- (1) Static Method (2) Quasistatic Method (3) Resonance Method.

For the present study, piezoelectric charge coefficient of poled samples was measured using Concord d_{33} meter (Model-2, Concord Electroceramics Industries) as shown in Figure 2.13 which is a Quasistatic method. This is based on Berlin court principle. D-meter consists of force head, electronic driver and d_{33} read out. The force head has an electromagnetic driver which vibrates the internal calibration piezo element as well as the piezo test specimen which are mechanically in series. It is so designed that it facilitates measurement of d_{33} coefficient for a

variety of piezoelectric materials of varying sizes and shapes. The piezoelectric sample under test is clamped within the jaws of the force head unit for testing. The oscillator and electromagnetic driver provide ac voltage to the electromagnetic driver in the force head and the charge developed by the sample is measured and displayed digitally in d_{33} read out. The measurable d_{33} range by D-meter is 50-1000 pC/N depends on the piezo sample with accuracy up to ±5.0%.

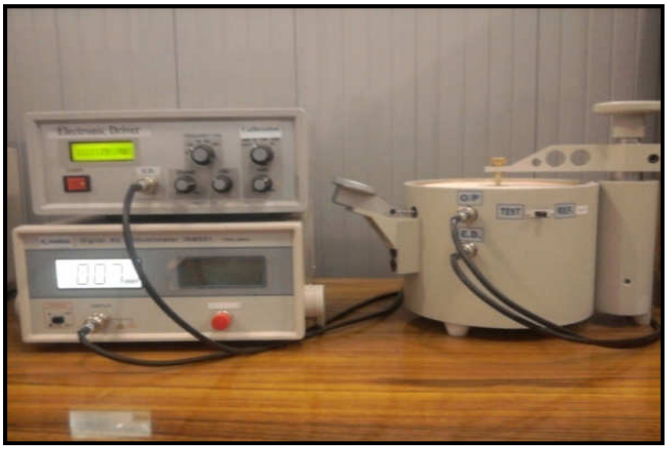

Figure 2.13 Piezo d- meter for Measuring the Piezoelectric Coefficient

2.2.10 Magnetic hysteresis loop set up- Vibrating Sample Magnetometer (VSM)

The ferroelectric properties of composite samples are characterized by P-E Hysteresis loop; similarly magnetic properties are characterized by magnetic hysteresis loop. Magnetic hysteresis loops can be obtained from various techniques such as Vibrating sample magnetometer, Superconducting Quantum Interference Device (SQUID) and B-H Loop tracer.

For the present study, VSM technique was employed for obtaining the M-H hysteresis loop. Lake Shore 735 VSM Controller, Model 662 was used for measurement of M-H hysteresis loops.VSM is based on the change in flux in a coil when a sample is made to vibrate. The vibrating sample is placed in an adjustable uniform magnetic field to magnetize the sample (as shown in Figure 2.14). Hysteresis curve of the material is obtained by measuring the induced voltage in pickup coils using lock-in amplifier and measuring the intensity of field produced by electromagnets. The magnetic moment of the sample is detected by pickup coils (induced voltage

in pickup coils is directly proportional to the magnetic moment of the sample and does not depend on the strength of the applied magnetic field). The vibrating sample magnetometer measures the magnetization of a small sample of magnetic material placed in an external magnetizing field by converting the dipole field of the sample into an ac electrical signal. From these loops, magnetic parameters i.e. saturation magnetization (M_s), coercive field (H_c) and remnant magnetization (M_r) were determined from graphs.

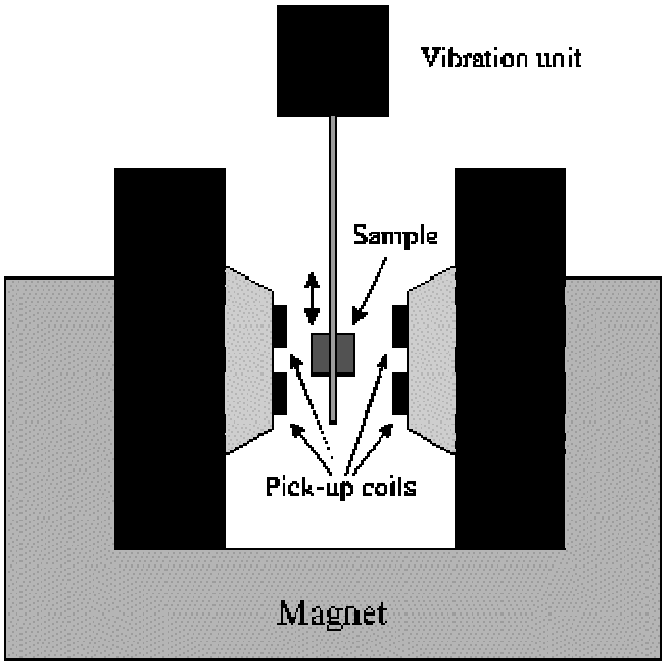

Figure 2.14 Schematic for Vibrating Sample Magnetometer

2.2.11 Magnetoelectric (M-E) Measurement

The magnetoelectric effect is a coupled two field effect in which induction of electric polarization by applying an external magnetic field and induction of magnetic polarization by applying an external electric field. The ME effect in composite is a result of the interaction of magnetic and piezoelectric phases through strain – stress coupling. ME voltage coefficient depends on mechanical coupling, resistivity and molar ratio of constituent phases and applied DC magnetic field. ME coefficient was measured in terms of variation of the change in electric field with respect to change in magnetic field as a function of dc magnetic bias field. ME characterization in the ceramic was studied by measuring the voltage response of the ceramic subjected to alternating and constant (bias) magnetic field. The bias magnetic field (H_{dc}) was

obtained using an electromagnet and the alternating magnetic field was generated by Helmboltz coil. ME effect was characterized by a ME voltage coefficient α which is given by [19].

$$\alpha = \frac{V}{H_{ac} \times d} \qquad \text{…….2.19}$$

Where V is the voltage generated due to magneto electric effect, H_{ac} is the amplitude of alternating magnetic field and d is the thickness of the sample.

For the present study, ME coefficient has been measured by dynamic method involving simultaneous application of AC as well as DC magnetic field [20]. ME measurement set up is shown in Figure 2.15. Electric voltage was noted using lock in amplifier. Magnetoelectric (ME) coupling coefficient (dE/dH) as a function of dc magnetic field (0- 5000 Oe), keeping AC magnetic field constant at 1 Oe, was studied using ME setup consisting of lock in amplifier (7265 DSP), electromagnets (10" poles) and sample holders.

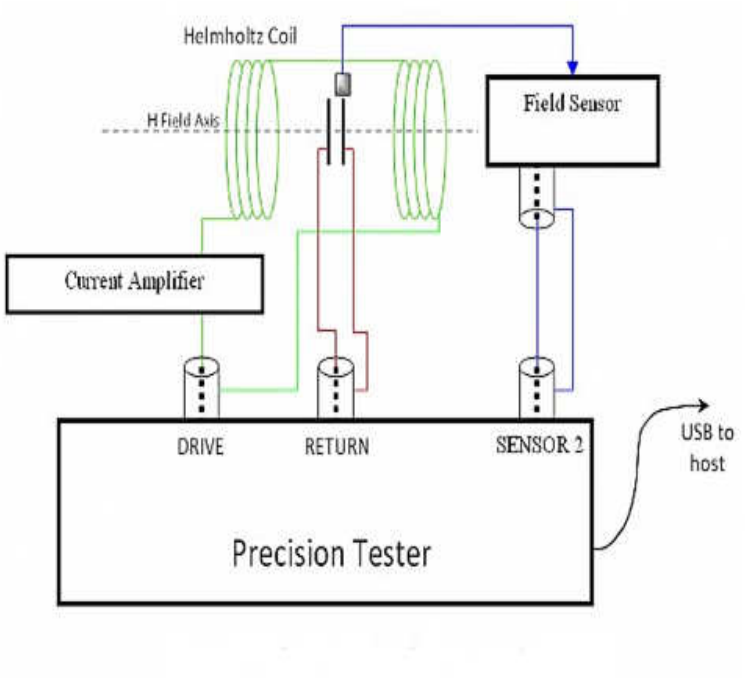

Figure 2.15 Magnetoelectric coupling measurement setup

References

1. P. Consin and R. A. Ross, Mater. Sci. and Engg. A., **130** (1990) 119.

2. M. K. Naskar and M. Chattarjee, J. Am. Ceram. Soc., **88** (2005) 38.

3. C. R. Bickmore, K. F. Waldner and D.R. Treadwell, J. Am. Ceram. Soc., **79** (1996) 1419.

4. C.T. Wang, L.S. Lin and S. J. Yang, J. Am. Ceram. Soc., **75** (1992) 2240.

5. J. Moulson and J. M. Herbert, Electroceramics: Materials, Properties and applications, Chapman and Hall, New York, USA (1997).

6. M. W. Barsoum, Fundamental of Ceramics, (1997).

7. K. Uchino, Processing of Ceramics (1982).

8. O.P. Thakur, Chandra Prakash and D. K. Aggarwal, J. Ceram. Process. Res., **3** (2002) 75.

9. S. K. Chatterjee, X-ray Diffraction: It's Theory and Applications, Prentice Hall of India Private Limited, New Delhi (1999).

10. B. D. Cullity, Elements of X-ray Diffraction, Addison-Wesley Publication Company Inc., Massachusetts, Menlo Park, California (1978).

11. M. W. Barsoum, Fundamentals of Ceramics, The McGraw- Hill Companies Inc., New York (1997).

12. W. F. Smith, Principles of Materials Science and Engg., MC Graw-Hill, U.S.A.

13. B. Jaffe, W. Cook and H. Jaffe, Piezoelectric Ceramics, Academic Press, London (1971).

14. R. C. Buchanan, Ceramic Materials for Electronics, Marcel Dekker Inc., New York (1998).

15. A. K. Jonscher, J. Mater. Sci., **16** (1981) 2037.

16. S. S Choughle and B. K. Choughle, Mat. Chem. Phys., **108** (2008) 408.

17. C. B. Sawyer and C.H. Tower, Phys. Rev., **35** (1930) 269.

18. C. M. Kanamadi, S.R. Kulkarni, K. K. Patankar, S. S. Chougule, S. J. Patil and B. K. Chougule, J. Mater. Sci., **42** (2007) 5080.

19. R. Grossinger, G.V. Dong and R. Sato-Turtelli, J. Magn. Magn. Mater., **320** (2008) 1972.

20. J. G. Wan, X. W. Wang, Y. J Wu, M.Zeng, Y. Wang, H. Jaing, W. Q. Zhou, G. H. Wang and J.- M. Liu, Appl. Phys. Lett., **86** (2005) 122501.

Chapter – 3

Synthesis and Characterizations Of CFO-PZT Composites

Chapter-III

Synthesis and Characterization of CFO-PZT Composites

In this chapter, details of composite samples of (x) CFO – (1-x) PZT, x= 0.00, 0.05, 0.10, 0.15 and 1.0, prepared by solid state reaction method, are given. The processing parameter eg:sintering temperature and time, heating and cooling rates, were optimized to get good quality,dense ceramic samples and the details are given here. The sintered samples were prepared for characterization and all the properties of techniqual importance eg: structural, physical, dielectric, ferroelectric, magnetic, piezoelectric and magnetoelectric effect were studied. The details are presented in this chapter.

3.1 Synthesis of Samples

3.1.1 Synthesis of Individual Phases

Our first objectives was to select the individual ferrite and ferroelectric phases to obtain the good ferrite and ferroelectric propertieswhich was done by exhaustive literature survey and finally to synthesize and study for properties of magnetoelectriccomposites. In this view, $PbZr_{0.55}Ti_{0.45}O_3$ was chosen as ferroelectric phase and $CoFe_2O_4$ was chosen as ferrite phase.The individual phases (ferrite and ferroelectric) were prepared separately by conventional solid state reaction method. AR grade $CoCo_3$, and Fe_2O_3 for the ferritephase and PbO, ZrO_2 and $TiO_2$for ferroelectric phase were weighed in the required molar proportions for synthesis. The mixing and grinding of raw material for both the phases individually were done by ball milling in distilled water using zirconia balls as the milling media. The dried powder of ferroelectric phase was calcined at 800 ^oC for 4 hours while ferrite was calcined at 900 ^oC for 4 hours. The calcined mixture was ball milled again, dried separately and then recalcination was done at 850 ^oC for 4 hours for ferroelectric phase and 950^oC for 4 hours for ferrite phase. An excess of 2% of PbO was taken to compansate lead loss during sintering. Various steps involved in the synthesis of individual phases are shown in Figure 2.1(a) (Chapter II). After synthesis, the samples were characterized for various properties.

XRD analysiswas carried out for phase identification of both phases. XRD patterns for individual phases (PZT & CFO) are shown in Figure 3.1. The patterns for PZT and CFO show well-defined peaks with specific indices characteristic of both the phases,perovskite tetragonal and spinel structures, respectively. This confirms the perovskite structure in the ferroelectric phase (PZT) and the cubic spinel structure in the ferrite phase (CFO).

3.1.2 Synthesis of Composites

After synthesis of individual phases, composite were prepared (ferroelectric and ferrite) by mixing 0.5% (by weight) ferrite phase with 95% (by weight) ferroelectric phase. The mixed powder was ball milled and dried.

Then dried powder was mixed with small amount of diluted polyvinyl alcohol (3% by weight) as binder. Thepowder was compacted into pallet form using uniaxial hydraulic press and was conventionally sintered in a programmable furnace.

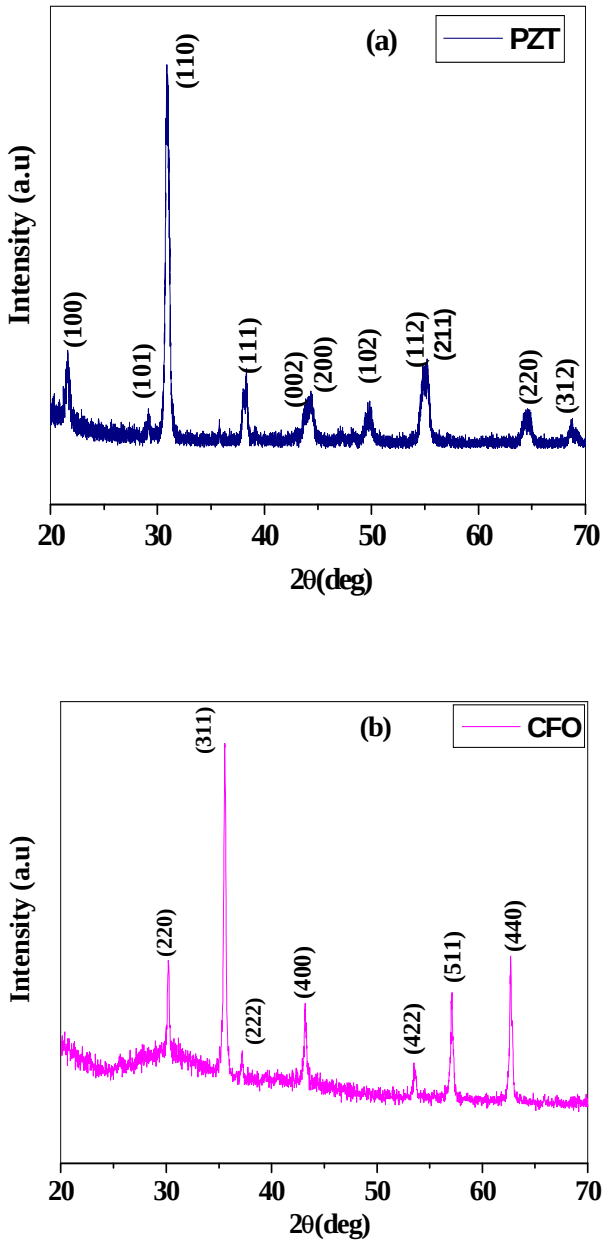

Figure 3.1 XRD patterns for (a) PZT and (b) CFO

3.2 Optimization of Sintering Temperature

As sintering temperature significantly influences the system properties including phase evolution, microstructure and density of the material [1-3], particularly involving PZT due to volatile nature of PbO. In order to obtain the optimum temperature, green bodies of sampleswere sintered at different temperatures from 1150^{o}C - 1250^{o}C in step of 50^{o}C for 4 hours. For the present work, (0.05) CFO- (0.95) PZT sample was selected to optimize the sintering temperature and time and sample was sintered at three different sintering temperatures from 1150^{o}C- 1250^{o}C in step of 50^{o}C for 4 hours.

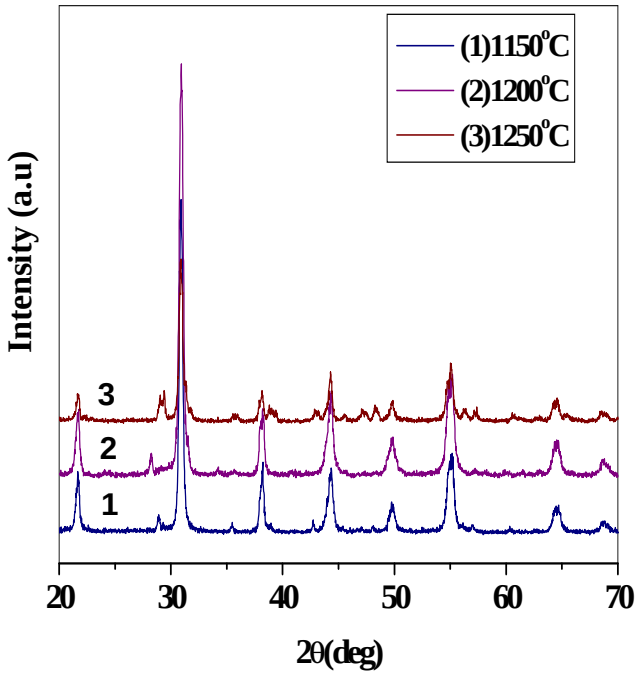

Figure 3.2 XRD patterns for(0.05) CFO – (0.95)PZTcomposite at different sintering temperatures

Figure 3.2 shows the XRD patterns for(0.05) CFO – (0.95) PZT composite prepared at different sintering temperatures (1150^{o}C - 1250^{o}C). From figure, it is observed that XRD pattern of samples sintered at 1250^{o}C shows some extra peaks other than constituent phases. That may be due to chemical reaction between the constituent phases during high temperature sintering process.No extra peaks other than the constituent phases were observed for samples sintered at

1150^{o}C and 1200^{o}C which shows that no chemical reaction takes place between the constituent phases. All XRD patterns show well defined peaks with specific indices of both phases. It is also observed thatintensity for ferrite phase is lower as compared to ferroelectric phase due to small concentration of ferrite content in the composite sample. So from the XRD patterns, the optimized temperature could be 1150^{o}C and 1200^{o}C but will depend on the other properties also. Lattice Parameters of composite sample sintered at three different temperature are calculated using X-Ray data and are listed in Table 3.1

Table 3.1 Lattice parameters of (0.05)CFO – (0.95) PZT composite sample sintered at Three different Temperatures

Sintering Temperature(^{o}C)	Lattice parameters(Å)			
	a (Ferrite phase)	a (Ferroelectric)	c (Ferroelectric)	c/a
1150	8.442	4.089	4.107	1.0044
1200	8.682	4.087	4.106	1.0046

The variation of dielectric constant and tangent loss with temperature for all samples sintered at three different sintering temperatures is shown in Fig 3.2 at 100 kHz. All samples show a dielectric peak at ferroelectric transition temperature.The value of ferroelectric Curie temperature (T_c), room temperature dielectric constant (ε_{RT}), maximum dielectric constant (ε_{max}) and loss tangent (tan δ)for all samples are given inTable 3.2. From Table, we can say that room temperature dielectric constant (ε_{RT}) is higher for sample sintered at 1150^{o}C and it decreases with increase in sintering temperature.

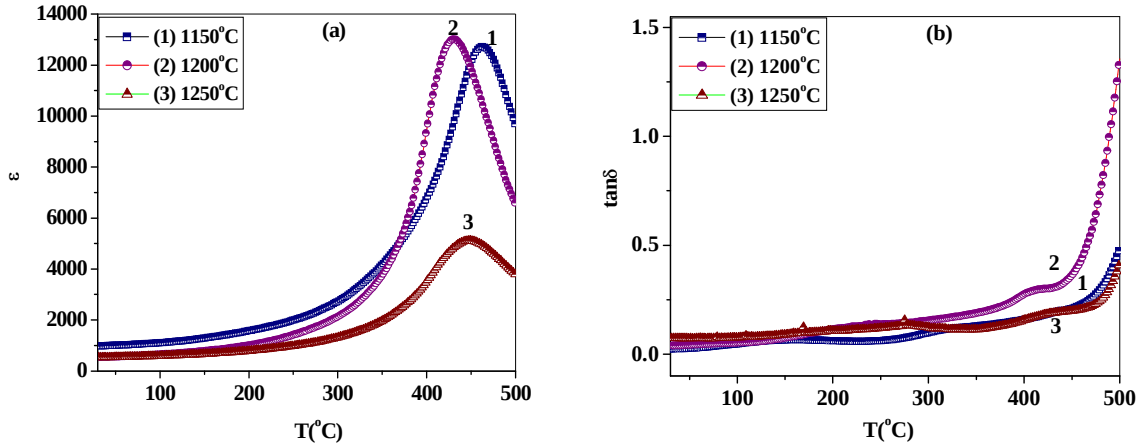

Figure 3.3 Variation of (a) Dielectric constant (ε) with temperature (T(°C)) (b) Dielectric Loss (tanδ) with temperature measured at 100 kHz for (0.05) CFO- (0.95) PZT composite at different sintering temperatures

Table 3.2 Dielectric parameters of (0.05) CFO- (0.95) PZT sample at 100 kHz for different sintering Temperatures

Sintering Temperature (°C)	ε_{RT}	T_c(°C)	ε_{max}	$\tan\delta_{RT}$	$\tan\delta_{max}$
1150	980	462	12725	0.023	0.23
1200	605	415	12810	0.021	0.23
1250	540	448	5115	0.074	0.19

Figure 3.4 shows the room temperature P-E Hysteresis loops of (0.05) CFO – (0.95) PZT sample sintered at different temperatures. Ferroelectric parameters are given in Table 3.3. Maximum saturation is observed for sample sintered at1150°C and decreases with increase in sintering temperature. Coercive field increases with increase in sintering temperature. To confirm magnetic ordering, M-H hysteresis loops were recorded and are shown in Figure 3.5.

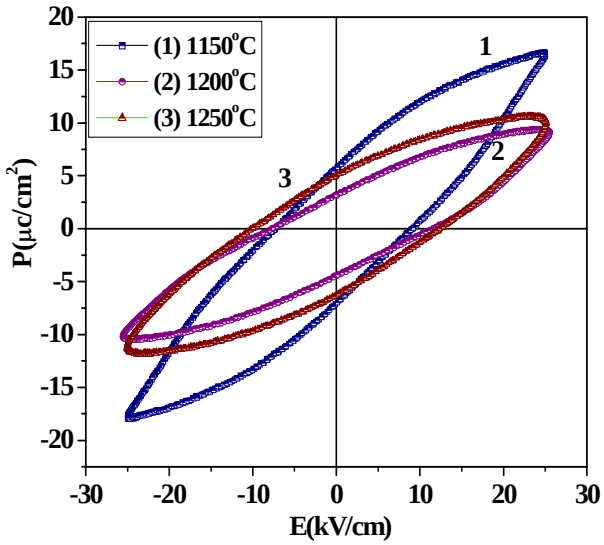

Figure 3.4 P-E Hysteresis loops for (0.05)CFO – (0.95)PZT composite at different sintering Temperatures

Table 3.3 Ferroelectric Parameters for (0.05) CFO – (0.95) PZT recorded at room temperature

Sintering Temperature (^oC)	P_s ($\mu C/cm^2$)	E_c (kV/cm)	P_r ($\mu C/cm^2$)
1150	17.34	8.15	6.45
1200	10.01	9.67	3.84
1250	11.30	11.31	5.66

From the above results, it can be concluded that sintering temperature affects the material properties. Dielectric constant (ε_{RT}),Remanant polarization (P_r), Saturation polarization (P_s), were observed to be optimum for the sample sintered at 1150^{o}C as compared to other sintering temperature and dielectric loss (tanδ) is also minimum. Hence, the 1150^{o}C for 4 hours temperature was chosen as the optimized sintering temperature for further studies of the composite samples.

3.3 Synthesis and Characterization of(x) $CoFe_2O_4$ - (1-x) $PbZr_{0.55}Ti_{0.45}O_3$

(x) $CoFe_2O_4$ - (1-x) $PbZr_{0.55}Ti_{0.45}O_3$, x = 0.05, 0.10 and 0.15 were prepared by conventional solid state reaction method. All composite samples were sintered at optimized temperature at 1150 ^oC for 4 hours. After sintering, samples were characterized for various properties.Existence of both phases was confirmed by XRD. XRD patterns were recorded using Bruker AXS D8 Advance computer controlled powder X- ray diffractometerat room temperature in a range of Bragg angles ($20^\circ \leq 2\theta \leq 70^\circ$) with step size of 0.02°. The microstructures of samples were studied by scanning electron microscope (JEOL JSM 6510LV, Japan). For measuring electrical properties, the sintered pellets were mechanically lapped on the glass surfacethoroughly cleaned and then electroded by using silver epoxy and subsequently heated at 400^{o}C for 30 minutes to ensure good ohmic contacts. The dielectric properties of the samples as a function of temperature at discrete frequencies were measured by using HIOKI 3532-50 LCR meter and room temperature measurement of dielectric constant (ε)and loss tangent (tanδ) as a function of ac frequency (100Hz to 1MHz) were measured using same meter. The ferroelectric nature (P-E) of the samples was analyzed using an automatic PE loop tracer system (Marine India Pvt. Ltd.). Electrical poling was done at 100^{o}C -120^{o}C in silicon oil bath by applying electric field strength of ~15kV/cm for 1 hr. Then the sample was allowed to cool up to room temperature by switching off the heater in applied electric field and after coolingthe field was removed.

Magnetic properties were recorded using a Lake shore 735 Vibrating Sample Magnetometer (VSM) Controller, Model 662, interfaced with a computer. The magnetoelectric signal (voltage) was determined as a function of increasing DC magnetic field (0–5000Oe) using 7265 DSP lock-in amplifier in the presence of small AC magnetic field. Electric voltage (V) was noted from lock in amplifier and magnetoelectric coupling coefficient (μV/cm.Oe) or (mV/cm.Oe) was calculated by using the relation:

$$\alpha = \frac{V}{H_{ac} \times d} \qquad \text{……..3.1}$$

Where d is the thickness of the sample and H_{ac} is the ac magnetic field.

Here, we discuss the structural, dielectric, ferroelectric, piezoelectric, ferromagnetic properties of CFO- PZT magnetoelectric composites.

3.3.1 X-Ray Diffraction

Figure 3.5 shows the X-ray diffraction (XRD) patterns of all samples (x = 0.00, 0.05, 0.10, 0.15 and 1.00). The XRD patterns show the presence of both the constituent phases: perovskite tetragonal structure offerroelectric phase (PZT) and cubic spinel structure of ferrite phase (CF) and both phases in the composite samples. The diffraction peaks are indexed with specific indices of both the phases. In XRD pattern, noadditional peak other than the constituent peak is observed which confirms that no chemical reaction between the constituent phases occurred at high sinteringtemperature. The intensity of the major peak depend on their individual phase fraction in the composite**.** With increasing the volume fraction of CFO content, number of diffracting points corresponding to ferrite phase increases which in turn increases the intensity of major peak.

Calculated values of lattice parameters for all samples (x = 0.00, 0.05, 0.10, 0.15 and 1.00) are given in Table 3.5. The change in parameter may also be due to interdiffusion of ions of individual phases at grain boundaries as they are sintered at higher temperature which can not be avoided or we can say that change in parameter is due to stress exerted by one phase on another. As observed from the lattice parameters, tetragonality (c/a) goes on decreasing with increase in ferrite content.The values of experimental densities, theoretical and relative density of composites were determined from Archimedes principal and X-Ray diffraction pattern (as already discussed in Chapter-II) and their values are given in Table 3.4. From table, it is observed that there is decrease in density with increase in ferrite content which may be due to low density of ferrite phase (CFO) added in the ferroelectric phase [4]. The composite sample for x = 0.15 has slightly higher density which may be due to better sinterability and better compaction [5].

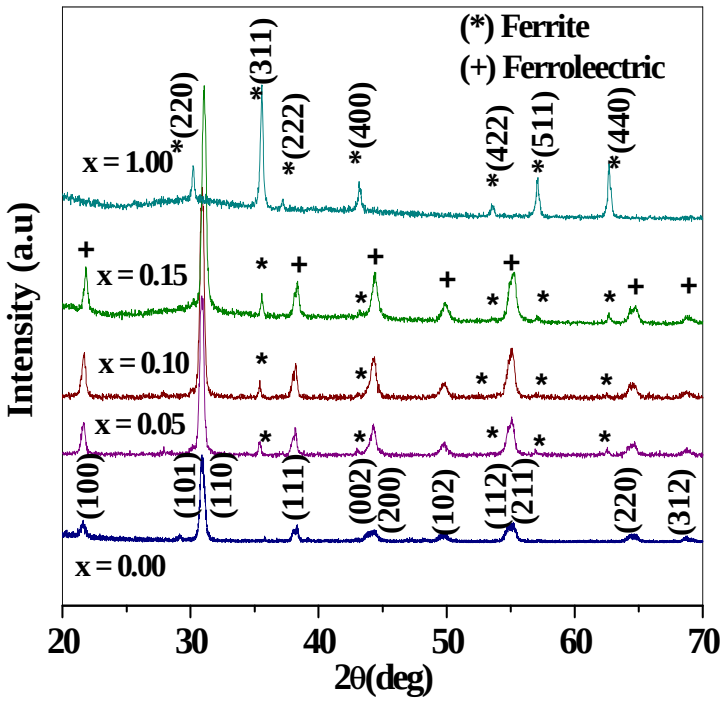

Figure 3.5 X-Ray Diffraction Pattern for (x)CFO-(1-x) PZT composites; (1) x= 0.00 (2) x = 0.05(3) x = 0.10 (4) x = 0.15 and (5) x = 1.00

3.3.2 Scanning Electron Microscope

Microstructure features are basically governed by transport of matter during heating process. SEM analysis is important because it influences the ferroelectric, dielectric, magnetoelectricand piezoelectric properties of ferroelectric as well as composites.Figure 3.6 shows SEM micrographs of freshly broken surfaces for all samples. The Micrographs show the closely packed and well oriented grains. The shape, size and distribution of grains confirm the polycrystalline nature. As seen in the micrograph,forpure PZT, grains are larger and rounded shape. In composites, two types of grain are observed, larger and smaller. Smaller or sharp edged grainsmay be due to the ferrite phase. The average grain sizeof the samples was calculated by linear intercept method and is given in Table 3.4.From Table, it is observed that average grain size for pure ferroelectric phase is larger than the pure ferrite as clearly seen in picture. As the

volume fraction of ferrite content in the composite sample is much smaller as compared to ferroelectric, the ferrite (CFO) and ferroelectric (PZT) grains are difficult to differentiate.

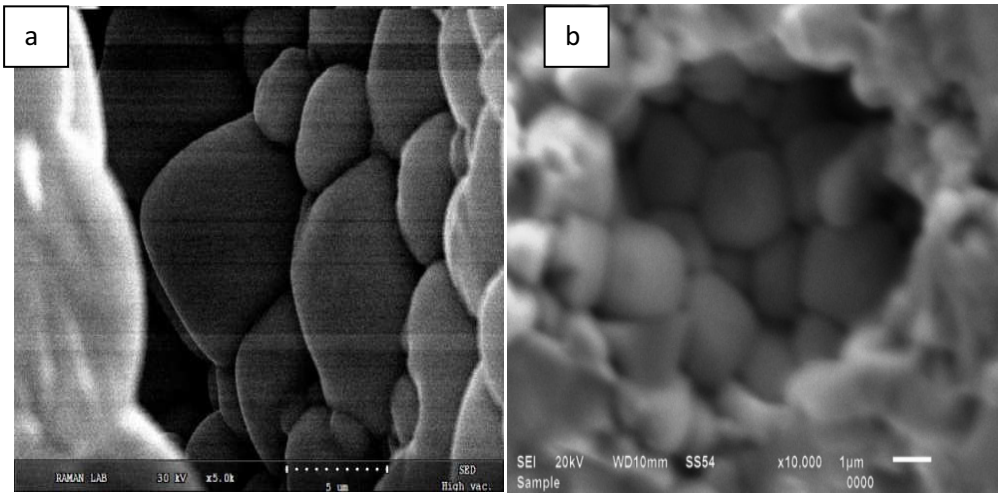

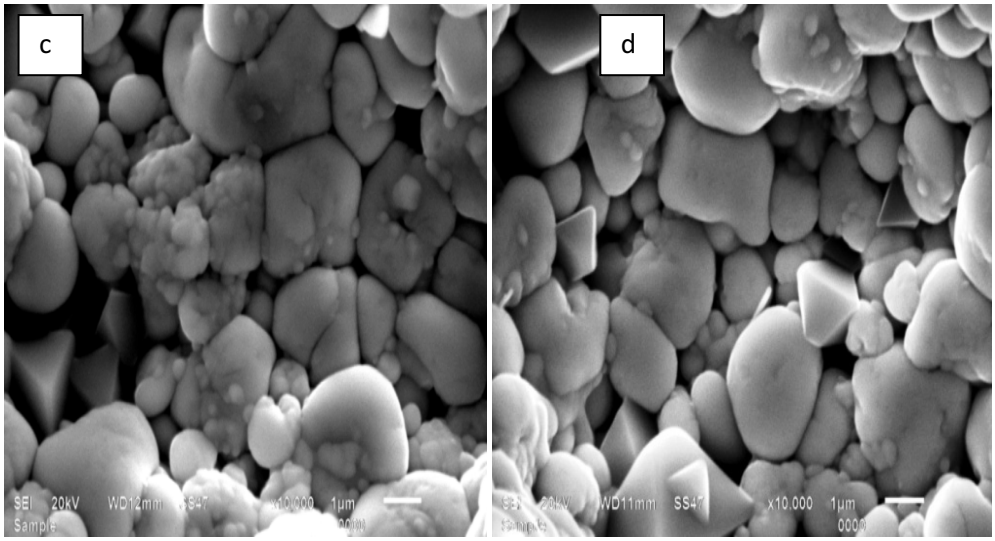

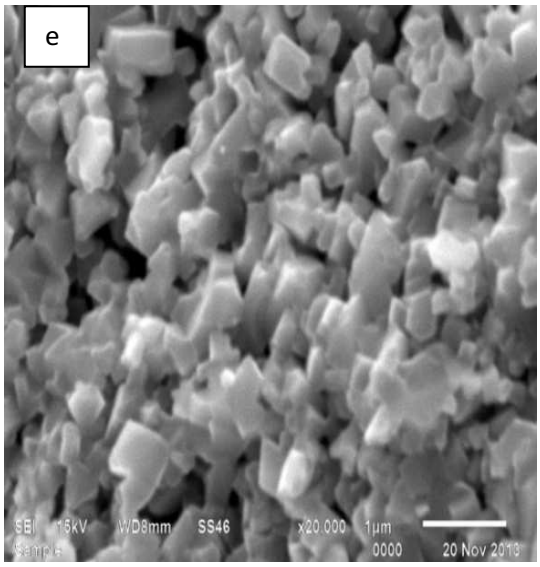

Figure 3.6 SEM Micrograph for (x)CFO-(1-x) PZT Composites; (a) x= 0.00 (b) x = 0.05 (c) x = 0.10 (d) x = 0.15 and (e) x = 1.00

Table 3.5 Structural Parameters of (x) CFO-(1-x) PZT composites

Parameters / **x**	**Ferrite a (Å)**	**Ferroelectric a (Å)**	**Ferroelectric c (Å)**	**d_{exp} (g/cc)**	**d_{th} (g/cc)**	**Relative Density (%)**	**Average Grain Size (µm)**
0.00	-	4.081	4.129	7.56	8.006	94.39	4.7
0.05	8.422	4.089	4.107	7.33	8.021	94.36	1.5
0.10	8.414	4.085	4.099	7.05	7.783	91.87	1.6
0.15	8.386	4.074	4.082	6.97	7.859	91.93	1.4
1.00	8.376	-	-	4.72	5.294	89.11	1.0

3.3.3 Dielectric Properties

The variation of dielectric constant and dielectric loss with frequency and temperature for all samples are discussed here.

3.3.3.1 Frequency dependence of dielectric properties

The variation of dielectric constant with frequency for all the samples at room temperature is shown in Figure 3.7(a). From Figure it is observed that all samples show dispersion and it is also observed that dielectric constant is higher at lower frequency then decreases rapidly with further increase in frequencies and remains constant at higher frequencies. The higher value of dielectric constant at lower frequencies is due to dislocations and defects for pure phases.The dispersion can also be explained by Maxwell Wagner type interfacial polarization in agreement with Koop's phenomenological theory [6-9]. However, in composites, the higher value of dielectric constant at lower frequencies is attributed tothe fact that ferroelectric region is surrounded by non ferroelectric region [11]. At higher frequencies, the dielectric constant decreases and remains constant for further increase in frequencies. This may be due to diminution of ionic and dipolar polarization and for further increase in frequencies, dipoles cannot follow the alternation of electric field, resulting into constant value of the dielectric constant. From figure, it is also observed that there is random values of dielectric constant which may be due to different permittivity and conductivity of two phases resulting into inhomogeneous dielectric structure. The inhmogeneities present in composite system are impurities, porosity and grain boundaries [10].

Figure 3.7(b) shows the variation of tangent loss (tanδ) with frequency for all the samples. The dispersion in tangent loss is similar to the dispersion in dielectric constant. At lower frequencies, the value of tanδ is higher and it decreases rapidly with increase in frequency. At higher frequencies, conduction losses get reduced and dipoles contribute to the polarization [12]. The tanδof the composites increases with increase in ferrite concentration. The tanδ of pure ferrite phase is shown in inset of Figure 3.7(b), Maximum dielectric loss is observed in pure ferrite phase, which may be due to high conductivity of ferrite phase. As seen from the inset figure a peak is observed at lower frequencies.The peak appears when the hopping frequency of

the electrons between the different ions, with different valance state, is close to that of external electric field.

Figure 3.8 shows the variation of log σ_{ac} with frequency for all the samples. The AC conductivity of the sampleswas calculated using relation:

$$\sigma_{ac} = \omega\varepsilon\varepsilon_o tan\delta$$

Where ω is the angular frequency, ε_o is the permittivity of the free space, ε is the dielectric constant andtanδ is the loss tangent.From this figure, it is observed that for all samples, conductivity increases with increase in frequency. The linear variation of ac conductivity with frequency indicates that conduction occurs due to small polaron hopping. Similar variation of Ac conductivity with frequency has also been reported by various researchers [13, 14].

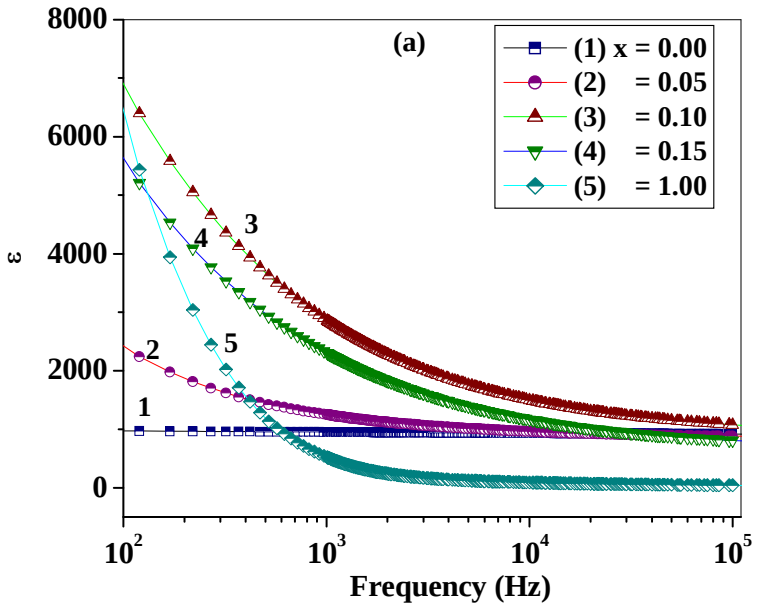

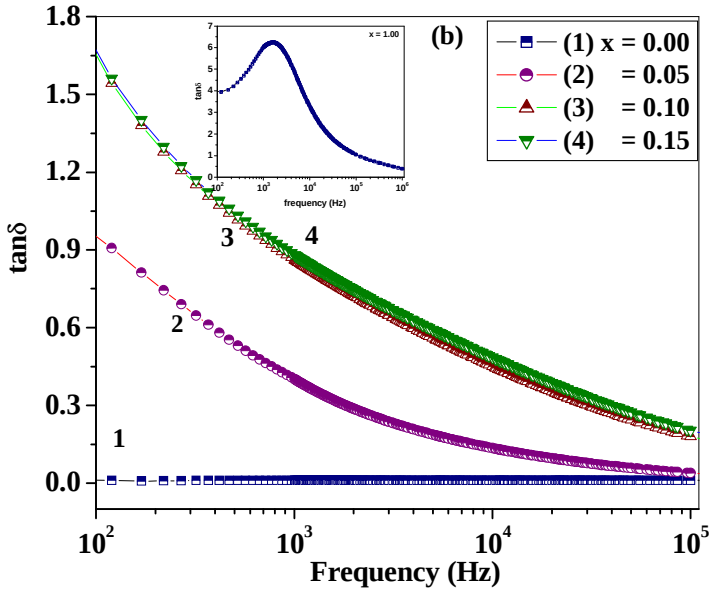

Figure 3.7 Variations of (a) Dielectric Constant and (b) Tangent Loss with Frequency at Room Temperature for (x) CFO-(1-x) PZT Composites; x = 0.00, 0.05, 0.10, 0.15 and 1.00

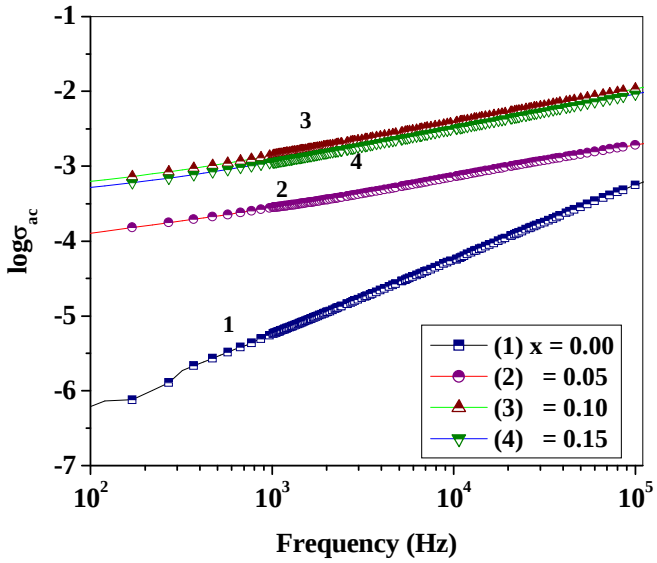

Figure 3.8 Variation of AC Conductivity with Frequency at 100 kHz for (x) CFO-(1-x) PZT Composites (x = 0.00, 0.05, 0.10, 0.15 and 1.00)

3.3.3.2 Temperature dependence of dielectric properties

The variation of dielectric constant (ε) and tangent loss (tanδ) with temperature for all the samples at 1 kHz, 10 kHz and 100 kHz is shown in Figure 3.9. It is observed that for all the samples, dielectric constant increases slowly with increase in temperature and attains maxima at a particular temperature called Curie temperature (T_c) and then it decreases with further increase in temperature. Dielectric constant and loss tangent for x = 1.00 increases with increase in temperature up to the particular temperature that particular temperature is known as dielectric transition temperature T_d. however, beyond this temperature dielectric constant is found to decrease continuously. This behavior is typical behavior of ferrites. Similar variation of dielectric constant with temperature for ferrites has also been reported earlier[15, 16]. In composites, a dielectric dispersion is observed over a wide range of temperature around T_c and broad dielectric peak are also observed.With increase in ferrite content, dielectric peak also gets broadened. This broadening of peak may be due to microscopic heterogeneity in the composites i.e. presence of two phases, ferrite and ferroelectric phase [17-19]. It is also observed that at lower frequency (1 kHz), there is increase in dielectric constant with increase in temperature (above 450^{o}C or in paraelectric region) for x = 0.05, 0.10 and 0.15.But with increase in measurement frequencies (10 kHz and 100 kHz), this behavior reduces showing that it could be related to lowfrequency relaxation process [20]. This increase in dielectric constant at higher temperatures is due to increase in dielectric polarization which arises from thermally activated electron hopping between Fe^{2+}& Fe^{3+} and Co^{2+}& Co^{3+} ions present in ferrite phase. But at higher frequencies, electron hopping is relaxed out.

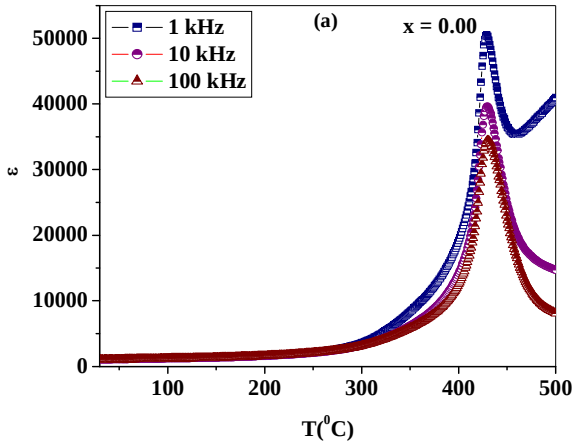
(a)
x = 0.00
1 kHz
10 kHz
100 kHz
ε
T(°C)

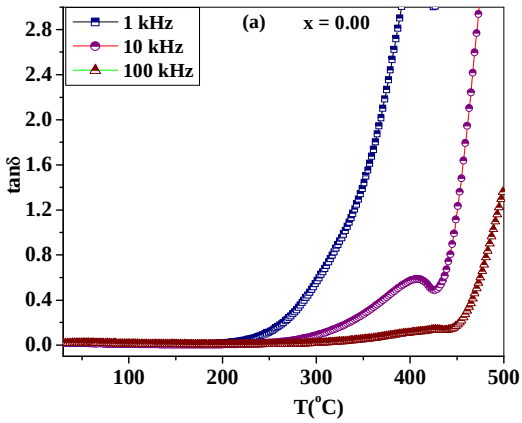
(a)
x = 0.00
1 kHz
10 kHz
100 kHz
tanδ
T(°C)

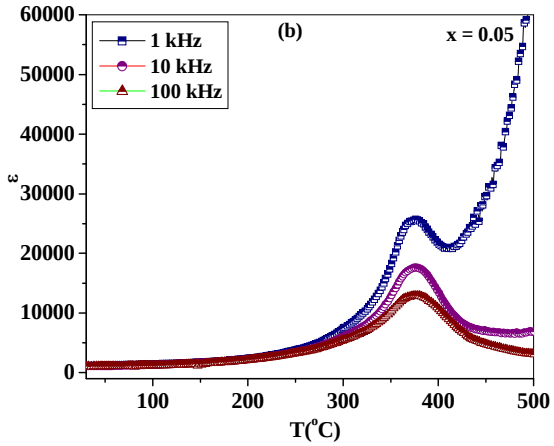
(b)
x = 0.05
1 kHz
10 kHz
100 kHz
ε
T(°C)

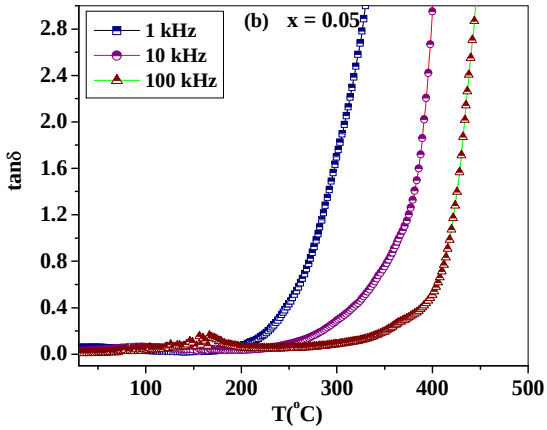
(b)
x = 0.05
1 kHz
10 kHz
100 kHz
tanδ
T(°C)

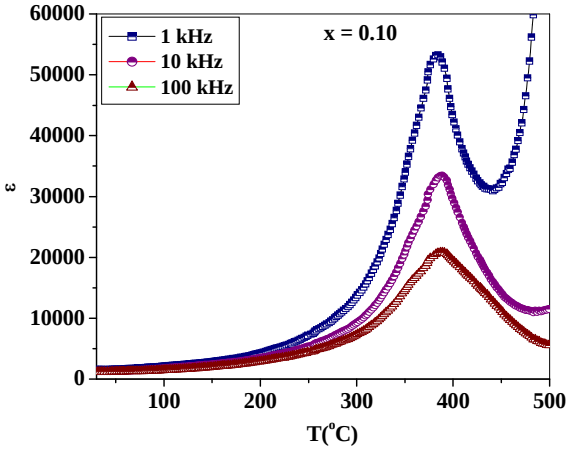
x = 0.10
1 kHz
10 kHz
100 kHz
ε
T(°C)

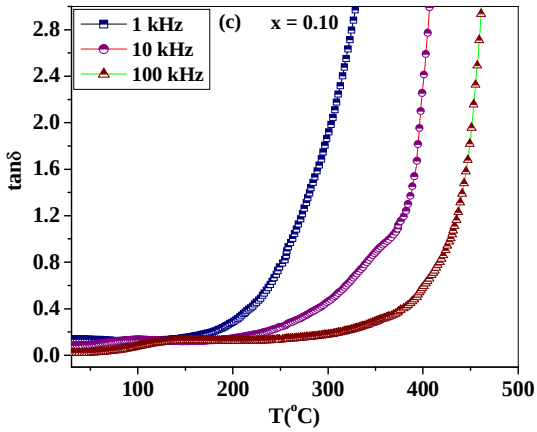
(c)
x = 0.10
1 kHz
10 kHz
100 kHz
tanδ
T(°C)

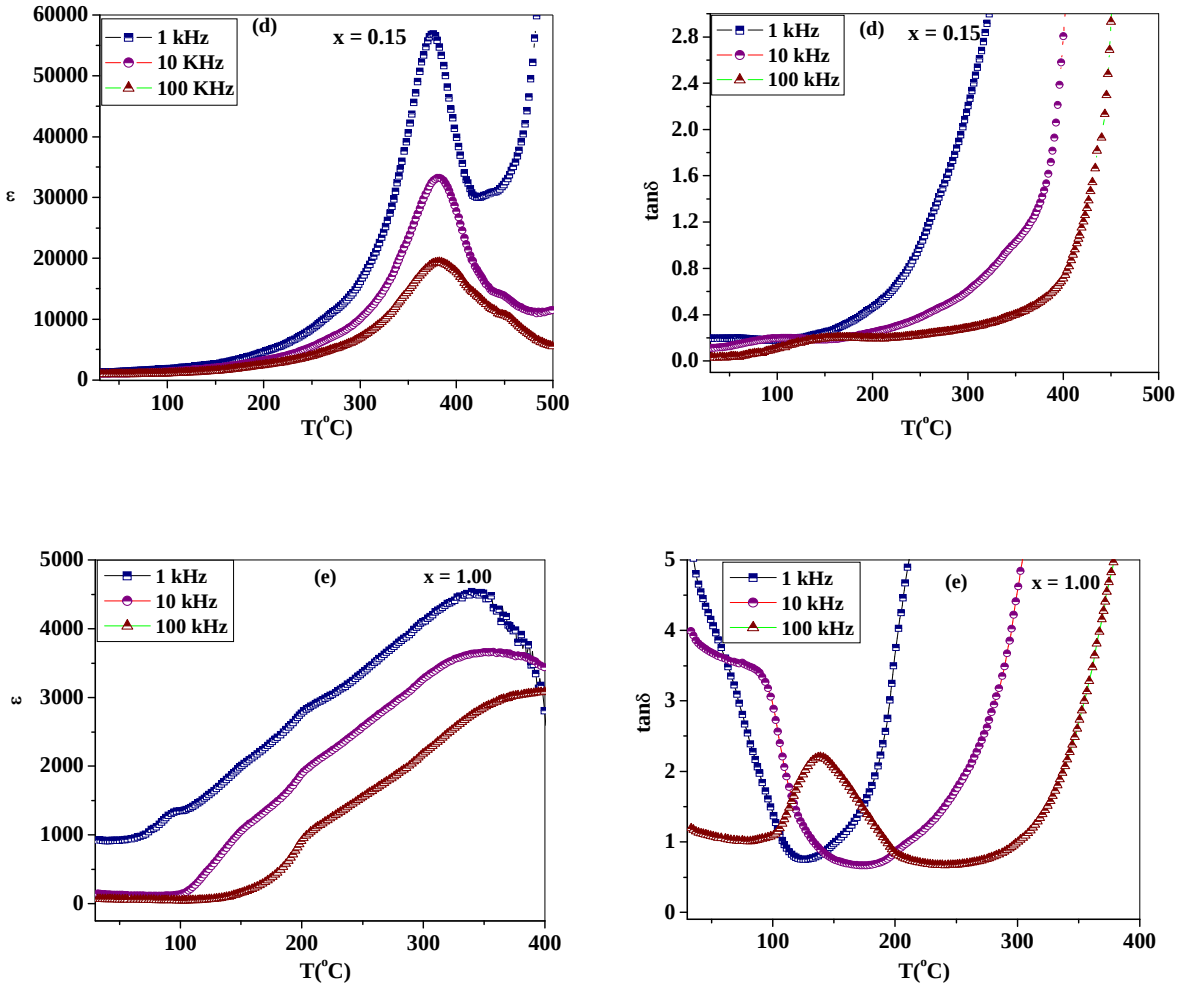

Figure 3.9 Variation of ε and tanδ with temperature for x CFO + (1-x) PZT composite (a) x = 0.00, (b) x= 0.05, (c) x= 0.10 and (d) x = 0.15 and (e) x = 1.00 measured at different frequencies (1 kHz, 10 kHz, 100 kHz)

Table 3.5 Variation of Dielectric Parameters at 100 kHz for all values of x

Parameters / **x**	ε_{RT}	T_c (^oC)	ε_{max}	$tan\delta_{RT}$	$tan\delta_{max}$
0.00	1010	430	34460	0.017	0.14
0.05	1055	373	12920	0.008	0.30
0.10	1235	387	20860	0.021	0.45
0.15	965	383	19385	0.030	0.55

The comparative study of dielectric constant (ε) and loss (tanδ) with temperature for samples except x = 1.00 at 100 kHz is shown in Figure 3.10. Room temperature dielectric constant (ε_{RT}), Curie temperature (T_c), room temperature loss tangent ($tan\delta_{RT}$), dielectric constant at T_c (ε_{max}) and loss tangent at T_c ($tan\delta_{max}$) at 100 kHz for all samples are given in Table 3.5. Room temperature dielectric constant increases with addition of 5% and 10% ferrite phase into 95% and 90% of ferroelectric phase, but decreases for 15% composite. The variation of dielectric constant with temperature is due to electron hoping in CFO phase. The Curie temperature and dielectric constant (at Curie temperature) are found to decrease in composite samples in comparison to pure PZT. In composite sample (x = 0.10), Curie temperature and dielectric constant (at Curie temperature) is found to increase which is due to fact thatthe electric field induced change in magnetization state depends on the strength of interaction between electric and magnetic ordering, which in turn depends on the molar ratio of phases that is why, Curie temperature of samples decreases [21]. The addition of ferrite phase in the ferroelectric phase dilutes the ferroelectric properties of the composites, resulting in the reduction of the dielectric constant and broadening of the peak.

The variation of dielectric loss (tanδ) as a function of temperature for the composites is shown in Fig. 3.10 (b).Dielectric loss is lower at lower temperature and then increases with further increase in temperature. The value of dielectric loss increases with temperature due to space charge conduction,which is related with transport of defects such as oxygen vacancies to

the electrode – dielectric interface [22]. Loss also increases with increase in ferrite content. Higher value of loss tangent is observed in paraelectric region, this may be due to thermal electrical conductivity losses which occur due to presence of ferrite and similar behavior for same materials has been reported by other researchers [14, 23].

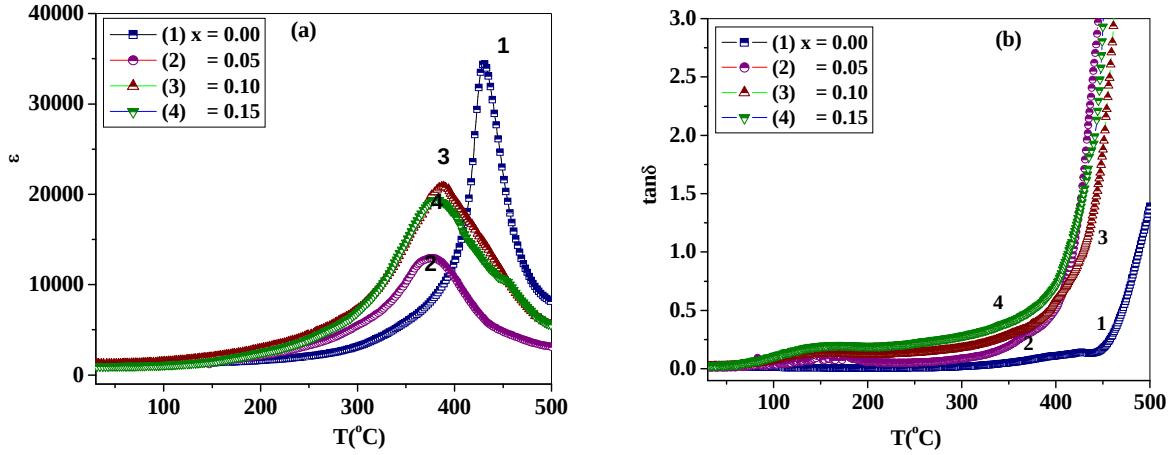

Figure 3.10 Comparison of Variation of Dielectric Properties ((a) dielectric constant and (b) tangent loss)with temperature at 100 kHz for (x)CFO-(1-x) PZT Composites (x = 0.00, 0.05, 0.10 and 0.15)

3.3.4 Ferroelectric Properties

To study the ferroelectric behavior of the composites, P-E Hysteresis loops for all samples were recorded at different electric field values (15 kV – 25 kV) at room temperature as shown in Figure 3.11. The ferroelectric hysteresis loop confirm the existence of ferroelectric structure. From this figure, Hysteresis loops for x = 0.05 and 0.10 confirmed the ferroelectric nature while for x = 0.15 loops are not well saturated as compared to other composites (x = 0.05 and 0.10) which may be due to presence of higher amount of ferrite resulting into increase in leakage of charges as compared to ferroelectric phase [24]. From the Figure, it is also observed that with increase in field, ferroelectric parameters (remanant polarization, coercive field and saturation polarization) increase. This arises due to alignment of domains with increase in field. As applied electric field increases from 15kV/cm to 25 kV/cm, there is increase in P_r from 2.3

$\mu C/cm^2$ to 6.4$\mu C/cm^2$, $P_s$from 6.3$\mu C/cm^2$ to 24.86$\mu C/cm^2$and E_c from 5.1 kV/cm to 8.12 kV/cm for x = 0.05 composite sample. Similarly for other samples, values of ferroelectric parameters increase with increase in field. With increase in electric field, area under the loop increases. This can be related to losses present in the samples which is due to the presence of ferrite content in the composite.

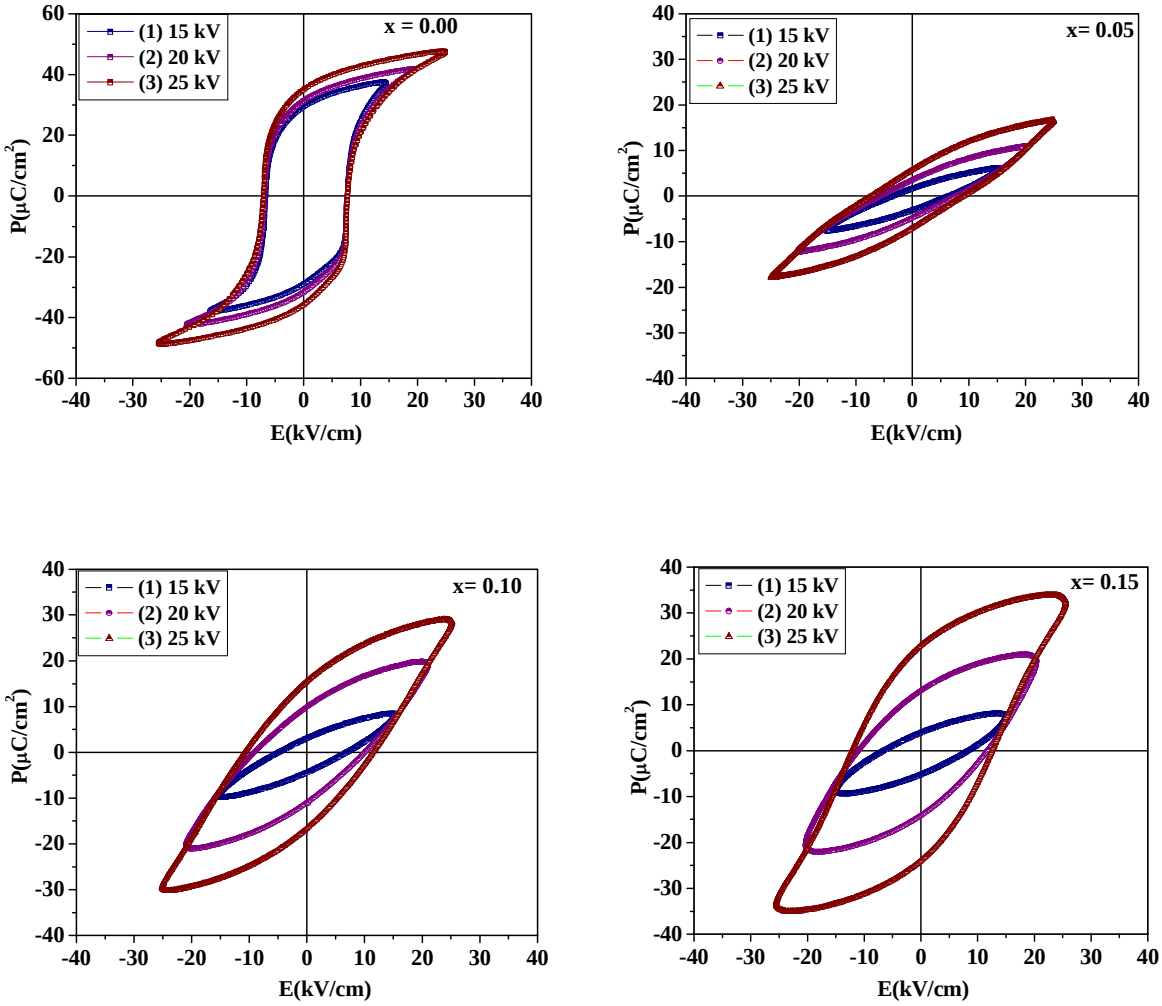

Figure 3.11 Ferroelectric P-E Hysteresis loop for all samples at different electric fields (15kV – 25kV)

A comparative study of ferroelectric hysteresis loops at 25 kV as shown in Figure 3.12. Ferroelectric parameters for all samples are given in Table 3.6. It is observed that in composite samples, value of polarization (P_r and P_s) increases with increase in the value of x. Ferrite phase (CF) has higher dielectric loss in comparison to pure PZT as we have already observed in

dielectric properties. Due to high tangent loss and space charge polarization in composites increases the polarization value of the samples.It is observed that the loops for composite samples are slightly asymmetric and this asymmetry increases with increase in ferrite content (x) which may be due to internal bias field developed in the ferroelectric phase, electrode/PZT interface or due to defects present in the sample [25].The coercivity of composites increases with increase in ferrite content. That may be due tofact that ferrite acts as obstacle to domain wall motion. Thus domain wall motion of the ferroelectric region becomes difficult as the ferrite content increases[23].

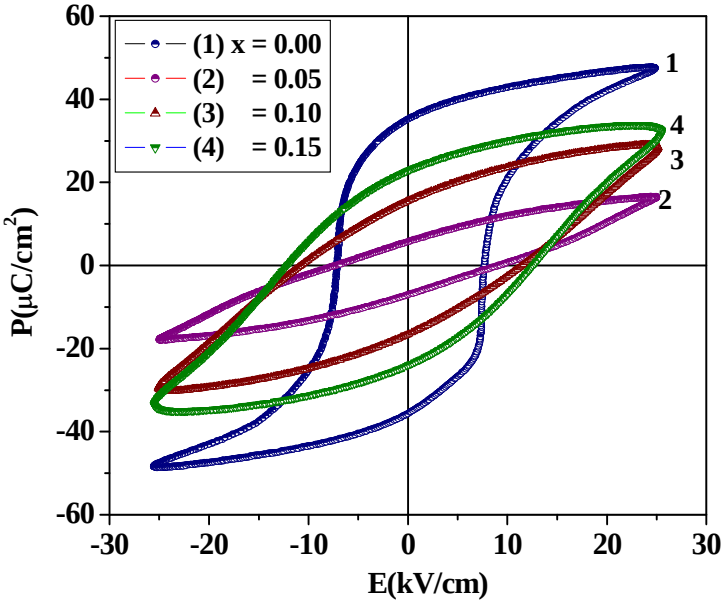

Figure 3.12 Comparisons of P-E Hysteresis Loops at 25°C for (x)CFO-(1-x) PZT Composites (x = 0.00, 0.05, 0.10 and 0.15)

Table 3.6 Ferroelectric Parameters (P_r, E_c and P_s) forall values of x

Parameters / **x**	**P_r ($\mu C/cm^2$)**	**P_s ($\mu C/cm^2$)**	**E_c (kV/cm)**
0.00	15.65	44.67	3.76
0.05	3.20	17.35	6.45
0.10	16.12	29.68	11.11
0.15	23.33	34.57	12.44

3.3.5 Ferromagnetic Properties

Figure 3.13 shows the Magnetic hysteresis loops of all composite samples at room temperature. All samples show well defined ferrimagnetic behavior confirming the existence of magnetic ordering in the composites [26]. The value of remnant magnetization, saturation magnetization and coercive field determined from M-H hysteresis loops are given in Table 3.7. In case of pure ferrite phase, saturation magnetization is 63.38 emu/g, while for composite samples, values of magnetiozation is very low. The magnetic properties of composites are smaller due to small content of ferrite phase.This isdue to the fact that magnetic properties are affected by the presence of non- magnetic ions [27].. In Composite samples, PZT particles act as obstacle thus reducing elastic interaction between the particles which in turn dilutes the magnetic properties in comparison to pure ferrite phase (CF).

The saturation magnetization (M_s) and remnant magnetization (M_r) are found to increase with increase in ferrite content

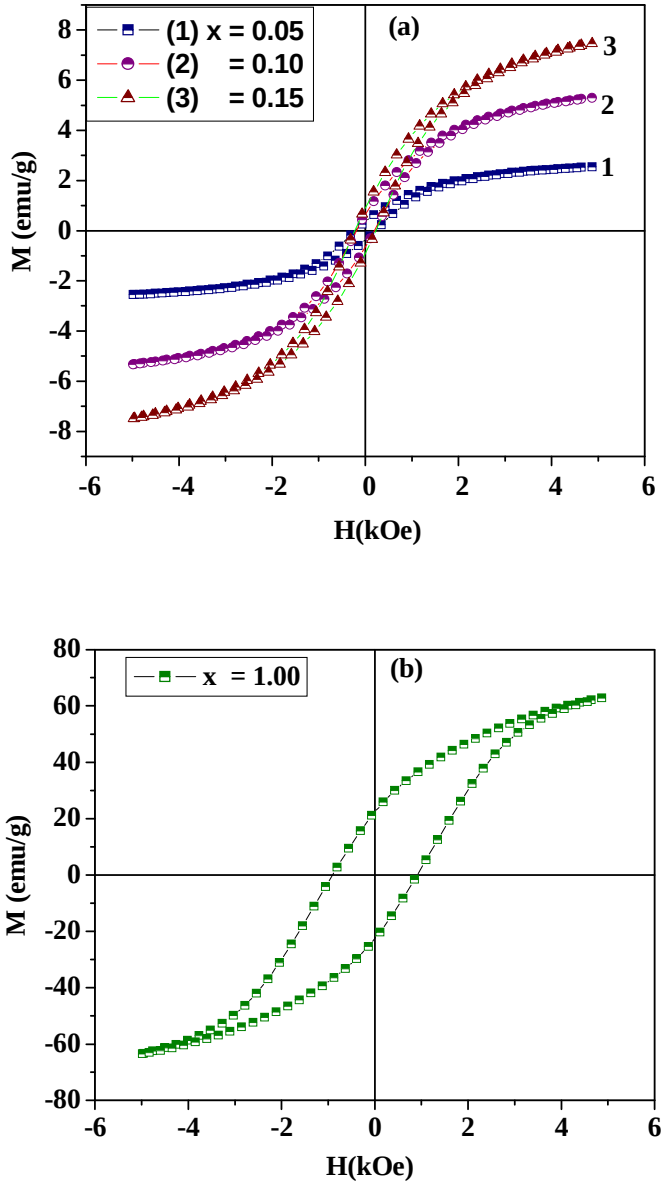

Figure 3.13 Ferromagnetic M-H Hysteresis Curve for (x)CFO-(1-x) PZT Composites (a) (x = 0.00, 0.05, 0.10 and 0.15) and (b) x = 1.00

3.3.6 Piezoelectric Properties

The values of piezoelectric charge coefficient of pure PZT and composite samples are given in Table 3.7. The piezoelectric property depends not only on the dopant concentration but also on the homogeneity, grain size and density of the samples. To determine the piezoelectric

charge coefficient of samples, each piece of composite samples was electrically poled at 15kV/cm in silicon oil bath for 1 hour and then piezoelectric coefficients was measured. The maximum d_{33} value for pure PZT ceramic is 130 pC/Nand with increase in ferrite content d_{33} decreases. This may be due to decreasein ferroelectric content (PZT) [28].This is due to the reason thatresistivity of ferrite phase (CF) is much smaller than that of the ferroelectric phase(PZT) resulting into increase in leakage current which leads to the loss of induced voltage which in turn makes the poling difficult. Hence the piezoelectriccharge coefficient decreases [29].

3.3.7 Magnetoelectric Properties

Magnetoelectric effect is a product property of piezoelectric and piezomagnetic phase. The ME effect depends on the mechanical coupling, resistivity and mole fraction of ferrite (CFO) and ferroelectric phase (PZT) phases in the composites [30].The ME output in ferrite-ferroelectric composites by applying magnetic field is due to the strain induced in ferrite phase (magnetostriction) which results in generation of charge in ferroelectric phase (piezoelectricity).

To determine the magnetoelectric(ME) coupling coefficient (α), the variation of ME coefficient as a function of applied dc magnetic field was studied and shown in Figure 3.14 for x = 0.05 and 0.15. In the present case, AC magnetic field of amplitude 1 Oe and 1 kHz is applied along with DC magnetic field of varying magnitude up to 5 kOe. The ME coefficient(α) was measured using relation [31].

$$\alpha = \frac{V}{H_{ac} \times d} \qquad \ldots\ldots\ldots\ldots\ldots\ldots\ldots\ldots 3.2$$

Where d is the thickness of the sample and H_{ac} is the ac magnetic field.

It is observed that as the applied magnetic field is increases, M-E output increases slowly for lower values of magnetic field due to initial increase in strain in magnetic material and attains a maximum value and then decreases with further increase in field for all samples because After a certain value of applied magnetic field, there is saturation instrain induced lattice distortions resulting in almost constant values of electric field in piezoelectric phase and hence ME coefficient decreases. Similar behavior has been reported by a number of researchers [32-34].The ME values of 298μV/cm.Oe, 389 μV/cm.Oe were observed for composite samples with x = 0.05 and x = 0.15, respectively. Increase in value of ME coefficient for x = 0.15 as compared to x=

0.05 is due to higher ferrite content. The values of ME coefficient (α) for composite samples is given in Table 3.7.

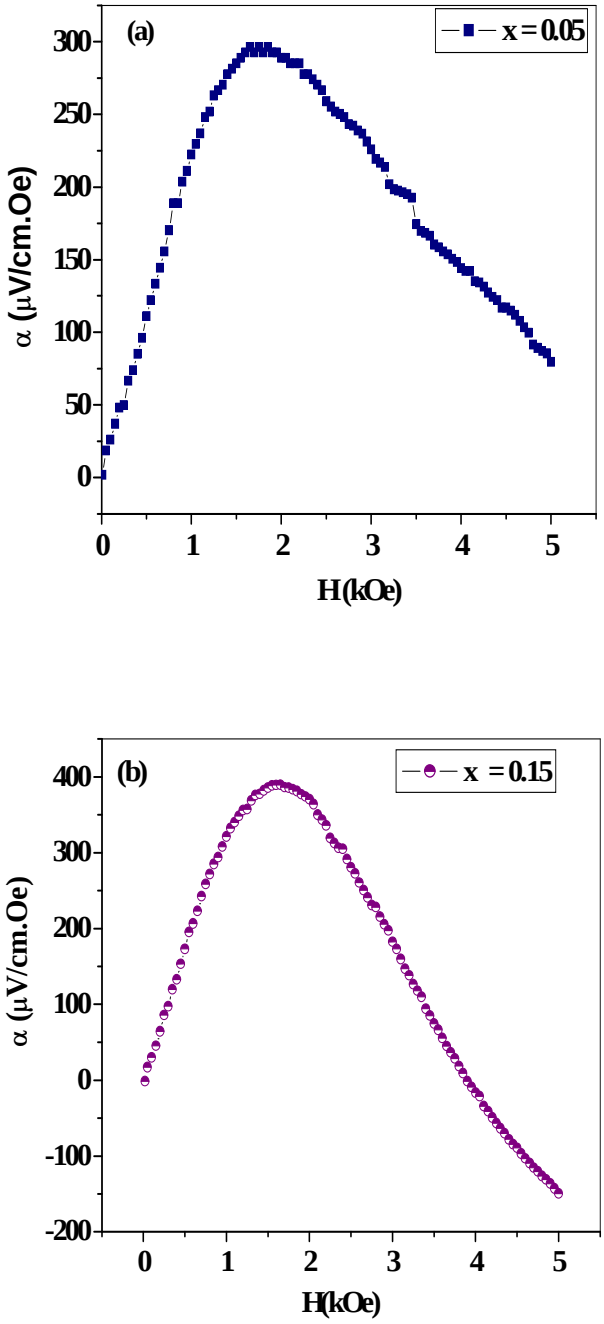

Figure 3.14 Variation of ME coupling coefficient with DC magnetic field for (a) x = 0.05 and (b) x = 0.15

Table-3.7 Magnetic parameters (H_c, M_r andM_s), Magneto-electric Coefficient (α) and Piezoelectric coefficient for (x)CFO-(1-x) PZT Composites (x = 0.00, 0.05, 0.10 and 0.15)

Magnetic Parameters					**Piezoelectric Coefficient**
Parameters / x	**H_c (Oe)**	**M_r (emu/g)**	**M_s (emu/g)**	**α (μV/cm .Oe)**	**d_{33} (pC/N)**
0.00	-	-	-	-	130
0.05	195	0.356	2.56	298	90
0.10	206	0.715	5.29	-	72
0.15	241	0.962	7.49	389	68
1.00	918	22.78	63.38	-	-

References

1. Y. Xu, Ferroelectric Materials and Their Applications, Elsevier Science Pub. Co.; NewYork, USA (1991).

2. S. L. Swartz and T. R. Shrout, Mater. Res. Bull.,**17** (1982) 1245.

3. K. Katayama, M. Abe, T. Akib and H. Yanagida, J. Euro. Ceram. Soc.,**5** (1989) 183.

4. R. Rani, J.K. Juneja, K.K. Raina and Chandra Prakash, J. Ceram. Proc. Res., **13** (2012) 76.

5. W.E. Kramer, R.H. Hopkins and M.R. Daniel, J. Mater. Sci. Lett., **12** (1997) 409.

6. C.G. Koop's, Phys. Rev. B., **83** (1951) 121.

7. J.C. Maxwell, Electricity and Magnetism, Oxfrod University Press, London, (1993) 828.

8. P.Kumar, P. Singh, J.K. Juneja, K.K. Raina, R.P. Pant, Chandra Prakash and S. Singh, J. Alloys. Compd., **601** (2014) 207.

9. N.K. Mishra, R. Sati and R.N.P Choudhary, Mater. Lett., **24** (1995) 313.

10. M.A EI-HiTi, J. Magn. Magn. Mater.,**164** (1996) 187.

11. L.M. Hrib and O.F. Caltun, J. Alloys Comp., **509** (2011) 6644.

12. K.K. Patankar, R.P. Nipankar, V.L. Mathe, R.P. Mahajan and S.A. Patil, Ceram. Int.,**27** (2001) 853.

13. S.A. Lokhare, R.S. Devan and B.K. Chougule, J. Alloys Comp., **454** (2008) 471.

14. R.S. Devan, Y.D. Kolekar and B.K. Chougule, J. Alloys Comp., **461** (2008) 678.

15. S.A. Olofa, J. Magn. Magn. Mater. **131** (1994) 103.

16. S. Bera and R.N.P Choudhary, Mater. Lett. **22** (1995) 197.

17. K.K. Patankar and V.L. Mathe, J. Electroceram., **6** (2001) 115.

18. J. Chen, Z. Xu and X. Lu, Ferroelectrics, **410** (2011) 29.

19. S. Basu, K.R. Babu and R.N.P. Choudhary, Mater. Chem. Phys., **132** (2012) 570.

20. A.P. Barranco, J.D.S.Guerra, R.L. Noda and E.B. Araujo, J. Phys. D: Appl. Phys., **41** (2008) 215503.

21. S. Upadhyay, D. Kumar and O. Prakash, Bull. Mater. Sci., **19** (1996) 513.

22. S. Zhang, S. Priya, T.R. Shrout and C.A. Randall, J. Appl. Phys., **93** (2003) 2880.

23. J. Paledo, G. Grange, R. Goutle and L. Fyrand, J. Phys. D., **7** (1994) 78.

24. X. Chao, Z. Yang, M. Dong and Y. Zhang, J. Magn. Magn. Mater.,**323** (2011) 2012.

25. S.K. Pandey, O.P. Thakur, A. Kumar and C. Prakash, J. Appl. Phys. **100** (2006) 014104.

26. L. Mitoseriu, I. Pallecchi, V. Buscaglia, A. Testino, C.E. Ciomaga and A. Stancu, J.Magn, Magn. Mater.,**316** (2007) e603.

27. S.A. Lokre, D.R. Patil and B.K. Chougule, J. Alloys Compd., **453** (2008) 58.

28. R. A. Islam and S.Priya, Integr. Ferroelectr., **82** (2006) 1

29. D. Wu, W. Gong, H. Deng and M.Li, J. Phys. D: Appl. Phys., **40** (2007) 5002.

30. B.K. Bammannavar, L.R. Naik and B.K Chougule, J. Appl. Phys., **104** (2008) 064123.

31. R. Grossinger, G.V. Dong and R. Sato-Turtelli, J. Magn. Magn. Mater.,**320** (2008) 1972.

32. R.F. Zhang, C.Y. Deng, L. Ren, Z. Li and J.P. Zhou, Mater. Res. Bull.,**48** (2013) 4100.

33. K. Sadhana, S.R. Murthy, S. Jei, Y. Xie and Y. Lui, J. Appl. Phys., **113** (2013) 17C731.

34. R.A. Kunale, R.H. Kadam and D.R. Mane, Int. J. Adv. Res. Tech., **2** (2013) 37.

Chapter – 4

Synthesis and Characterizations Of CNFO-PZT Composites

Chapter-IV

Synthesis and Characterization of CNFO-PZT Composites

The studies on structural, micro-structural, dielectric, ferroelectric, ferromagnetic and magnetoelectric properties of (x) CNFO - (1-x) PZT composites are discussed in this chapter. PZT and Ni doped $CoFe_2O_4$ were prepared by solid state reaction route. Formation of the phases was confirmed by XRD analysis and microstructure was studied by recording SEM micrographs of the broken samples. Dielectric properties were studies as a function of frequency and temperature and Curie temperature was determined from ε vs. T plots. In order to study ferroelectric and ferromagnetic behavior, P-E and M-H hysteresis loops were recorded. Magnetoelectric coefficient was determined from measurement of electric signal via applied magnetic field. The results are discussed in detail in this chapter.

4.1 Synthesis of Composites

The composite samples were synthesized by conventional solid state reaction as per details given in section 3.1 (chapter III). For the synthesis of ferrite phase, $Co_{0.8}Ni_{0.2}Fe_2O_4$ (CNFO), AR grade $CoCo_3$, NiO and Fe_2O_3 were used as raw materials and weighed in required molar proportions. The mixing process was carried out by ball milling using distilled water as milling media and Zirconia balls as grinding media. After ball milling and drying, the powder mixture was calcined at 900^{o}C for 4 hrs. After calcination, the powder was again ball milled followed by drying. The dried powder mixture was recalcined at 950^{o}C. Details of synthesis of ferroelectric phase, PZT are given in Chapter 3.

(x) $Co_{0.8}Ni_{0.2}Fe_2O_4$ – (1-x) $PbZr_{0.55}Ti_{0.45}O_3$ with x = 0, 0.05, 0.10, 0.15 were prepared by mixing the two phases in desired ratio. Powder mixture was ball milled in ball mill using distilled water and zirconia balls. After drying, the powder was mixed with small amount of diluted polyvinyl alcohol (3% by weight) as binder. This dried mixture was uniaxially pressed into pellets having 15 mm diameter and 1 mm thickness. The pellets were finally sintered in a programmable furnace at optimized temperature i.e. 1150^{o}C for 4 hrs with heating rate of 5^{o}C/min.

After sintering, experimental density of the samples was determined using Archimedes principle. Theoretical density of the samples was calculated using the lattice parameters. XRD was done using Bruker AXS D8 Advance computer controlled powder X- ray Diffractrometer in a range of Bragg angles ($20^o \leq 2\theta \leq 70^o$) with step size of 0.02^o. The micro structures of freshly broken sintered samples were studied by scanning electron microscope (JEOL JSM 6510LV, Japan). For measuring electrical properties, the sintered pellets were mechanically lapped on the glass surface and then electroded using silver epoxy and subsequently heated at 400^{o}C for 30 min to ensure good ohmic contact. The dielectric properties of the samples as a function of temperature at discrete frequencies were measured using HIOKI 3532-50 LCR meter and room temperature measurement of dielectric constant (ε) and loss tangent ($\tan\delta$) as a function of ac frequency (100Hz to 1MHz) were measured by same meter. The ferroelectric nature of the composite samples was analyzed using an automatic PE loop tracer system (Marine India Pvt. Ltd.). Electrical poling was done at 100^{o}C -120^{o}C in silicon oil bath by applying electric field of ~15kV/cm for 1 hr. Then the samples were allowed to cool up to room temperature by switching

off the heater in applied electric field and then the field was removed. Magnetic properties were recorded by using a Lake shore 735 Vibrating Sample Magnetometer (VSM) Controller, Model 662, interfaced with a computer. The magnetoelectric signal (voltage) was measured as a function of increasing DC magnetic field (0–5000 Oe) using 7265 DSP lock-in amplifier in the presence of small AC magnetic field (H_{ac} = 1Oe). Electric voltage (V) was noted from lock in amplifier and magnetoelectric coupling coefficient (μV/cm.Oe) was calculated using formula:

$$\alpha = \frac{V}{H_{ac} \times d} \qquad \text{.....4.1}$$

Where d is the thickness of the sample and H_{ac} is the AC magnetic field.

4.2 Effect of Ni Substitution in Co-Ferrite

In this section, comparative studies on DC resistivity, structural and magnetic properties of $CoFe_2O_4$ and Ni doped $CoFe_2O_4$ are discussed.

4.2.1 Characterization of $CoFe_2O_4$ and $Co_{0.8}Ni_{0.2}Fe_2O_4$

4.2.1.1 XRD

Phase analysis of both samples was done using XRD analysis. XRD pattern of both samples i,e. $CoFe_2O_4$ and Ni doped $CoFe_2O_4$ is shown in Figure 4.1. The analysis shows that XRD patterns for samples have well defined diffraction peaks with specific indices confirming cubic spinel structure. Both samples show all the characteristic peaks of ferrites with most intense peak (311). Most intense peak of Ni doped $CoFe_2O_4$ shift towards lower angle side due to lower ionic radii of Ni^{2+} (0.69 Å) as compared to Co^{2+} (0.74 Å) as shown in inset of Figure 1.

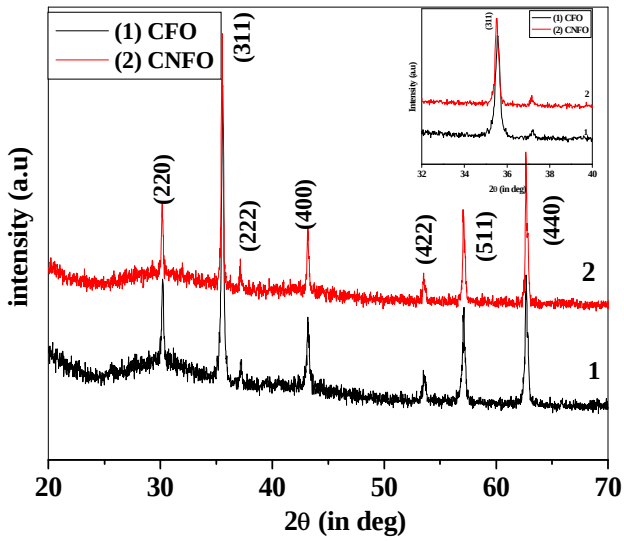

Figure 4.1 XRD pattern of $CoFe_2O_4$ and Ni doped $CoFe_2O_4$ samples.

4.2.1.2 DC Resistivity:

The temperature variation of DC resistivity of $CoFe_2O_4$ and Ni doped $CoFe_2O_4$ sample is shown in Figure 4.2. Both samples show decrease in resistivity with increase in temperature which corresponds to semiconducting behavior of the materials. The decrease in resistivity with increase in temperature may be due to increase in drift mobility of the charge carriers [1]. The resistivity of ferrite can be explained on the basis of cation distribution in spinel structure (AB_2O_4). The resistivity of ferrite is controlled by the Fe^{2+} concentration at B-site. With substitution of Ni in $CoFe_2O_4$, Ni^{2+} ions occupy the octahedral site B, while Co^{2+} and Fe^{3+} ions occupy both the A and B sites. When Ni^{2+} is substituted at A site, Co^{2+} ion concentration decreases which causes the shifting of ion from B to A site. As a result, the number of Fe^{3+} and Fe^{2+} ions at the B sites decreases resulting in increase in resistivity [2]. From this figure, it is also observed that Ni doped $CoFe_2O_4$ has high resistivity as compared to $CoFe_2O_4$ which results in high magnetoelectric properties.

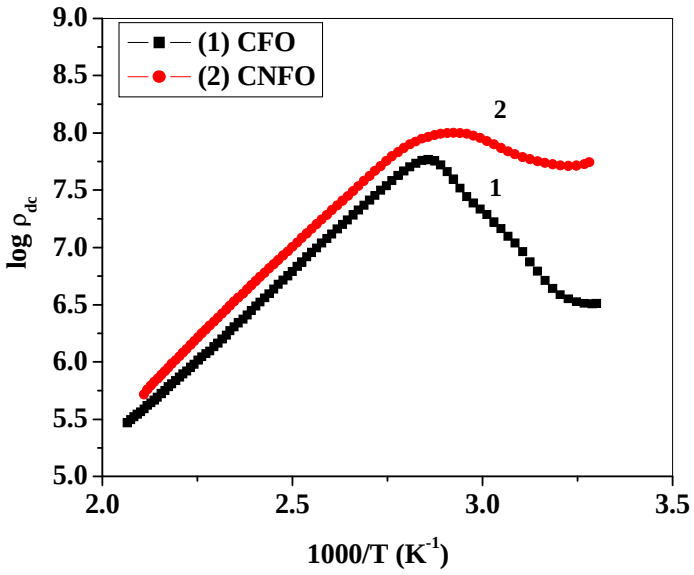

Figure 4.2 Variation of DC resistivity with temperature for $CoFe_2O_4$and Ni doped $CoFe_2O_4$ samples.

4.2.1.3 Magnetic Properties:

The M-H hysteresis loops for both the samples are shown in Figure 4.3. The magnetic properties of the inverse spinal structure can be explained in terms of the distribution of cations and the magnetization. In case of Ni doped $CoFe_2O_4$, Ni^{2+} ions occupy octahedral sites in place of Co^{2+}, while Co^{2+} and Fe^{3+} ions occupy both octahedral as well as tetrahedral sites [3]. The magnetic moment per ion for Ni^{2+} (2μB) is smaller than that for Co^{2+} ion (3μB) which results in the reduction in the magnetization of Ni doped $CoFe_2O_4$ sample. From M-H hysteresis loops, it is also observed that remnant magnetization and coercive field of Ni doped $CoFe_2O_4$ sample decreases which are suitable for recording media.

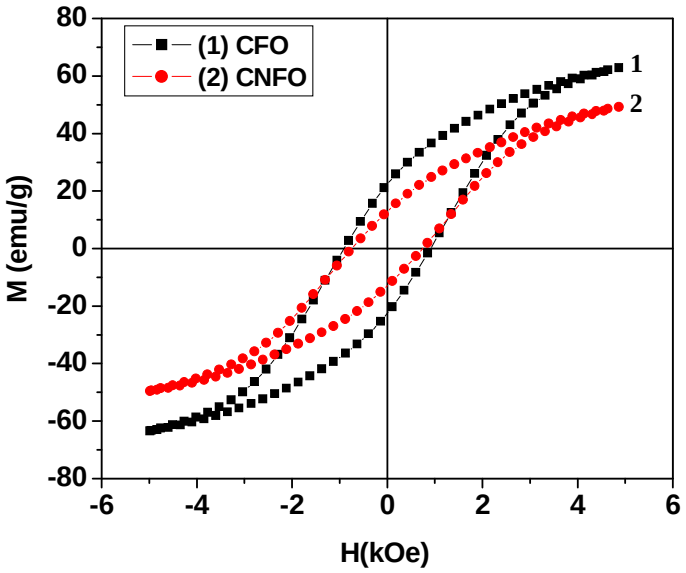

Figure 4.3 M-H Hysteresis loops of $CoFe_2O_4$ and Ni doped $CoFe_2O_4$ samples.

From above results it can be concluded that Ni substitution in $CoFe_2O_4$ not only increases the resistivity of the sample but also helps to measure the magnetoelectric properties of composites as discussed in following section.

4.3 Characterization of CNFO-PZT Composites

The properties of magnetoelectric composites depend on the molar ratio of constituent phases and resistivity of the both the phases. Here, the effect of CNFO on structural, electrical, ferroelectric, piezoelectric and magnetic properties of PZT is discussed.

4.3.1 X-Ray Diffraction

Figure 4.4 shows XRD diffraction patterns for all the samples with x = 0.00, 0.05, 0.10, 0.15 and 1.00. The XRD patterns for x = 0.00 (PZT) and x = 1.00 (Ni doped $CoFe_2O_4$) shows well defined peaks of perovskite tetragonal structure and spinel structure respectively. In composite samples (x = 0.05, 0.10 and 0.15) these XRD pattern confirm the co-existence of both perovskite

structure (ferroelectric phase) and spinel cubic structure (ferrite phase). No extra peaks were observed in XRD pattern which confirms that no chemical reaction has taken place between the two constituent phases during sintering. Intensity of diffraction peaks depends on the amount of ferrite and ferroelectric content in the composites. The intensity of ferrite peak increases with increase in ferrite content in the composite [4].

Calculated values of the lattice parameters for both the phases are given in Table 4.1. The ferroelectric phase has lattice constant a = 4.081 Å and c = 4.129 Å and ferrite phase with lattice parameter a = 8.375 Å. From table, we have seen that there is slight variation in lattice parameters of both phases of composite samples. This may be due to stress exerted on each other by the two phases [5].

Experimental, x-ray and relative density for all the samples were calculated and given in Table 4.1. From table it is observed that the relative density of composite samples is lower as compared to PZT. This is due to low density of CNFO (x = 1.00) in the composite. However, the composite with x = 0.10 has slightly higher value of relative density and that may be due to better compaction and sinterability [6].

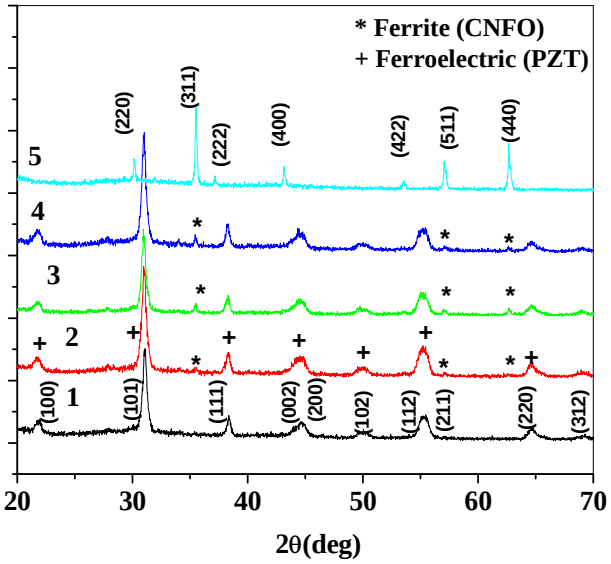

Figure 4.4 X-Ray diffraction for x CNFO + (1-x) PZT (1) x = 0.00 (PZT) (2) x = 0.05 (3) x = 0.10 (4) x = 0.15 and (5) x = 1.00 (CNFO)

Table 4.1 Structural Parameters of (x) CNFO-(1-x) PZT composites

Parameters / x	Ferrite (a) (Å)	Ferroelectric a (Å)	Ferroelectric c (Å)	d_{exp} (g/cc)	d_{th} (g/cc)	Relative Density (%)	Average Grain Size (µm)
0.00	-	4.081	4.129	7.56	8.01	94.4	4.7
0.05	8.409	4.042	4.067	7.12	8.00	88.9	0.99
0.10	8.390	4.0542	4.073	6.99	7.81	89.5	0.92
0.15	8.377	4.0585	4.081	6.85	7.64	89.5	0.88
1.00	8.375	-	-	4.280	5.26	80.8	1.2

4.3.2 Scanning Electron Micrograph (SEM)

Since electrical and magnetic properties of both the constituent phases ferrite and ferroelectric strongly depend on the microstructure so it is necessary to observe the scanning electron microscope and to determine the average grain size. Scanning electron micrograph of freshly broken surfaces for all the sintered samples are shown in Figure 4.5. The shape, size and distribution of grains confirm the polycrystalline nature. As seen in the micrograph, for pure PZT, grain size is larger in comparison to composite samples. The average grain size of the samples were calculated using linear intercept method and the values are given in Table 4. 1. As observed from the Table that the average grain size of ferroelectric phase is larger as compared to ferrite phase. The average grain size decreases with addition of ferrite which may be due to difference in grain size of the constituent phases. Grains of the constituent phases cannot be distinguished individually due to low concentration of ferrite phase.

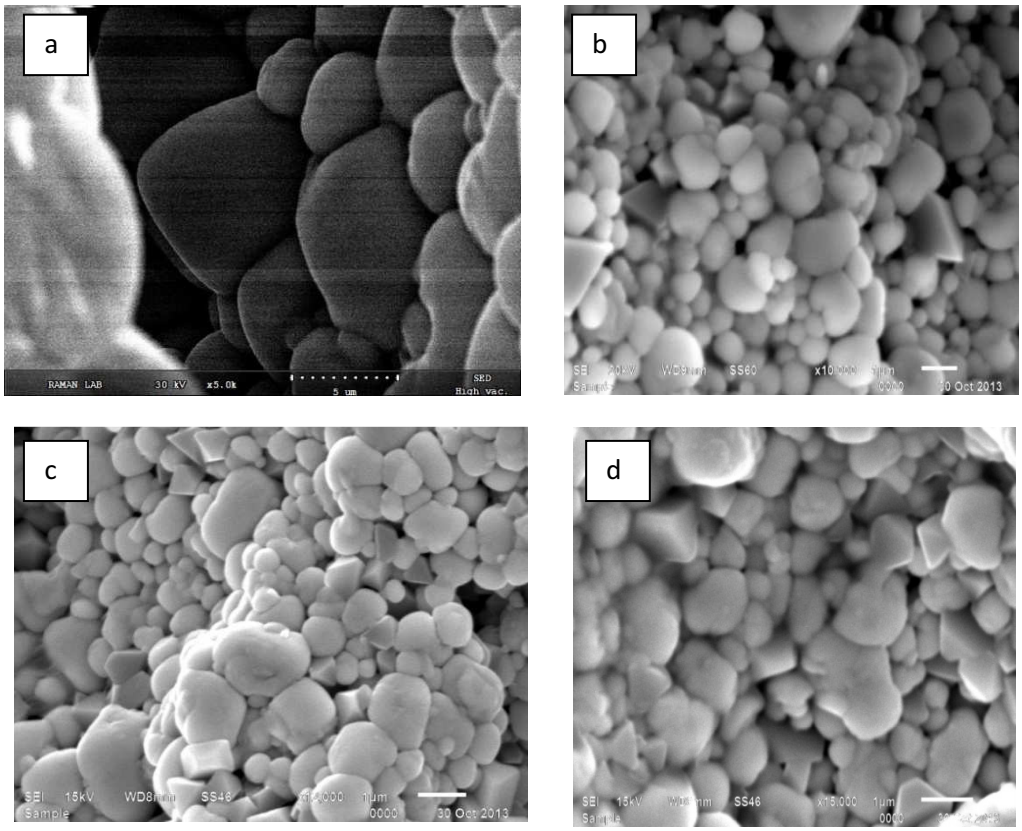

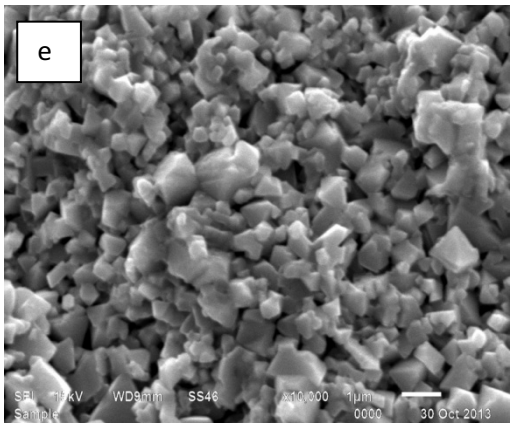

Figure 4.5 SEM Micrographs for x CNFO - (1-x) PZT (a) x = 0.00 (PZT) (b) x = 0.05 (c) x = 0.10 (d) x = 0.15 and (f) x = 1.00 (CNFO)

4.3.3 Dielectric Properties

The variation of dielectric constant and dielectric loss with frequency and temperature for all samples are discussed here.

4.3.3.1 Frequency Dependence of Dielectric properties

Dielectric measurements (dielectric constant and loss tangent) of constituent phases and composites as a function of frequency (100 Hz – 100 kHz) at room temperature were done and are shown in Figure 4.6(a) and 4.6(b). It is clear from the figure 4.6(a) that dielectric constant decrease rapidly with increase in frequency and then reaches a constant value for all samples. The large values of dielectric constant at lower frequencies are associated with space charge polarization and inhomogeneous dielectric structure. The inhmogeneities in the samples are impurities, grain structure and pores [7]. In composites, higher value of dielectric constant may be due to the fact that ferroelectric grains are surrounded by non ferroelectric grains which give rise to interfacial polarization [8]. Dielectric dispersion is also observed at lower frequencies. The dispersion at lower frequencies can also be explained by Maxwell Wagner type interfacial polarization in agreement with Koop's phenomenological theory [9-11]. The values of dielectric constant rapidly decrease with further increase in frequency and remain constant at higher frequencies. At higher frequencies, ionic and orientation polarization decreases. Beyond the external field, the electron exchange between Fe^{2+}/ Fe^{3+} cannot follow the alternating field and

hence reaches a constant value. Similar type of behavior has also been reported by various researchers [12-14].

Further in composites, it is observed that the values of dielectric constant at room temperature increase up to x = 0.10 and after that it decrease. The increase in dielectric constant may be due to increase in interfacial polarization at grain boundaries. With increase in ferrite content, resistivity of the composite sample (x = 0.15) decreases resulting into decrease in polarization hence dielectric constant decreases [15].

Figure 4.6 (b) shows the variation in loss tangent with frequency for the composites at room temperature. Variation in tanδ for all composites is similar to the variation in έ with frequency. Loss tangent is higher at lower frequencies and it decreases with increase in frequency. High value of loss factor is observed due to domain wall resonance at lower frequencies. It is also observed that loss increases with increase in ferrite content. This may be due to low resistivity of ferrite CNFO in comparison to ferroelectric which would produce leakage path for stored charge carriers [16].

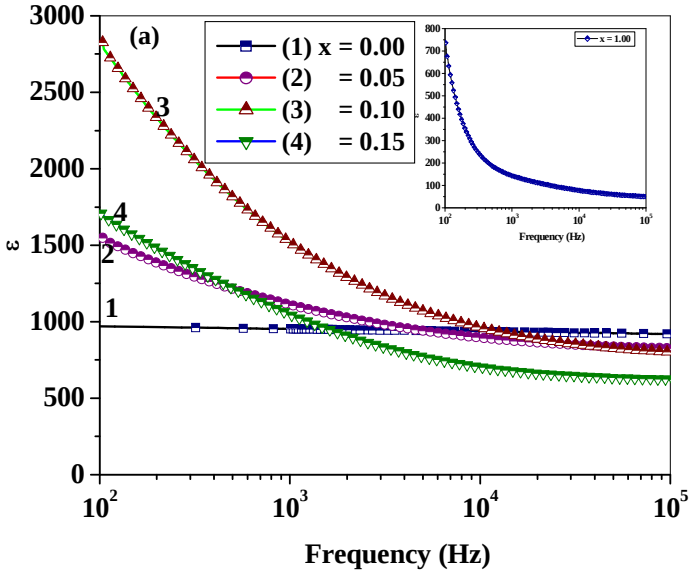

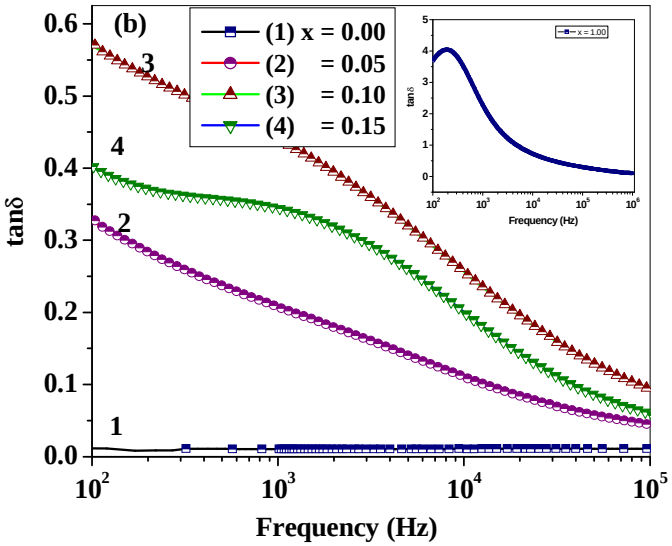

Figure 4.6 (a) Variation of Dielectric Constant with frequency at room temperature for all samples (b) Variation of dielectric loss with frequency for all samples.

AC conductivity is an important property of material which reveals the conduction mechanism, types of polaron responsible for conduction. AC conductivity at room temperature was determined in the frequency range (100 Hz- 100 kHz) from measured dielectric data. Figure 4.7 shows the variation of AC conductivity with frequency at room temperature. The plots are almost linear indicating that conductivity increases with frequency. From this figure it is clear that conductivity of composite samples is high as compared to ferroelectric phase due to presence of ferrite phase. The conduction mechanism in ferrite, ferroelectric and their composites can be explained by polaron hopping process [17]. The conduction in the composites is due to small polaron hopping [18, 19].

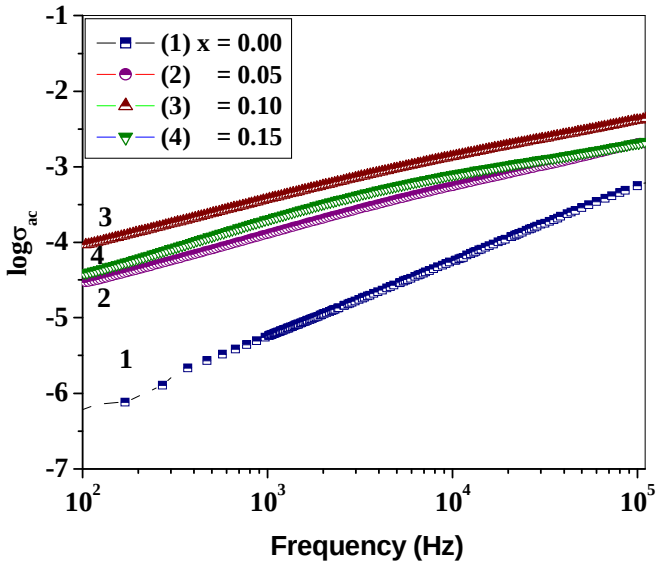

Figure 4.7 Variation of AC Conductivity with Frequency at 100 kHz for x CNFO-(1-x) PZT Composites (x = 0.00, 0.05, 0.10, 0.15 and 1.00).

4.3.3.2 Temperature dependence of dielectric properties

Figure 4.8 (a-e) shows the variation of dielectric constant and loss tangent with temperature (30^{o}C - 500^{o}C) at different frequencies (1 kHz, 10 kHz and 100 kHz) for all samples. Dielectric Constant was calculated using the relation $\varepsilon = Ct / \varepsilon_0 A$, where C is the capacitance, t is the thickness of the pallet, A is the area of the electrode surface of the pallet and ε_0 is the permittivity of free space (8.85×10^{-12} F/m). From these figures, it is observed that the dielectric constant increases with increase in temperature up to particular temperature and after that decreases. With increase in temperature, the mobility of charge carrier increases, hence conductivity and polarization of samples also increases with increase in temperature resulting in increase in dielectric constant [20]. It is also observed that the region around dielectric peak get broadened in composites, which may be due to the microscopic heterogeneity of the composites due to presence of two phases [21]. From figure, it is also observed that in paraelectric region, there is an increase in the dielectric constant with increase in the temperature for all samples but with an increase in the measurement frequency, values of dielectric constants gradually decreases. This may be due to a low frequency relaxation process [22]. This increase in dielectric

constant at high temperatures is due to an increase in the dielectric polarization which is a result of thermally-activated electron hopping between $Fe^{+2} \leftrightarrow Fe^{+3}$ ions as well as $Ni^{+2} \leftrightarrow Ni^{+3}$ ions present in the ferrite phase.

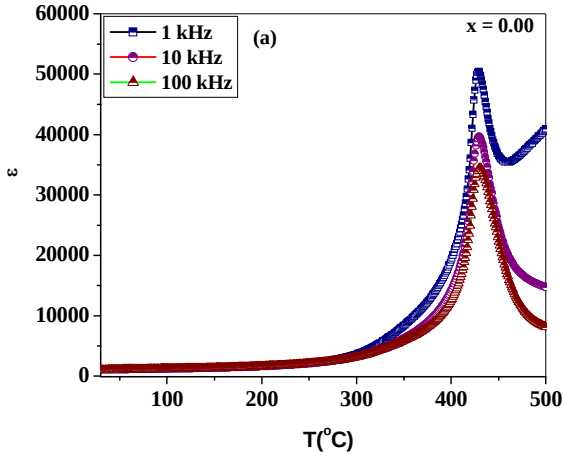

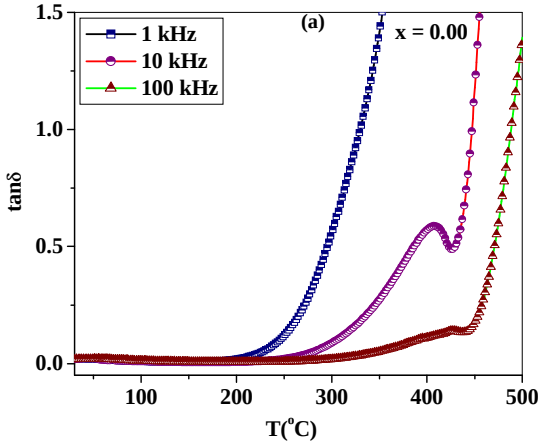

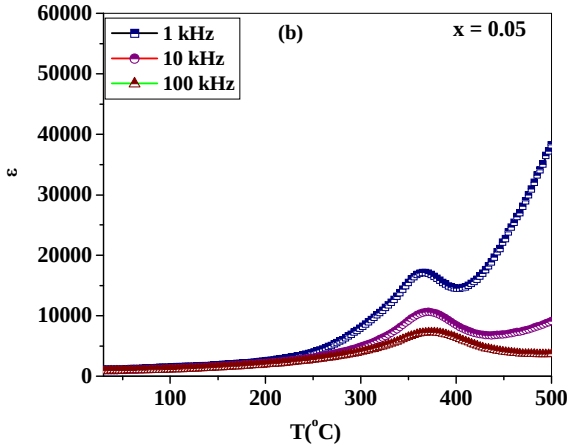

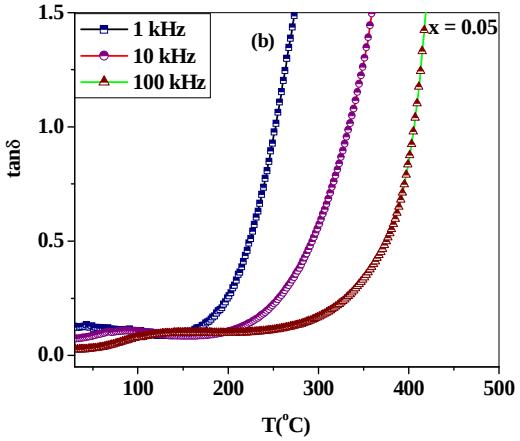

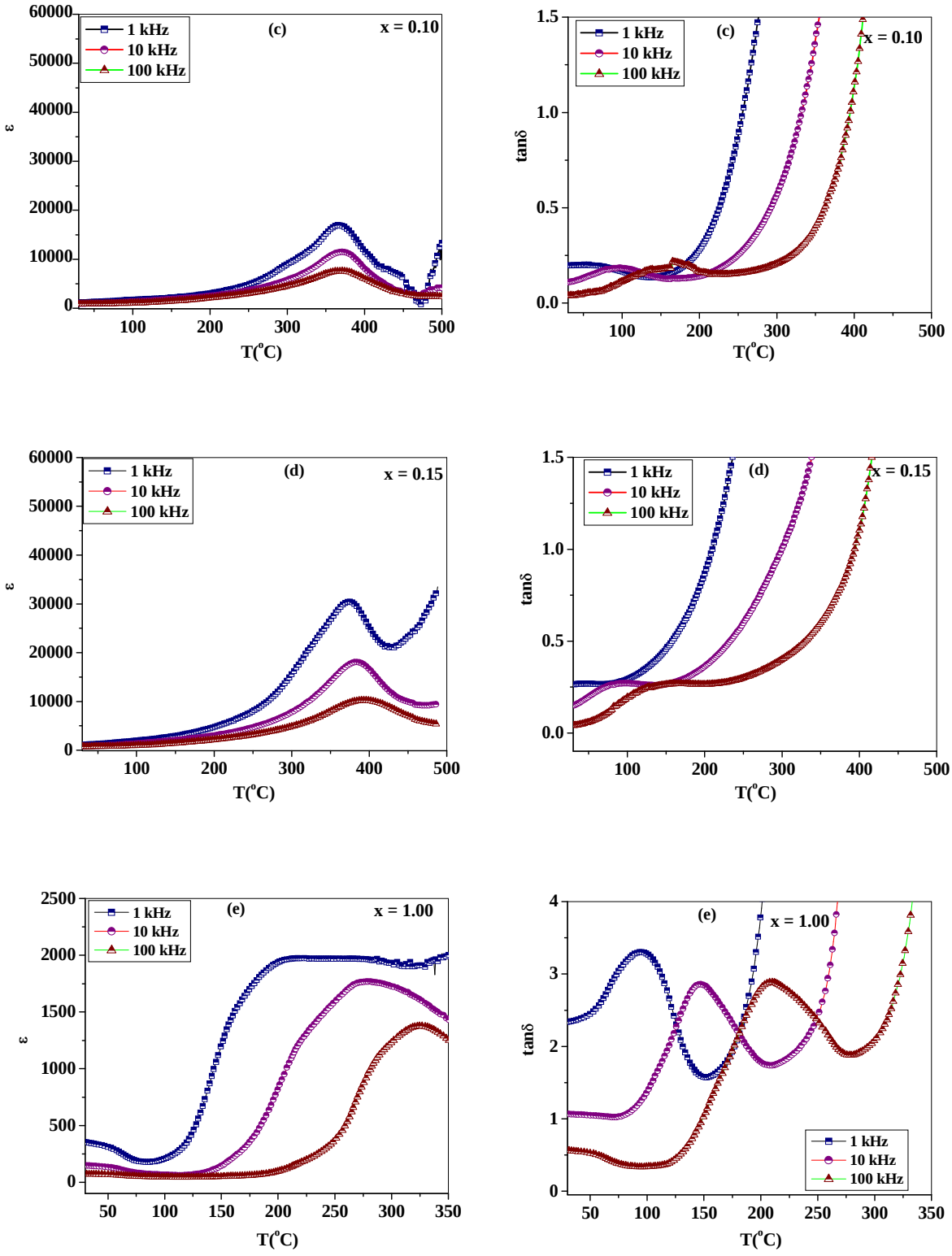

Figure 4.8 Variation of ε and tanδ with temperature for x CNFO + (1-x) PZT composite (a) x = 0.00, (b) x= 0.05, (c) x= 0.10 and (d) x = 0.15 and (e) x = 1.00 at different frequencies (1 kHz, 10 kHz, 100 kHz)

Table 4.2 Variation of Dielectric Parameters (ε_{RT}, T_c (^oC), ε_{max}, $\tan\delta_{RT}$, $\tan\delta_{max}$) at 100 kHz for all values of x

Parameters / **x**	**ε_{RT}**	**T_c (^oC)**	**ε_{max}**	**$\tan\delta_{RT}$**	**$\tan\delta_{max}$**
0.00	1025	430	34460	0.01	0.14
0.05	930	373	7275	0.02	0.47
0.10	895	370	7595	0.04	0.58
0.15	760	393	10240	0.04	0.99

A comparative study of dielectric constant and loss (tanδ) with the temperature for all samples at 100 kHz is shown in Figure 4.9. The values of room temperature dielectric constant (ε_{RT}), Curie temperature (T_c), room temperature loss tangent ($\tan\delta_{RT}$), dielectric constant at T_c (ε_{max}) and loss tangent at T_c ($\tan\delta_{max}$) at 100 kHz for all samples are given in Table 4.2. It is observed from table that room temperature dielectric constant decreases with increase in ferrite content. This decrease in dielectric constant may be attributed to Ni substitution in $CoFe_2O_4$ phase. It is reported that Ni is well known for improving electrical resistivity of soft ferrites and dielectric constant decreases when resistivity of soft ferrites increases. It is also observed that the Curie temperature of composites changes with the change in ferrite content. This may be due to the fluctuation in the compositions in the micro regions [23]. Curie temperature is found to decrease with increase in ferrite content up to x = 0.10 and then increases for x = 0.15. T_c shifts towards the higher temperature side with ferrite content (x = 0.15). This may be due to the presence of two types of charge carriers (p and n type). The presence of Ni^{3+} / Ni^{2+} and Co^{3+} / Co^{2+} ions give rise to p- type charge carriers. Since the mobility of p type carriers is smaller than that of n type carriers, then it is assumed that their contribution to polarization appears only at high temperatures [24]. The dielectric constant at Curie temperature (ε_{max}) decreases with ferrite content (x = 0.05) [25] and then increases with increase in ferrite content. This may be due to the reason that the conduction in ferrite due to electron exchange and polarization in ferroelectric

influences the dielectric polarization of composites. Value of dielectric loss also increases with temperature. Due to the presence of ferrite phase, higher value of loss tangent is observed in paraelectric region. This loss is higher due to thermal conductivity losses at higher temperature and similar behavior of these materials has been reported by other researchers [26, 27].

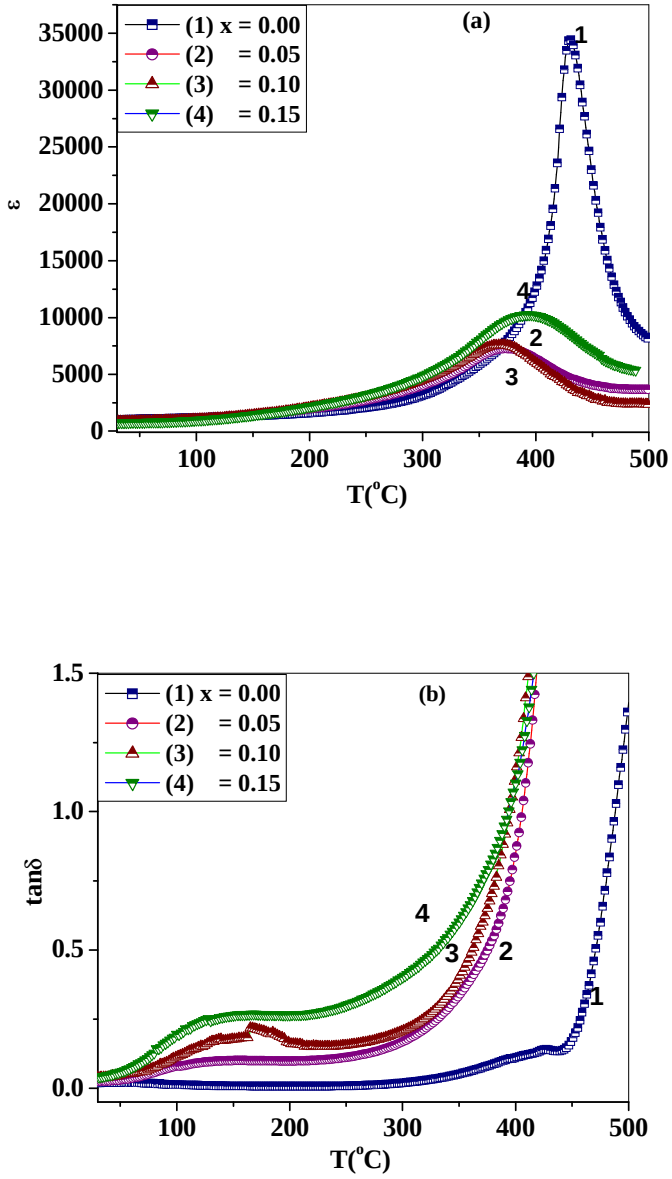

Figure 4.9 Comparison of Variation of Dielectric Properties ((a) dielectric constant and (b) tangent loss) with temperature at 100 kHz for x CNFO-(1-x) PZT Composites (x = 0.00, 0.05, 0.10 and 0.15)

4.3.4 Ferroelectric Properties

To study the ferroelectric nature of composites, P-E hysteresis loops of (x) CNFO - (1-x) PZT composites were recorded at different electric field as shown in Figure 4.10. P-E Hysteresis loops for all samples were taken at room temperature at 50 Hz. The hysteresis loops of x = 0.00, 0.05 and 0.10 confirm the well defined ferroelectric behavior while sample with x= 0.15 shows lossy loop. This may be due to presence of higher amount of ferrite phase having high conductivity resulting into leakage current in the sample [28]. It is also observed that the P-E loops are not symmetrical about the origin. This may be due to internal bias field caused by defects present in the sample and electrode interface [29]. As the applied field increases from 20 kV/cm to 35kV/cm for pure PZT (x = 0.00). There is increase in P_r, P_s and E_c, no further increase is observed at 30 kV and 35 kV while in composite samples as seen from the figure; there is continuous increase in the values of ferroelectric parameters and no saturation is observed.

A comparison of P-E hysteresis loop of (x) CNFO - (1-x) PZT composites are shown in Figure 4.11. The values of remnant polarization (P_r), saturation polarization (P_s) and coercive field (E_c) are given in Table 4.3. There is a significant decrease in the value of P_r, P_s and E_c of composites in comparison to pure PZT as seen from the table. There is decrease in the values of ferroelectric parameters in composites due to the low resistivity of ferrite content which causes increase in the leakage current, so the sample may not get fully polarized. There is increase in the values of P_r, P_s and E_c with increase in ferrite content. This increase in polarization may be due to space charge effect whose contribution to the ferroelectricity increases as ferrite content increases in the composites [30]. Similar behavior has been reported in various multiferroic systems [31, 32]. The value of coercive field also increases with increase in ferrite content; this indicates restricted motion of ferroelectric domain wall in the presence of ferrite phase [33, 34].

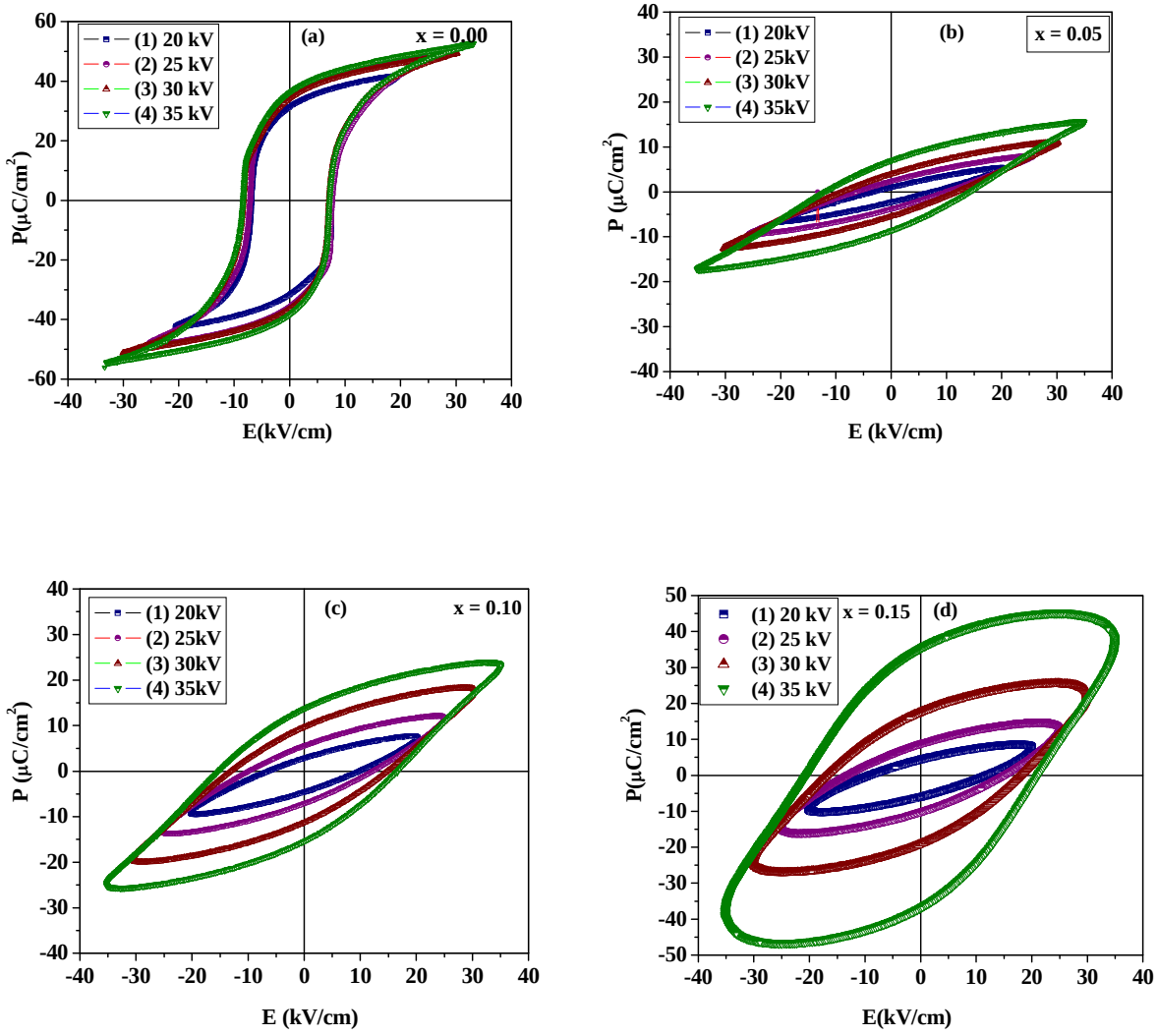

Figure 4.10 P-E hysteresis loop at different electric fields for x CNFO- (1-x) PZT ((a) x = 0.00, (b) 0.05 (c) x = 0.10 (d) x = 0.15

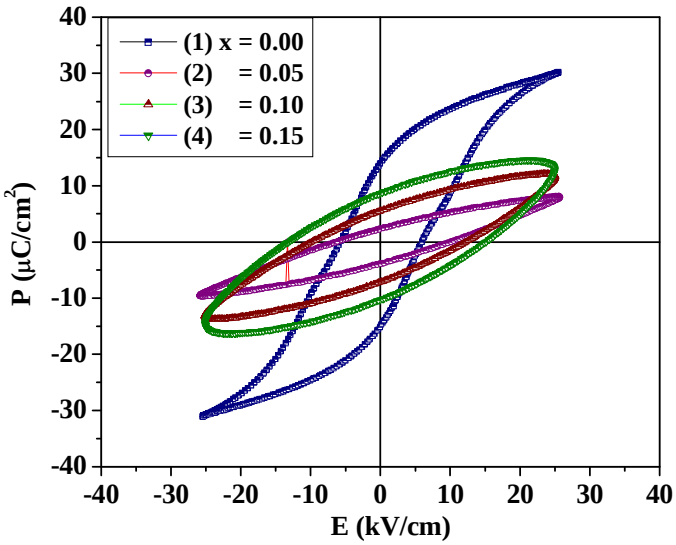

Figure 4.11 Comparisons of P-E Loops for all samples at 25 kV

Table 4.3 Ferroelectric Parameters (P_r, E_c and P_s) at 25 kV for all values of x

Parameters / x	P_r ($\mu C/cm^2$)	P_s ($\mu C/cm^2$)	E_c (kV/cm)
0.00	14.61	30.03	5.83
0.05	3.17	8.96	8.10
0.10	6.38	13.05	11.22
0.15	9.50	15.52	14.32

4.3.5 Magnetic Properties

The magnetic hysteresis (M-H) loops of (x) CNFO – (1-x) PZT composites were investigated at room temperature using VSM with an applied magnetic field of 6 kOe and are shown in Figure 4.12. All samples show well defined ferromagnetic behavior confirming the existence of magnetic ordering in the composite system [35]. The values of magnetic parameters of composite samples (x = 0.05, 0.10 and 0.15) are smaller than the pure ferrite (x = 0.00). This may be due to the fact that magnetic properties are affected by the presence of non- magnetic

ions (PZT) [22]. Comparison of M-H loops shows that as ferrite content increases from x = 0.05 to 0.15, saturation shifts towards high field axis [36]. The values of magnetic parameters of (x) CNFO – (1-x) PZT samples are smaller than the (x) CFO – (1-x) PZT which may be due to incorporation of Ni in ferrite phase.

The values of remnant magnetization (M_r), saturation magnetization (M_s) and coercive field (E_c) are determined from M-H hysteresis loops and are given in Table 4.4. The M_s and H_c of composite samples increase linearly with increase in ferrite content. This may be due to that individual ferrite grain acts as center of magnetization and the saturation magnetization is the vector sum of these entire individual grains of ferrites. This increase in magnetic contacts with ferrite content, results in the increase in magnetization [24, 37].

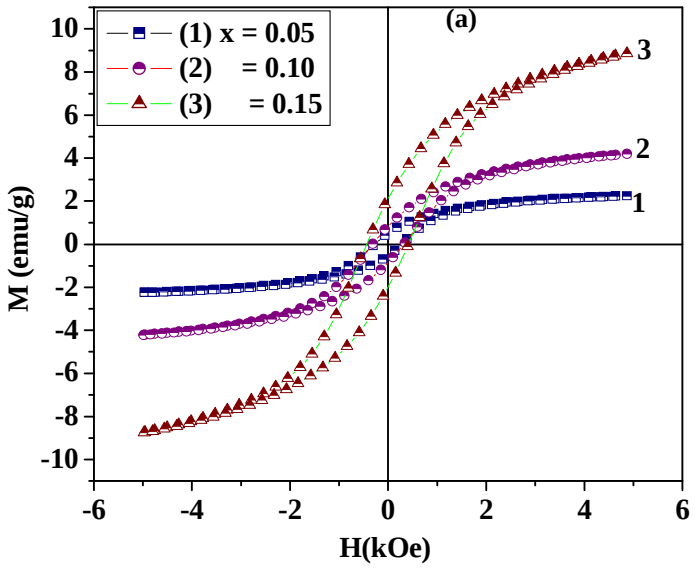

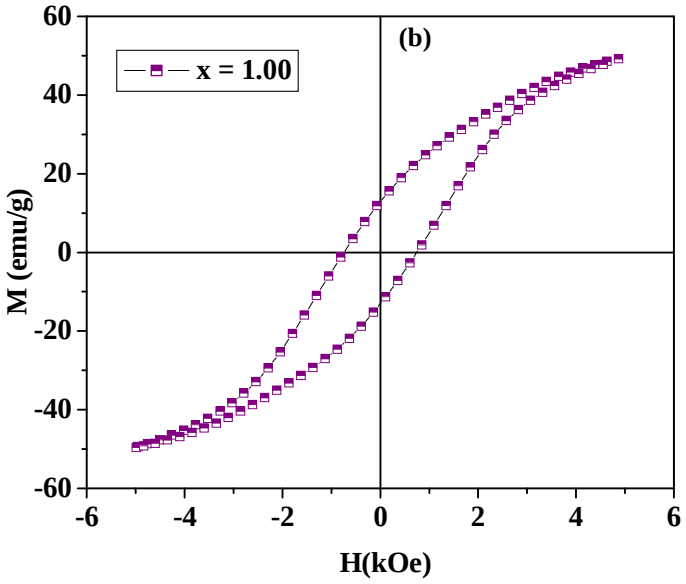
(b)
x = 1.00
M (emu/g)
H(kOe)
60
40
20
0
-20
-40
-60
-6
-4
-2
0
2
4
6

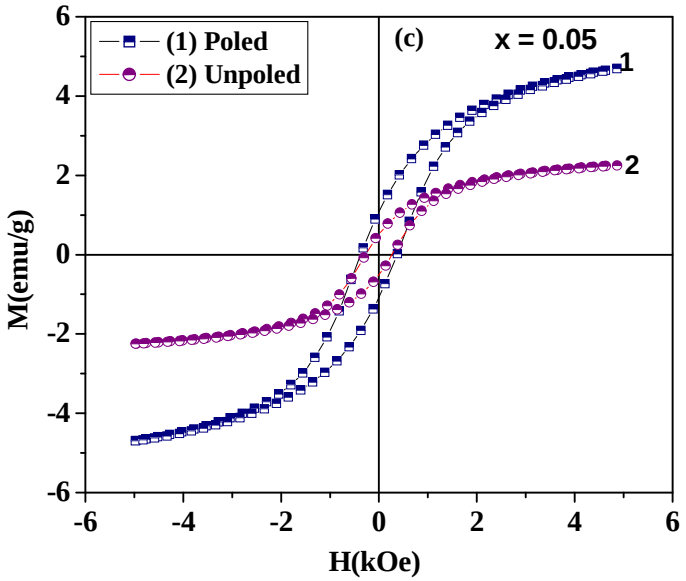
(c)
x = 0.05
(1) Poled
(2) Unpoled
1
2
M(emu/g)
H(kOe)
6
4
2
0
-2
-4
-6
-6
-4
-2
0
2
4
6

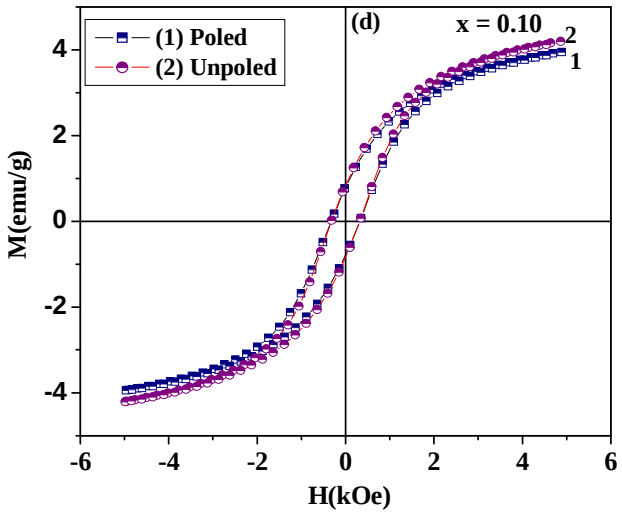

Figure 4.12 M-H Hysteresis curve for x CNFO + (1-x) PZT composite (a) x = 0.05, 0.10, 0.15 (b) x = 1.00 measured at room temperature (c) M-H Loops for Electrically Poled Sample and Unpoled Sample for x = 0.05 and (d) x = 0.10.

4.3.6 Piezoelectric Properties

The values of piezoelectric charge coefficient of pure PZT and composite samples are given in Table 4.4. To determine the piezoelectric charge coefficient of samples, each piece of composite samples were electrically poled at 15kV/cm in silicon oil bath tub for 1 hour and then piezoelectric coefficients were measured. The d_{33} values are found to be composition dependent because the composition influences the dielectric permittivity, electrostriction constant and spontaneous polarization [38]. These parameters play an important role in determining the piezo–coefficients and are directly related to d_{33} coefficients [39]. The maximum d_{33} value for pure PZT ceramic is 133pC/N. The decrease in d_{33} values with increase in ferrite content is due to decrease in ferroelectric phase (PZT) [40]. This is due to the fact that resistivity of ferrite phase (CNFO) is much smaller than that of the ferroelectric phase (PZT) resulting into increase in leakage current which leads to the loss of induced voltage which in turn makes the poling difficult. Hence the piezoelectric charge coefficient decreases [41].

4.3.7 Magnetoelectric Properties

To confirm the magnetoelectric coupling between ferrite ferroelectric phases, two pieces of single pallet were taken. One piece from each composite sample was electrically poled at 15 kV/cm. and other was unpoled. M-H hysteresis loops of both poled and unpoled composite samples were taken using VSM. Figure 4.12 (c-d) shows hysteresis loop of both poled and unpoled pieces of sample x= 0.05 and 0.10. From figures, it is observed that there is increase in both saturation and remnant magnetization of electrically poled samples. This increase in magnetization values of electrically poled samples may be due to poling of sample which may result into aligning of individual dipole moments within different electric domains along the magnetic field direction. The increase in magnetization can also be attributed to change in magnetic anisotropy and movement of domain walls [42].

Magnetoelectric coupling between PZT and CNFO phases is the interaction between the electric and magnetic dipoles. ME effect is the phenomenon of inducing magnetic polarization in a material in an external electric field and vice-versa. Magneto- electric effect in composites having ferrite and ferroelectric phases depends on the applied magnetic field, mole percentage of constituent phases, resistivity of the phases and mechanical coupling between the two phases [43]. Figure 4.13 shows the variation of the ME coupling coefficient (α = dE/dH) with applied DC magnetic field up to 6 kOe keeping ac magnetic field constant (1 Oe) at 1 kHz for composites at room temperature. The ME effect observed in samples is due to strain induced in the CNFO phase when a magnetic field is applied which is mechanically coupled to induce stress in ferroelectric due to piezoelectric effect that leads to change in polarization in PZT phase. From this figure, it has been observed that α increases with increase in magnetic field, reaches to maximum value and then decreases for the higher magnetic field. This increase in ME coefficient is due to the increase in magnetostriction induced strain in ferrite phase. The decrease in α with the increase in DC magnetic field may be due to the fact that the magnetostriction coefficient to ferrite phase reaches its saturation value at certain value of magnetic field [44]. Beyond a particular value of magnetic field, the produced magnetostriction and strain induce constant electric field in the ferrite phase resulting into decrease in the value of ME coefficient. The values of α = (dE/dH) obtained for composites are given in Table 4.4. The value of the ME coupling coefficient for 5% of CNFO in PZT is 854μV/ (cm. Oe). The ME coefficient is related

to magnetostriction coefficient (λ), piezoelectric coefficient (d), magneto mechanical coefficient (k_m) and dielectric constant (ε) [45] as

$$\alpha = \frac{\lambda \times d \times k}{\varepsilon}$$

piezoelectric coefficient (d) increases and dielectric constant decreases (ε) in case of PZT–CNFO sample which in turn increases the ME coefficient.

From the Figure 4.13, decrease in α is also related with piezoelectric coefficient. Piezoelectric coefficient (d_{33}) decreases with increase in CNFO content. The decrease in ME output is also due to the low resistivity of CNFO phase which leads to leakage of charges developed in the PZT grains through the low resistance of the surrounding CNFO grains [45]. The values of ME coupling coefficient obtained for given PZT-CNFO composite system are higher and comparable than those reported in ferrite – ferroelectric bulk composites [46, 47].

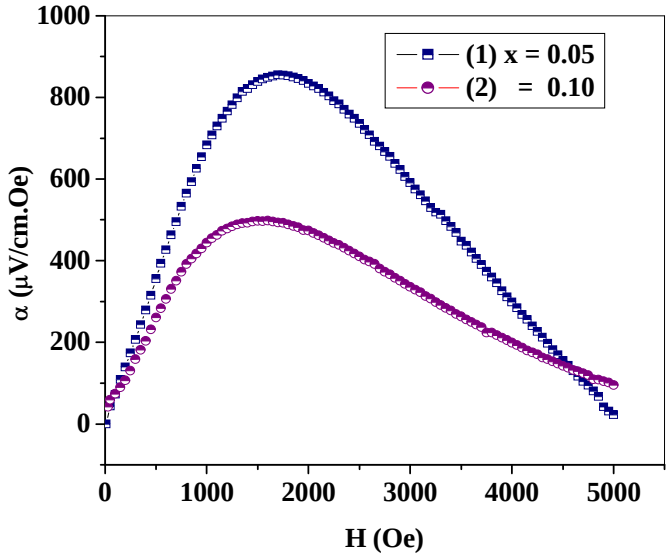

Figure 4.13 Variation of ME Coupling Coefficient (α) with a DC magnetic field for x = 0.05 and x = 0.10

Table-4.4 Magnetic parameters (H_c, M_r and M_s), Magneto-electric Coefficient (α) and Piezoelectric Properties for (x) CNFO-(1-x) PZT Composites (x = 0.00, 0.05, 0.10 and 0.15)

Magnetic Parameters					**Piezoelectric Coefficient**
Parameters / x	**H_c (Gauss)**	**M_r (emu/g)**	**M_s (emu/g)**	**α (μv/cm.Oe)**	**d_{33} (pC/N)**
0.00	-	-	-	-	130
0.05	265	0.45	2.26	855	77
0.10	334	0.83	4.23	498	70
0.15	424	2.063	8.78	-	60
1.00	724	13.08	49.45	-	-

References

1. B. K. Bammannnavar, G. N. Chavan, L. R.Naik and B. K.Chougule, Mater. Chem. Phys., **117** (2009) 46

2. R. S. Devan, Y. D. Kolekar and B. K.Chougule, J. Phys.: Condens.Matter., **18** (2006) 9809.

3. J. Paledo, G. Grange, R. Goutl and L. Fyrand, J. Phys. D., **7** (1994) 78.

4. A. D. Shiekh and V. L. Mathe, Smart Struct., **18** (2009) 797.

5. R. Rani, S. Singh, J. K. Juneja, Chandra Prakash and K. K. Raina, Ferroelectrics Lett., **38** (2011) 134.

6. W. E. Kramer, R. H. Hopkins and M. R. Daniel, J. Mater. Sci. Lett., **12** (1977) 409.

7. D. C. Agrawal, Asian J. Phys., **6** (1997) 108.

8. S. Upadhyay, D. Kumar and O. Prakash, Bull. Mater. Sci., **19** (1996) 513.

9. K. W. Wagner, Ann. Phys., **40** (1993) 818.

10. C. G. Koop's Phys. Rev. B., **83** (1951) 121.

11. J. C. Maxwell, Electricity and Magnetism, Oxfrod University Press, London, (1993) 828.

12. V. L. Mathe, K. K. Patanker, M. B. Kothale, S. B. Kulkarni, P. B. Joshi and S. A. Patil, Pramana, J. Phys., **58** (2002) 1105.

13. M. Zivkovic, D. Stojanovic, C. R. Foschini, V. Paunovic and D. Mancic, Sci. Sinter., **35** (2003) 133.

14. S. B. Narang and D. Kaur, Ferroelectrics Lett., **36** (2009) 20.

15. D. R. Patil and B. K. Chougule, J. Alloys Compd., **47** (2009) 531.

16. A. D. Sheikh and V.L Mathe, Mater. Chem. Phys., **119** (2010) 5074.

17. D. Adler and J. Feinlein, Phys. Rev. B: Condens. Matt., **2** (1970) 3112.

18. S. A. Lokare, R. S. Devan, D. R. Patil and B. K. Chougule, J. Mater. Sci.: Mater. in Elect., **18** (2007) 1211.

19. R. C. Kambale, P. A. Shaikh, C. H. Bhosale, K. Y. Rajpure and Y. D. Kolekar, Smart Mater. Struct., **18** (2009) 085014.

20. L. Mitoseriu and V. Buscaglia, Phase Trans., **79** (2006) 1.

21. K. K. Patanker, V. L. Mathe, A. N. Patil, S. D. Lotke, Y. D. Kolekar and P. B. Joshi, J. Electroceram., **6** (2002) 115.

22. A. P. Barranco, J. D. S. Guerra, R. L. Noda and E. B. Araujo, J. Phys. D: Appl. Phys., **41** (2008) 215503.

23. S. A. Lokre, D. R. Patil, R. S. Devan, S. S. Chougule, Y. D. Kolekar and B. K. Chougule, Mater. Res. Bull., **43** (2008) 326.

24. C. M. Kanamadi, B. K. Das, C. W. Kim, D. I. Kang, H. G. Cha, E.S. Ji, A.P. Jadav, B-E Jun, J. H. Jeong, B.C. Choi, B. K. Chougule and Y.S. Kong, Mater. Chem. Phys., **116** (2009) 6.

25. C. M. Kanamadi, L. B. Pujeri and B. K. Chougule, J. Magn. Magn. Mater., **295** (2005) 139.

26. J. Chen, Z. Xu and X. Lu, Ferroelectrics, **410** (2011) 29.

27. X. Chao, Z. Yang, M. Dong and Y. Zhang, J. Magn. Magn. Mater., **323** (2011) 2012.

28. S. L. Kadam, K. K. Patankar, C. M. Kanamadi and B.K. Chougule, Mater. Res. Bull., **39** (2004) 2265.

29. R. Y. Zheng, J. Wang and S. Ramakrishna, J. Appl. Phys., **104** (2008) 034106.

30. Y. Yang, Y. Yang, W. Rao, M. Wang, G. Li, Y. Li, J. Gao, W. Zhou and J. Yu, J. Mater. Sci: Mater. Electron., **23** (2012) 570.

31. A. Sharma, R. K. Kotnala and N. S. Negi, J. Alloys Compd., **582** (2014) 628.

32. W. Ye-An, W. Yun-Bo, R. Wei, G. Jun-Xiang, Z. Wen-Li and Y. Jun, Ceram. Phys. Lett., **29** (2012) 067701.

33. X. W. Qi, J. Zhou, B. Li, Y. C. Zhang, Z. Yue, Z. Gui and L. Li, J. Am. Ceram. Soc., **87** (2004) 1848.

34. L. Mitoseriu, I. Pallecchi, V. Buscaglia, A. Testino, C.E. Ciomaga and A. Stancu, J. Magn, Magn. Mater., **316** (2007) e603.

35. J. Zhai, N. Cai, Z. Shi, Y. Lin and C.W. Nan, J. Phys. D.: Appl. Phys., **37** (2004) 823.

36. R. S. Daven and B.K. Chougule, J. Appl. Phys., **101** (2007) 014109.

37. W. Wersing, K. Lubitz and J. Mohaupt, IEEE T. Ultrason. Ferr., **36** (1989) 424.

38. D. Wu, W. Gong, H. Deng and M. Li, J. Phys. D: Appl. Phys., **40** (2007) 5002.

39. R. A. Islam and S. Priya, Integr. Ferroelectr., **82** (2006) 1

40. D. Wu, W. Gong, H. Deng and M. Li, J. Phys. D: Appl. Phys., **40** (2007) 5002.

41. C. W. Nan, M.I. Bichurin, S. Dong, D. Viehland and G. Shrinivasan, J. Appl. Phys., **103** (2008) 031101.

42. M. Sertkol, Y. Koseoglu, A. Baykal, H. Kavas and M. S. Toprak, J. Magn. Magn. Mater., **322** (2010) 866.

43. S. A. Lokre, D. R. Patil and B. K. Chougule, J. Alloys Compd., **453** (2008) 253.

44. A. S. Fawzi, A. D. Shiekh and V. L. Mathe, Phys. B: Condens. Matter., **405** (2010) 340.

45. J. Hanumanian, T. Bhimasankaram, S. V. Suryanarayan and G. Kumar, Bull. Mater. Sci., **17** (1994) 405.

46. B. K. Bammannavar, L. R. Naik and B.K. Chougule, J. Appl. Phys., **104** (2008) 064123.

Chapter – 5

Synthesis and Characterizations Of La substituted PZT-CNFO Composites

Chapter –V

Synthesis and Characterization of La Substituted PZT-CNFO Composites

This chapter includes studies on the structural, dielectric, ferroelectric, ferromagnetic and magnetoelectric properties of La substituted PZT and Ni doped $CoFe_2O_4$ composite. *Following material series were synthesized and the details are presented here.*

Series A - $Pb_{(1-3y/2)}\,La_yZr_{0.55}\,Ti_{\,0.45}O_3$ (y = 0 - 0.0075 in step of 0.0025)

Series B - (x) $Co_{0.8}Ni_{0.2}Fe_2O_4$ - (1-x) $Pb_{0.99625}La_{0.0025}Zr_{0.55}Ti_{0.45}O_3$

Series C - (x) $Co_{0.8}Ni_{0.2}Fe_2O_4$ - (1-x) $Pb_{0.9925}La_{0.005}Zr_{0.55}Ti_{0.45}O_3$ } (x = 0 - 0.15 in step of 0.05)

Series D - (x) $Co_{0.8}Ni_{0.2}Fe_2O_4$ - (1-x) $Pb_{0.9887}La_{0.0075}Zr_{0.55}Ti_{0.45}O_3$

In series A, we have studied effect of La on various properties of $Pb_{(1-3y/2)}La_yZr_{0.55}Ti_{0.45}O_3$*, where y = 0.000 - 0.0075 in step of 0.0025. In series B, C, and D, we have studied the effect of different concentration of CNFO on PLZT keeping La fixed at y = 0.0025, 0.005 and 0.0075, respectively. Influence of* La^{3+} *substitution at* Pb^{2+} *site is found to be most effective substituent and is seen to yield significant improvement in properties of composites.*

5.1 Synthesis of Individual Phases and Composites

The ferrite and ferroelectric phase are synthesized by solid state reaction method. The synthesis method for $Co_{0.8}Ni_{0.2}Fe_2O_4$ has already been discussed in chapter 4. For ferroelectric phase, $Pb_{(1-3y/2)}La_yZr_{0.55}Ti_{0.45}O_3$, AR grade of PbO, La_2O_3, ZrO_2 and TiO_2 were used as raw materials. These oxides were weighed in required molar proportion after that ball milled for 4 hours using distilled water and zirconia balls as milling media and followed by drying. Dried powder of PLZT was calcined at 800^{o}C for 4 hours, so that constituent oxides can react with each other and form a compound. The calcined powder of PLZT was ball milled again and dried. Dried powder of PLZT was recalcined at 850^{o}C for 4 hours in order to make homogenous powder. For phase identification, XRD analysis was carried out. XRD pattern for $Pb_{(1-3y/2)}La_yZr_{0.55}Ti_{0.45}O_3$, y = 0.0025, 0.005 and 0.0075 are shown in figure 5.1 and for $Co_{0.8}Ni_{0.2}Fe_2O_4$, it has already been discussed in chapter-4.

Composites of ((x) $Co_{0.8}Ni_{0.2}Fe_2O_4$ - (1-x) $Pb_{1-3y/2}La_yZr_{0.55}Ti_{0.45}O_3$) where x = 0.05, 0.10 and 0.15 for y = 0.0025, 0.005 and 0.0075 were prepared by mixing both the phases. The mixing was done by ball milling followed by drying. After drying, powder was mixed with small amount of diluted PVA (poly vinyl alcohol) as binder. Dried mixtures were pressed in form pallet of diameter 15 mm and thickness of 1 mm using uniaxial pressing. The pallets were sintered at 1250^{o}C for 4 hours in programmable furnace followed by various characterizations.

5.2 Characterization of (x) $Co_{0.8}Ni_{0.2}Fe_2O_4$ - (1-x) $Pb_{1-3y/2}La_yZr_{0.55}Ti_{0.45}O_3$

5.2.1 X-Ray Diffraction

Figure 5.1(a) shows the XRD pattern for $Pb_{(1-3y/2)}La_yZr_{0.55}Ti_{0.45}O_3$ where y = 0.0000, 0.0025, 0.005 and 0.0075 (Series A). The XRD pattern shows well defined peaks and confirms the single phase compound with Perovskite tetragonal structure. The lattice parameters (c and a) were determined using Bragg's Law. It is observed that due to substitution of La^{3+} at Pb^{2+} site (as ionic radius of La^{3+} is smaller as compared to Pb^{2+}), there is slight decrease in lattice parameters of PLZT.

Figure 5.2 (b-d) shows the XRD pattern for all composite samples for (x) $Co_{0.8}Ni_{0.2}Fe_2O_4$ - (1-x) $Pb_{1-3y/2}La_yZr_{0.55}Ti_{0.45}O_3$ where x = 0.05, 0.10 and 0.15 for y = 0.0025, 0.005 and 0.0075

(series B, C and D). The XRD pattern shows the well defined peaks indexed with specific indices of both ferrite and ferroelectric phase. This confirms the co-existence of both the phases (cubic spinel structure in ferrite phase and perovskite tetragonal structure in ferroelectric phase). The XRD patterns of composite samples do not show any extra phase other than the constituent phases which confirms the no chemical reaction took place between two phases. From figure 5.2 (a-c), it is observed that the intensity of peaks and number of peaks corresponding to ferrite phase as compared to ferroelectric phase is smaller which is due to small concentration of ferrite phase in the composites. It is also observed from the figure that intensity of ferrite peaks increase with increase in ferrite content which shows that present composite follow the rule of mixture.

The lattice parameters of both ferrite and ferroelectric phase were calculated and are given in Table 5.1. It is observed that random variation in lattice constant is observed for ferroelectric phase for all the three series (B, C and D) which may be due to stress induced by ferrite phase on ferroelectric phase [1].

The experimental density, x – ray density and relative density were determined for all samples and are given in Table 5.1. It is observed that in composite samples for y = 0.0025, relative density decreases with increase in ferrite content, While for y = 0.005 and 0.0075, relative density initially decreases with ferrite content then increases for x = 0.15. Lower density for small concentration of substituent has already been reported in for similar ceramics [2, 3]. This variation in density can be explained by the number of Pb^{2+} vacancies which affect volume diffusion during densification for different concentrations of substituent's [4].

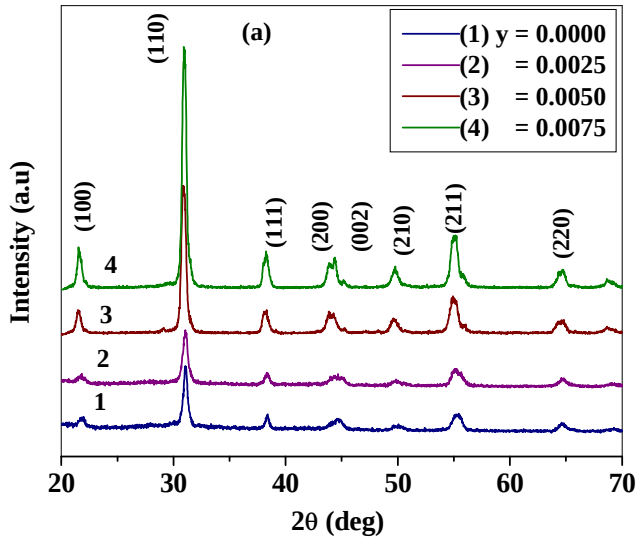
(a)
(1) y = 0.0000
(2) = 0.0025
(3) = 0.0050
(4) = 0.0075
(100)
(110)
(111)
(200)
(002)
(210)
(211)
(220)
4
3
2
1
Intensity (a.u)
2θ (deg)

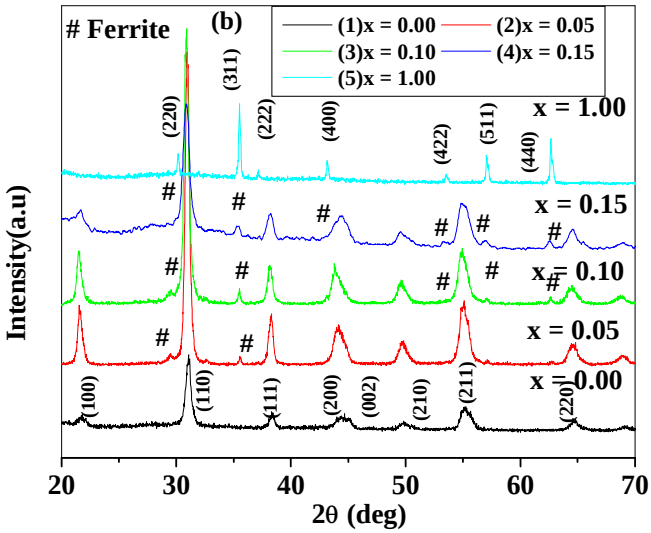
Ferrite
(b)
(1)x = 0.00
(2)x = 0.05
(3)x = 0.10
(4)x = 0.15
(5)x = 1.00
x = 1.00
x = 0.15
x = 0.10
x = 0.05
x = 0.00
Intensity(a.u)
2θ (deg)

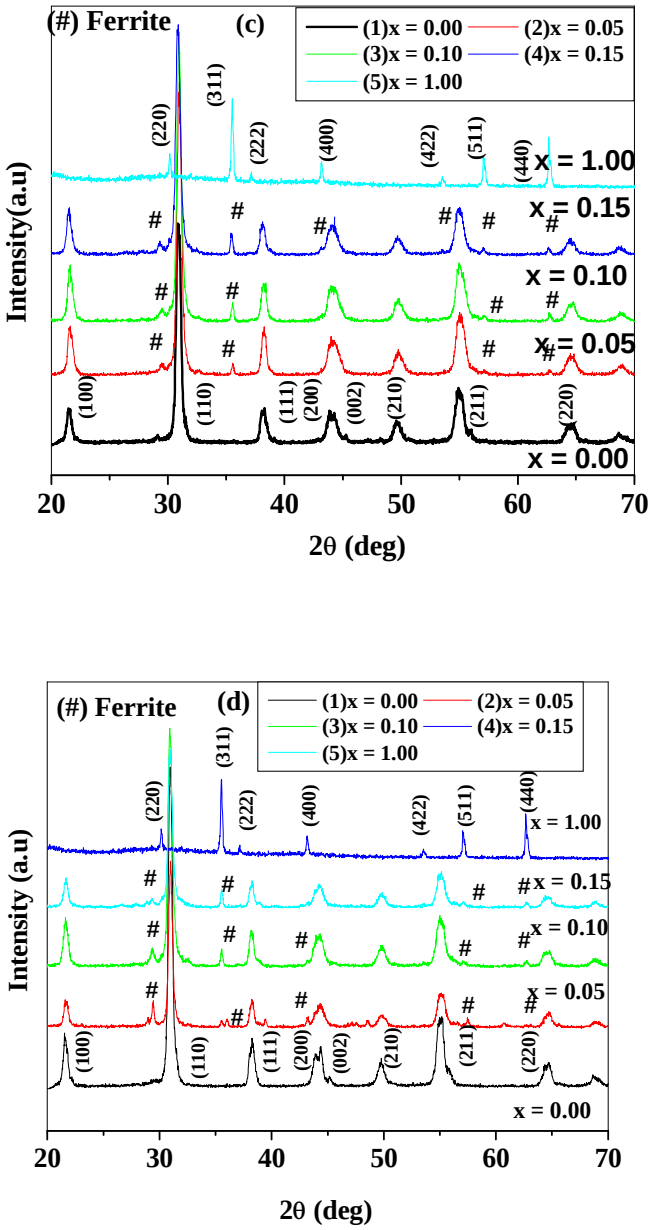

Figure 5.1 (a-d) XRD Pattern for all samples of (a) Series A (b) Series B (c) Series C and (d) Series D

Table 5.1: Lattice Parameters and relative density for (x) $Co_{0.8}Ni_{0.2}Fe_2O_4$ - (1-x) $Pb_{1-3y/2}La_yZr_{0.55}Ti_{0.45}O_3$ for all values of x of all values of y

Series A (x = 0.00)							
Parameter / y	**Ferrite phase a (Å)**	**Ferroelectric phase**			**Exp. Density d_{exp}(g/cc)**	**X–ray Density d_{th} (g/cc)**	**Relative Density d_{rel}(%)**
		a (Å)	**c (Å)**	**c/a**			
0.0000	-	4.048	4.105	1.0138	7.223	7.929	91.096
0.0025	-	4.056	4.108	1.0127	7.165	8.113	88.331
0.005	-	4.063	4.107	1.0108	6.936	8.079	85.850
0.0075	-	4.042	4.082	1.0099	7.425	8.231	90.221
Series B (y = 0.0025)							
x	**Ferrite phase a (Å)**	**Ferroelectric**			**Exp. Density d_{exp}(g/cc)**	**X–ray Density d_{th} (g/cc)**	**Relative Density d_{rel}(%)**
		a (Å)	**c (Å)**	**c/a**			
0.05	8.368	4.053	4.108	1.0135	7.79	7.22	92.7
0.10	8.382	4.062	4.121	1.0144	7.42	7.15	96.3
0.15	8.427	4.038	4.105	1.0165	7.65	7.04	91.9
Series C (y = 0.005)							
0.05	8.359	4.053	4.104	1.0126	7.95	6.97	87.802
0.10	8.368	4.052	4.103	1.0124	7.81	6.43	82.353
0.15	8.389	4.054	4.100	1.0115	7.66	6.80	88.777

Series D (y = 0.0075)							
0.05	8.386	4.066	4.081	1.0036	7.7108	6.0714	76.131
0.10	8.393	4.079	4.126	1.0113	7.7015	6.8542	88.998
0.15	8.414	4.057	4.102	1.0109	7.6777	6.8969	89.830

5.2.2 Scanning Electron Microscope

Figure 5.2 (A) shows the SEM micrograph for samples of series A (PLZT). The Micrographs show the closely packed and well oriented grains and shape, size and distribution of grains confirm the polycrystalline nature. The average grain size was calculated by intercept method. The average grain size as seen from the images is in the range of 1μm – 2μm.

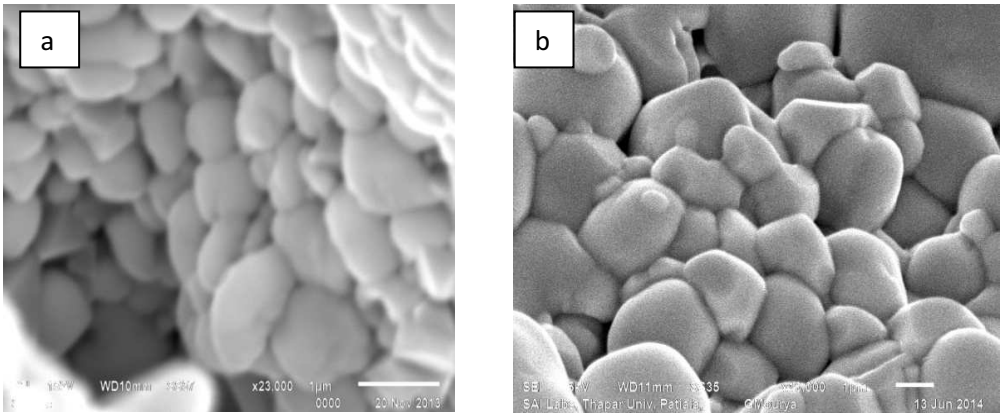

Figure 5.2 (A) SEM micrograph for **Series A (**PLZT**)** (a) y = 0.0025 and (b) y = 0.005

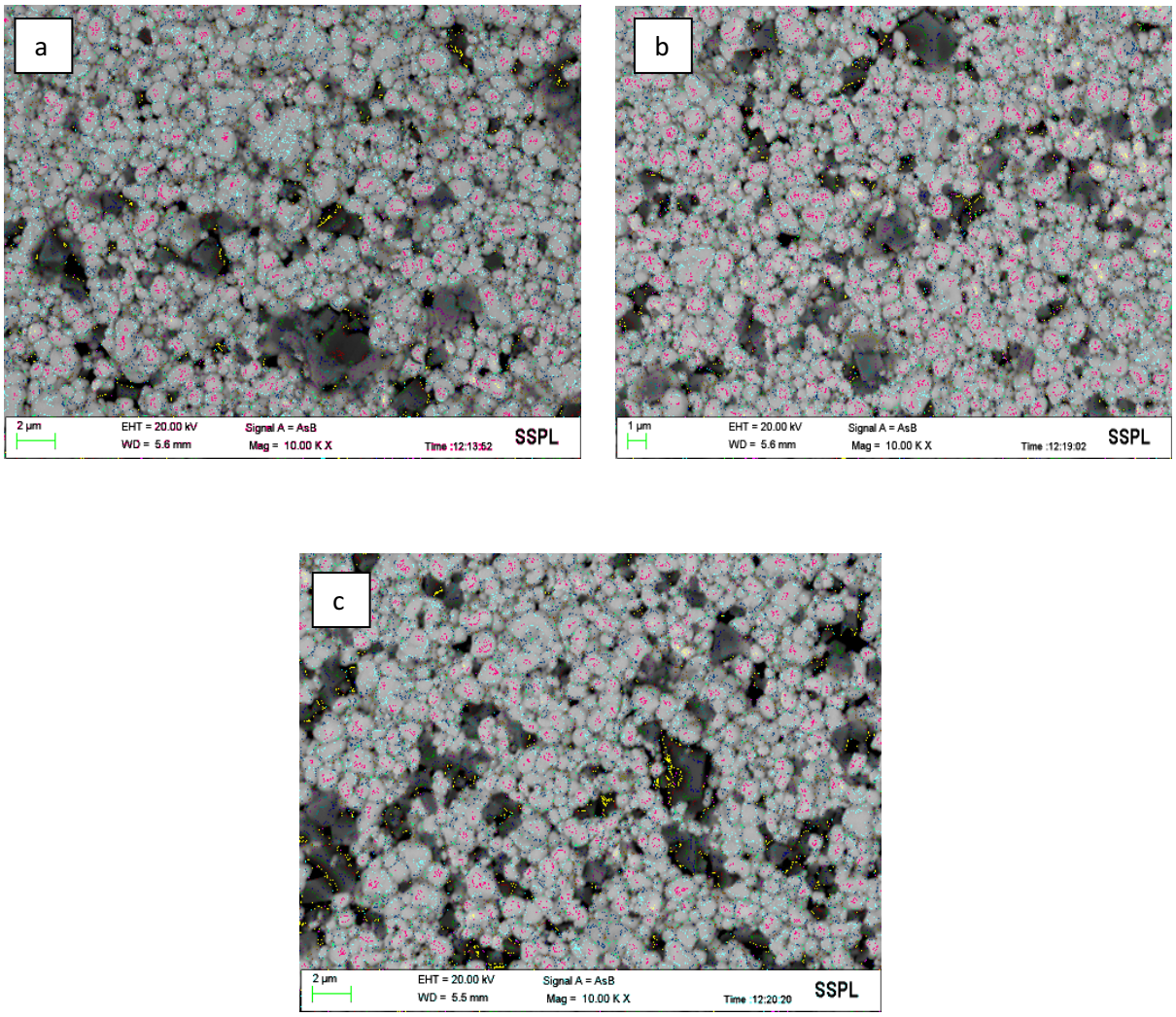

Figure 5.2 (B) SEM images for **Series B** (a) x = 0.05 (b) x = 0.10 (c) x = 0.15

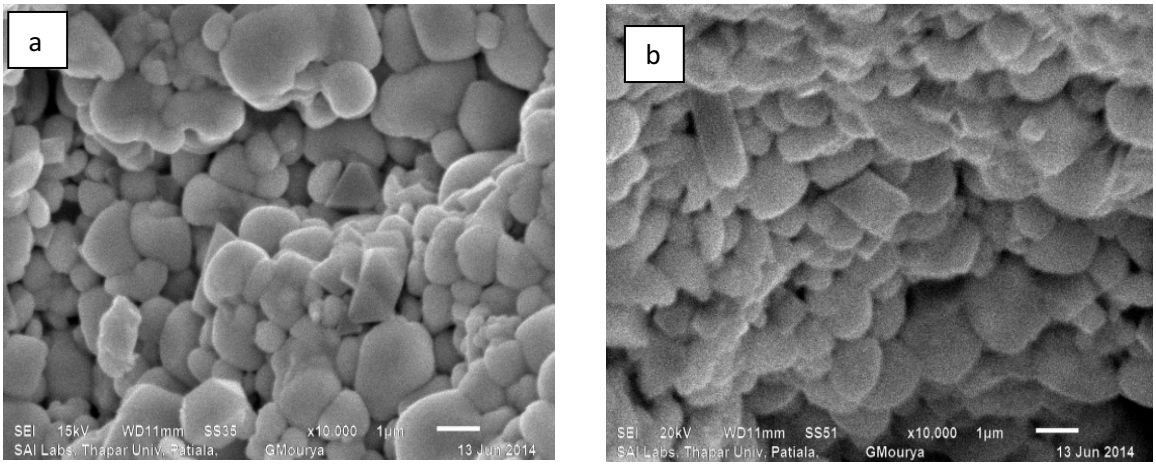

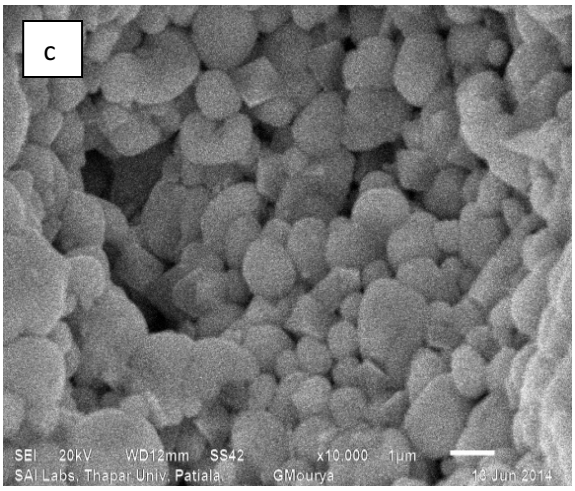

Figure 5.2 (C) SEM images for **Series C** (a) x = 0.05 (b) x = 0.10 (c) x = 0.15

Figure 5.2 (B) and 5.2 (C) shows the SEM micrograph for composites samples of series B and series C. SEM images of series B were recorded in back scattered mode. It can be seen from the micrograph that there is a mixture of white and black grains confirming the presence of two individual phases. As ferrites are conductive, electrons have path to go through that surface causing darkness while ferroelectrics are less conductive in comparison to ferrite, when an electron beams falls on the surface, beam is absorbed by that ferroelectric region resulting to charging effect i.e. accumulation of charges on the surface of the sample causing the brightness. This confirmed that the white grains are for ferroelectric (PLZT) and black grains are for ferrite (CNFO) as per composition. The volume fraction of black grains, corresponding to ferrite phase, is lesser than that of white grains, corresponding to ferroelectric phase. As ferrite content increases, volume fraction of black grains also increases.

SEM images of series C also show well defined and closely packed grains. Average grain size of the composites of series C was determined from linear intercept method. With increase the ferrite content in the composites, average grain size of the composites increases with increase in ferrite content. The values of average grain size with x = 0.05, 0.10 and 0.15 are 0.94, 0.97 and 1.02μm respectively. Individual phases of composites could not be distinguished because of small concentration of ferrite content in the composite.

5.2.3 Dielectric Properties

The variation of dielectric with frequency and temperature for all series (Series A and series B, series C and series D) are discussed here.

5.2.3.1 Frequency dependence of dielectric properties (ε and tanδ)

Frequency dependence of dielectric constant and dielectric loss at room temperature were studied for all series. Figure 5.3 (A-D) depicts the frequency dependence of dielectric constant and loss with frequency (100 Hz – 100 kHz). In general, it is found that dielectric constant decreases with increase in frequency for all samples. The higher value of dielectric constant at lower frequencies may be due to presence of all types of polarizations such as space charge, ionic, dipolar, electronic polarization [5]. The contribution of these polarizations ceases to respond at higher frequencies because of higher relaxation time which result into decrease in dielectric constant. At higher frequencies, only electronic polarization is dominant and other polarizations become ineffective. Similar type of frequency dependent dielectric behavior is found in many ferroelectric ceramics and ferrite–ferroelectric composites [6-9].

From Figure 5.3 (A), it is observed that dielectric constant increases with increase in La content. A small decrease in dielectric constant is observed at higher frequencies for all the samples and after that values of dielectric constant become constant at 10 kHz - 100 kHz. Dielectric dispersion is observed at lower frequencies in both variations (dielectric constant and dielectric loss). Similar behavior is observed in tangent loss of PLZT samples.

In composite samples, large dielectric dispersion is observed which may be due to mixing of two different materials having different conductivity and permittivity. This can also be explained by Maxwell- Wagner Polarization with Koop's phenomenological theory [10-12]. From Figure 5.3 (B), it is observed that dielectric constant increases with increase in ferrite content up to x = 0.10 after that it decreases for x = 0.15. From Figure 5.3 (C), it is also observed that values of dielectric constant decreases with increase in ferrite content for series C while in series D, values of dielectric constant varies randomly. This may be due to the fact that ferrite and ferroelectric having different permittivities are randomly mixed together. It can also be observed that tanδ of all samples of composite shows peaking behavior at lower frequencies which may represent relaxation process. The peaking behavior in tanδ occurs when frequency of electrons between Fe^{2+} and Fe^{3+} is equal to the frequency of the applied field [13, 14].

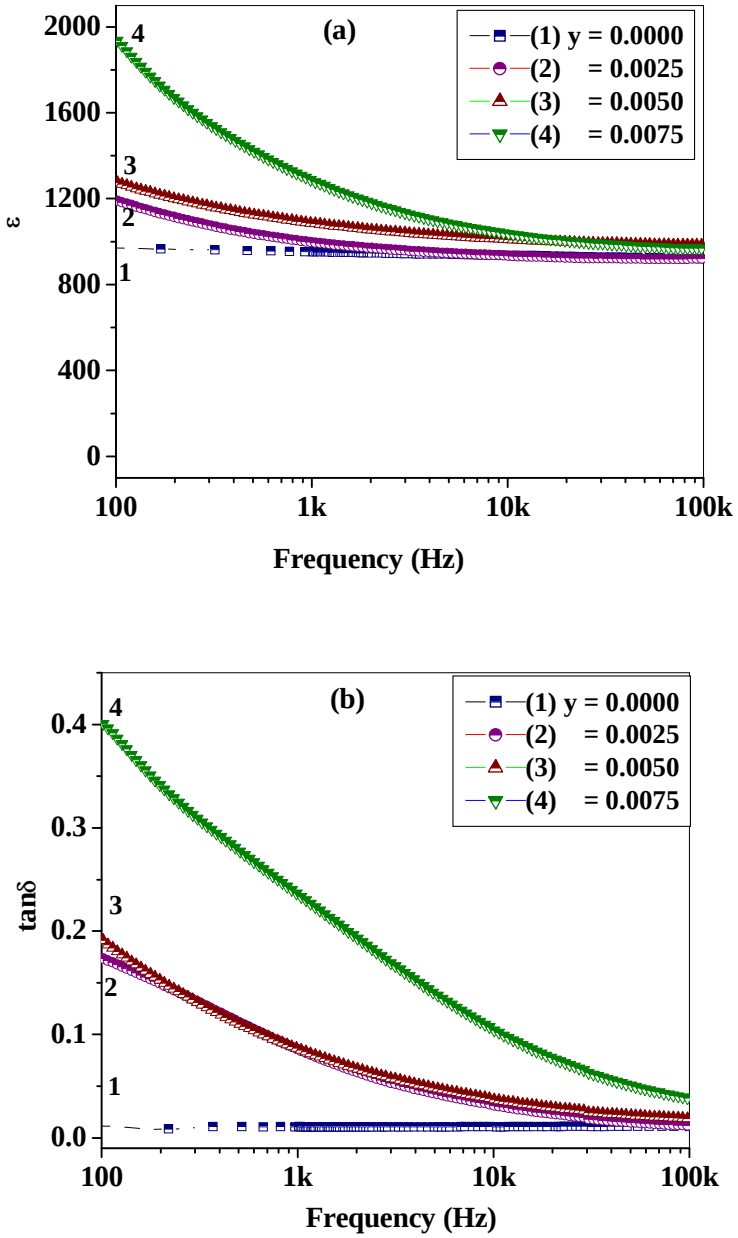

Figure 5.3 (A) Frequency dependence of (a) dielectric constant (b) dielectric loss for **Series A**

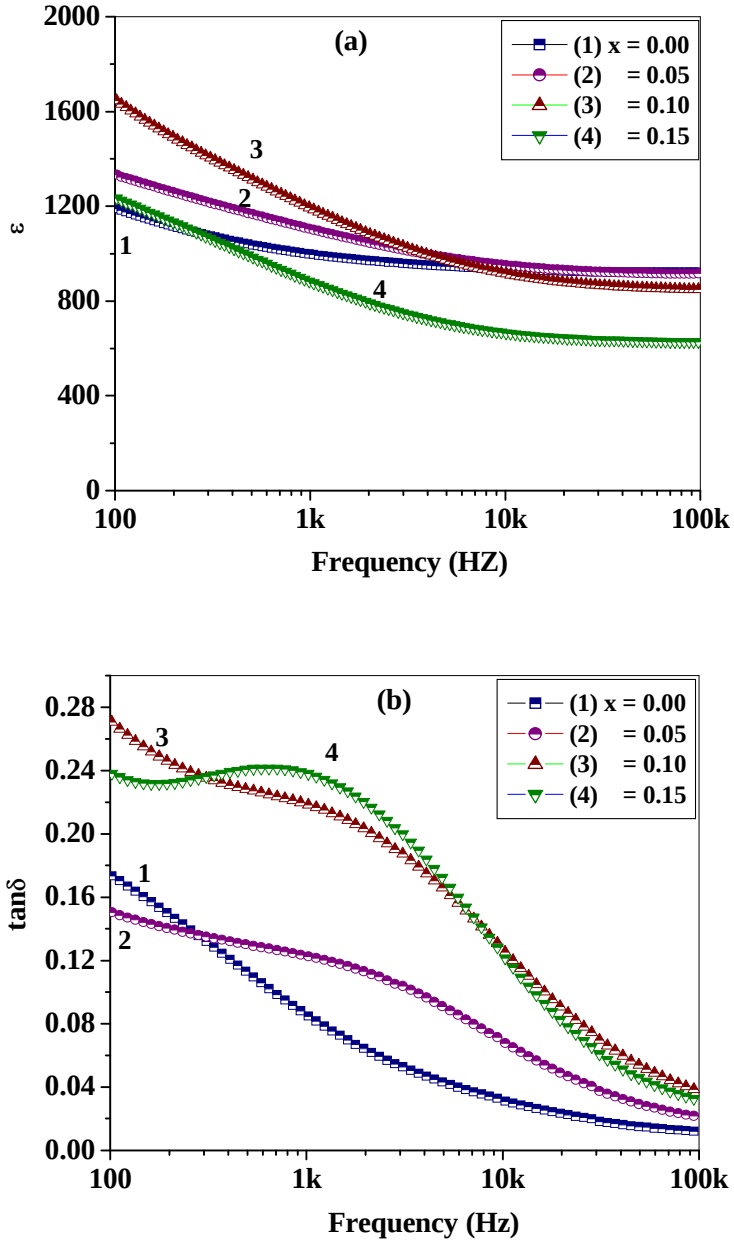

Figure 5.3 (B) Frequency dependence of (a) dielectric constant (b) dielectric loss for **Series B**

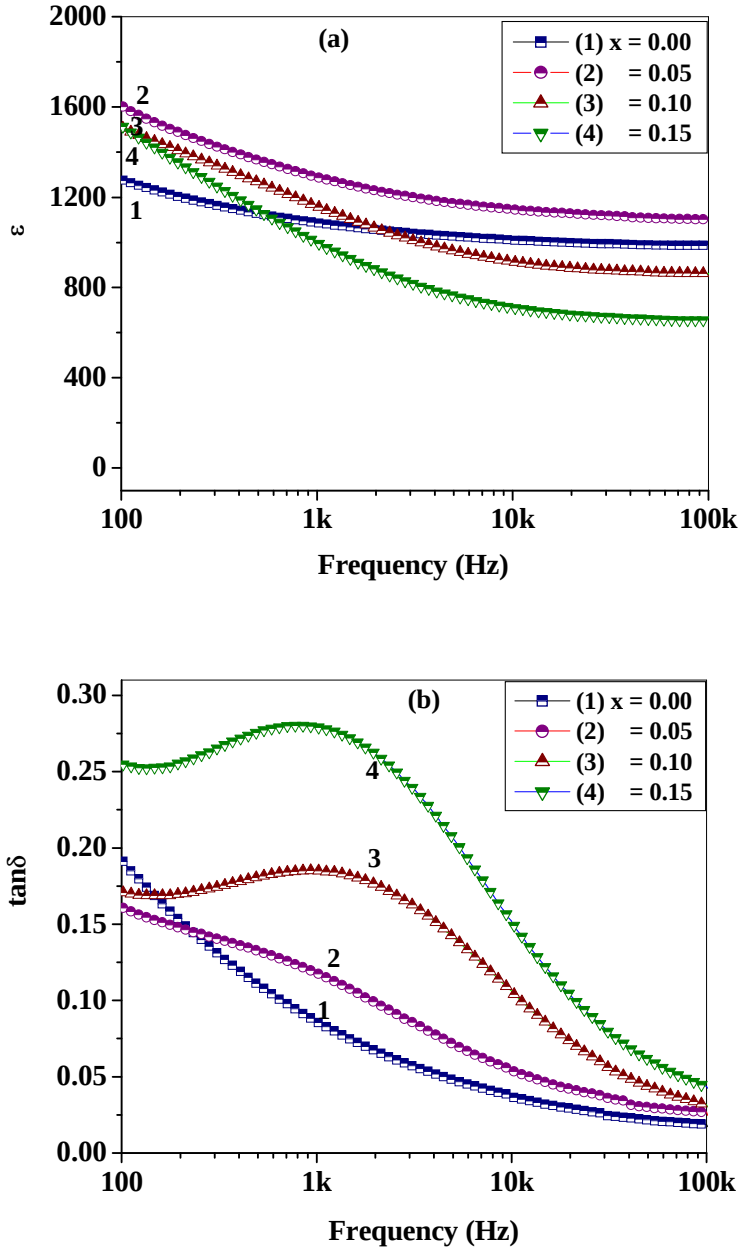

Figure 5.3 (C) Frequency dependence of (a) dielectric constant (b) dielectric loss for **Series C**

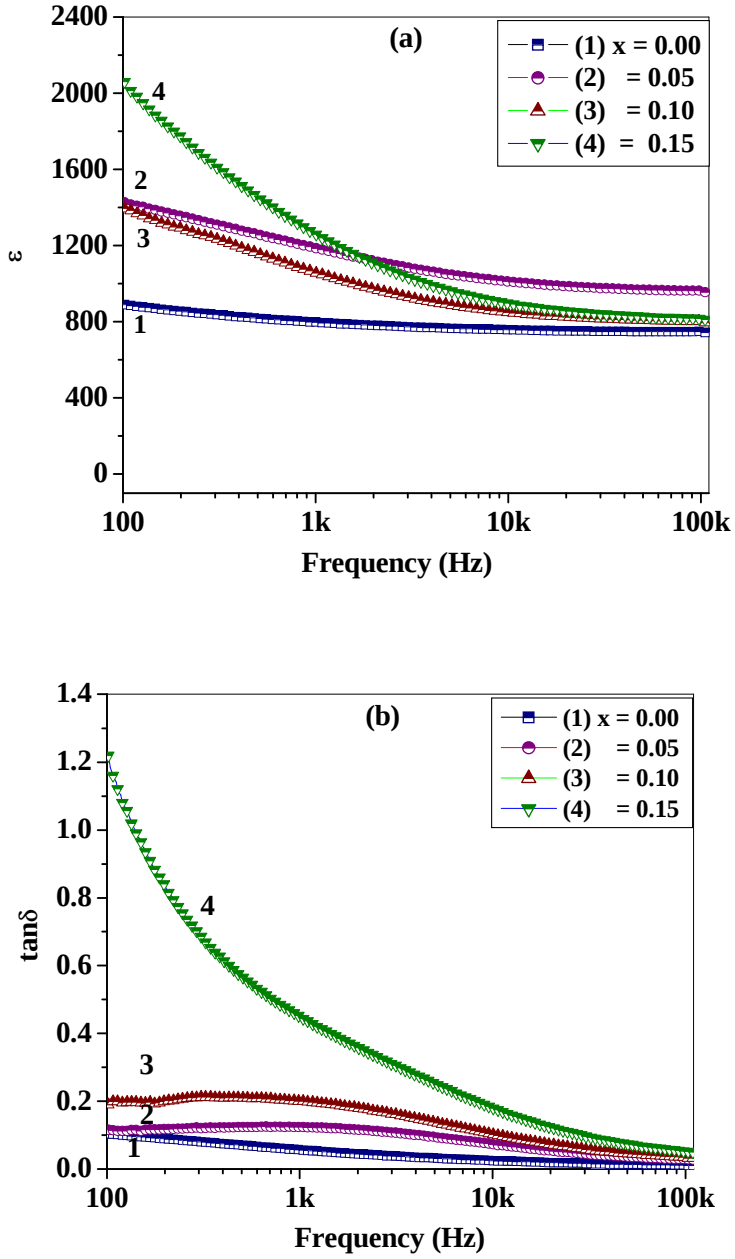

Figure 5.3 (D) Frequency dependence of (a) dielectric constant (b) dielectric loss for **Series D**

5.2.3.2 Temperature dependence of dielectric properties (ε and tanδ):

Figure 5.4 (A-D) shows the variation of dielectric constant (ε) and loss tangent (tanδ) with temperature (30^{o}C -500^{o}C) measured at three frequencies (1 kHz, 10 kHz and 100 kHz) for all samples for series A, series B, series C and series D. Values of dielectric parameters such as

dielectric constant at room temperature (ε_{RT}), Curie temperature (T_c), dielectric constant at Curie temperature (ε_{max}), loss tangent at room temperature ($\tan\delta_{RT}$) and loss tangent at Curie temperature ($\tan\delta_{max}$) were determined from these graphs and are listed in Table 5.2. In all samples (pure ferroelectric and composites), it is observed that dielectric constant increases with increase in temperature, reaches a maximum value at particular temperature and after that it decreases with further increase in temperature. The temperature at which maximum dielectric constant is observed is known as Curie temperature (T_c). The mobility of charge carriers increases with increasing temperature which leads to increase in polarization of the samples, hence increase in dielectric constant. The well defined peaks correspond to the transition from ferroelectric phase to paraelectric phase [15-17].

With substitution of La in PZT (Series A), Curie temperature of the samples is found to decrease. This decrease in T_c is observed due to decrease in crystal tetragonality which results in the reduction of the internal stress and which in turn reduces the transition temperature [18]. The results are well reported in literature [19, 20]. It is observed that dielectric loss decreases with substitution of La in PZT. This may be due to decrease in domain wall contribution.

Variation of dielectric constant with temperature for composite samples (Figure 5.4 (B-D)) also shows similar behavior (ferroelectric –paraelectric phase transition) as shown by ferroelectrics (Series A). It is observed from the figures (5.4 (B-D)) that in the paraelectric region dielectric constant increases with increase in temperature while for higher frequencies (10 kHz and 100 kHz), it follows decreasing trend in all composite samples. This can be related with low frequency relaxation process [21]. This increase in dielectric constant is observed due to increase in dielectric polarization which is a result of hopping of ions in CNFO phase [22]. Dielectric dispersion and broadening at dielectric maxima can also be seen in all composite samples. This may be due to microstructural heterogeneity in samples due to incorporation of ferrite phase in ferroelectric phase [23, 24].

Comparative study of variation of dielectric constant and dielectric loss with temperature for all samples of series (A, B, C and D) are shown in Figure 5.5. It is observed that from comparative study, room temperature dielectric constant of all composite samples decreases as compared to pure ferroelectrics as per composition. This may be due to addition of (CNFO) ferrite (having low dielectric constant) in ferroelectrics. The decrease in dielectric constant with increase in ferrite content is well reported in literature [25]. It is observed that Curie temperature

of composite samples (all Series- Series B, C and D) increases with increase in ferrite content. Similar behavior has been reported in (x) CFO- (1-x) PCT multiferroic system and in (1-x) BST – (x) CFO [26, 27].

The value of dielectric loss is low near room temperature and it increases with increase in temperature as observed from samples of all composites. This may be due to the space charge polarization and thermal conductivity losses which arise as a result of thermally activated electron hopping between the ions present in the CNFO phase. Loss peaks is observed at lower temperature as observed from the Figure. These peaks shift towards higher temperature side with increase in frequency, shows thermally activated relaxation process.

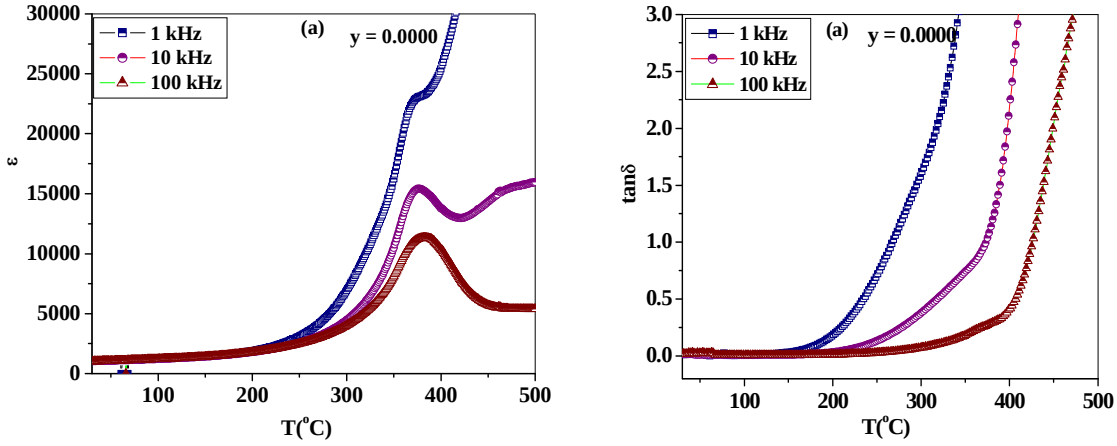

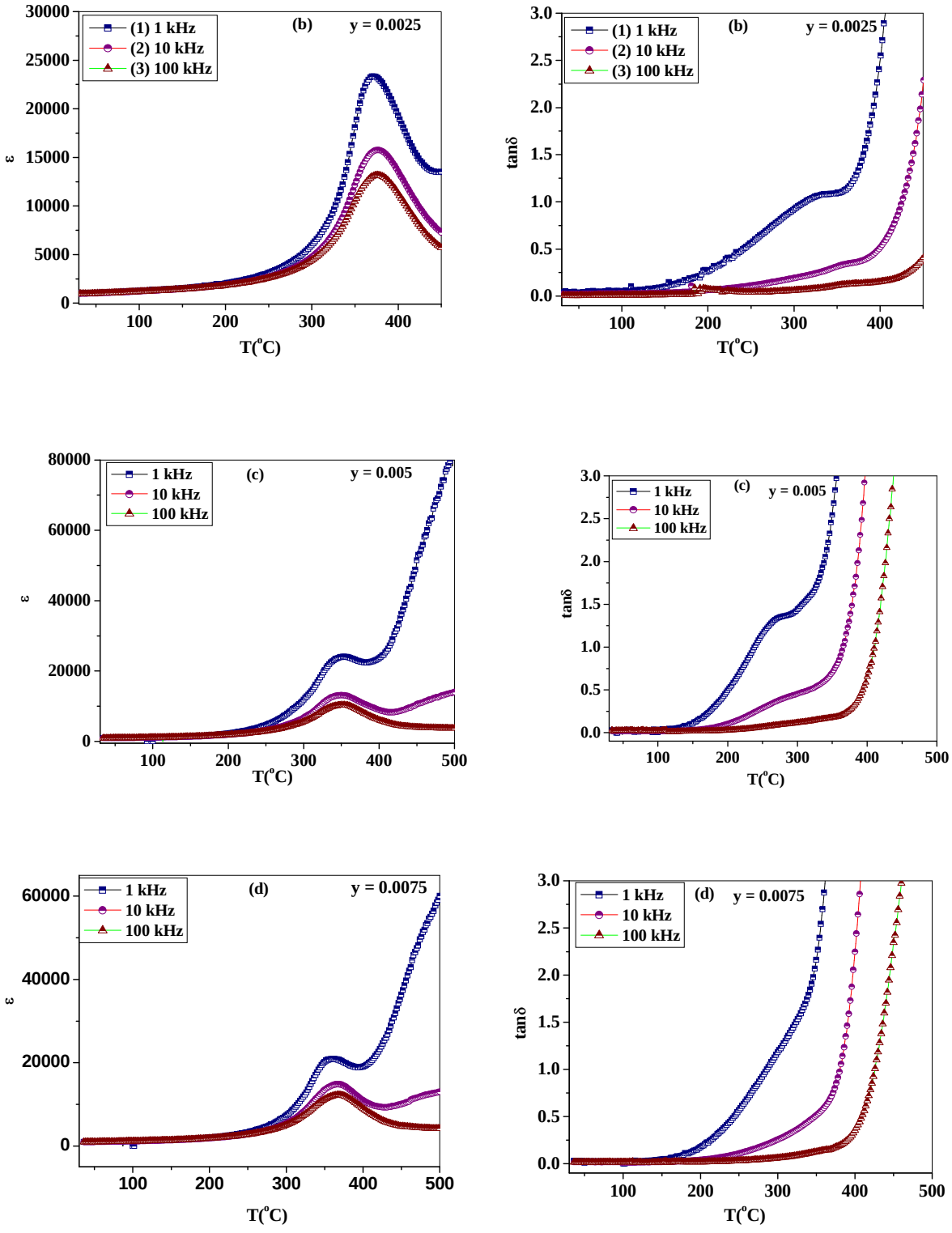

Figure 5.4 (A) Variation of ε and tanδ with temperature for **Series A** (a) y = 0.000, (b) y = 0.0025, (c) y = 0.005 (d) y = 0.0075 at different frequencies (1 kHz, 10 kHz, 100 kHz)

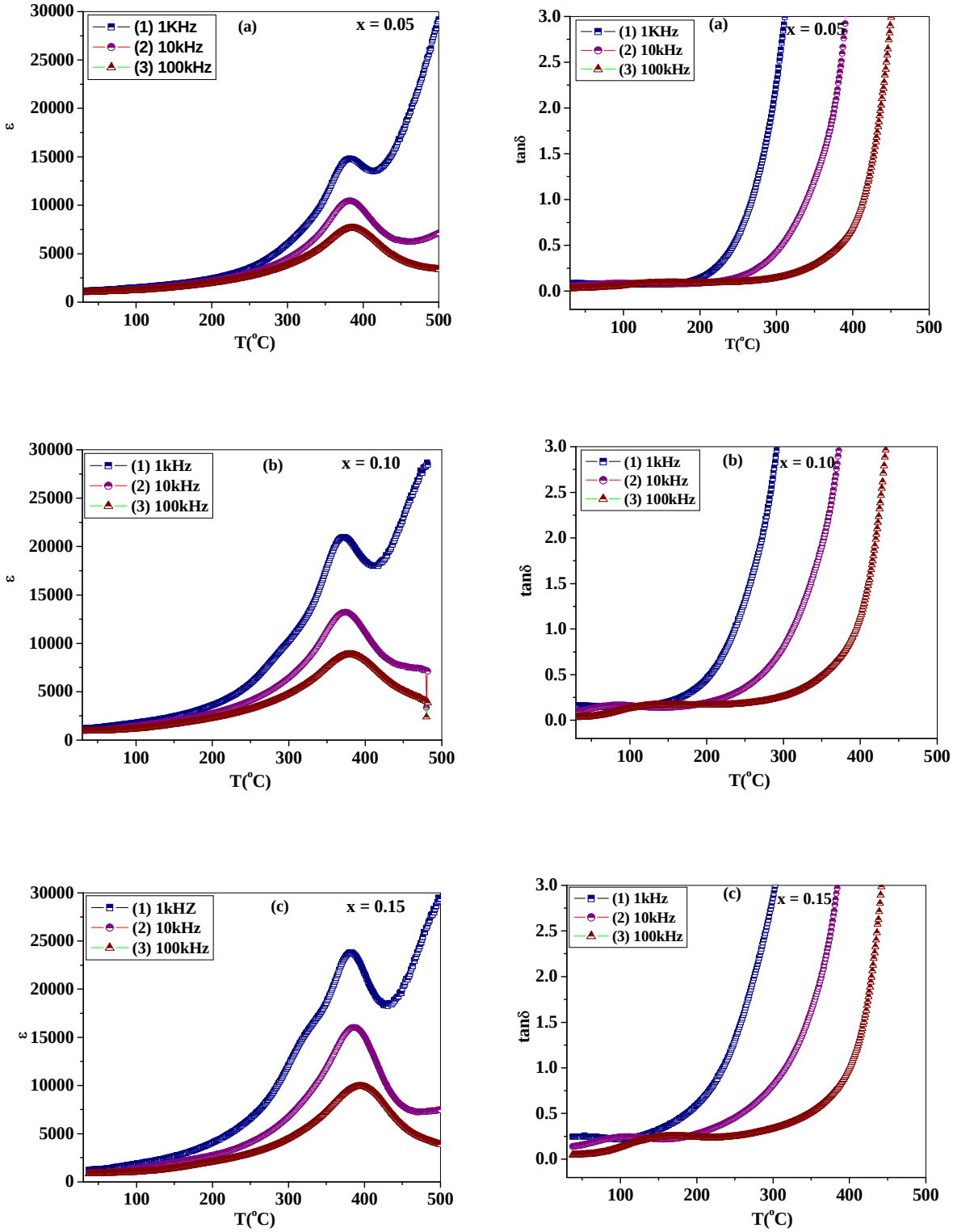

Figure 5.4 (B) Variation of ε and tanδ with temperature for **Series B** (a) x = 0.05 (b) x = 0.10 and (c) x = 0.15 at different frequencies (1 kHz, 10 kHz and 100 kHz)

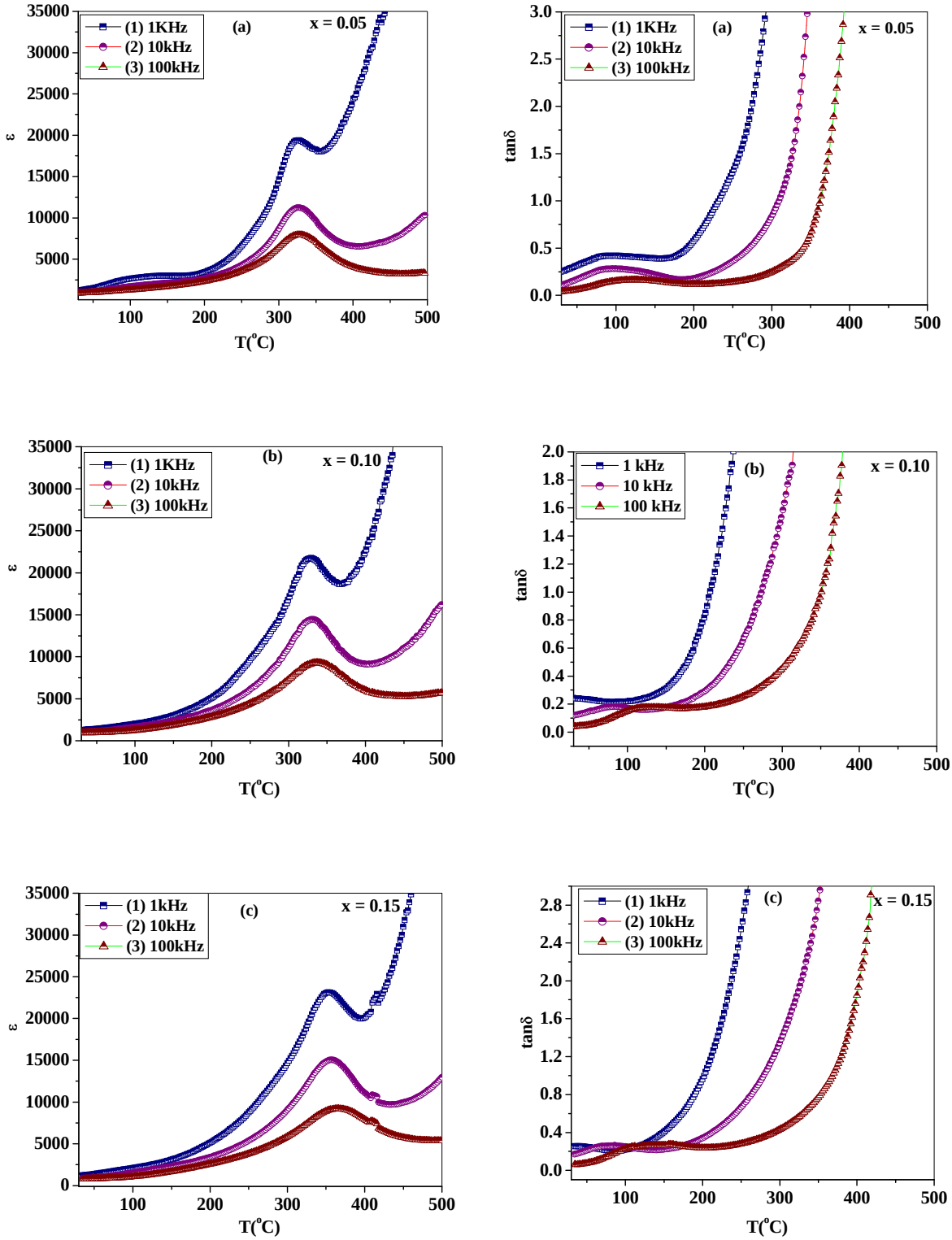

Figure 5.4 (C) Variation of ε and tanδ with temperature for **Series C** (a) x = 0.05 (b) x = 0.10 and (c) x = 0.15 at different frequencies (1 kHz, 10 kHz and 100 kHz)

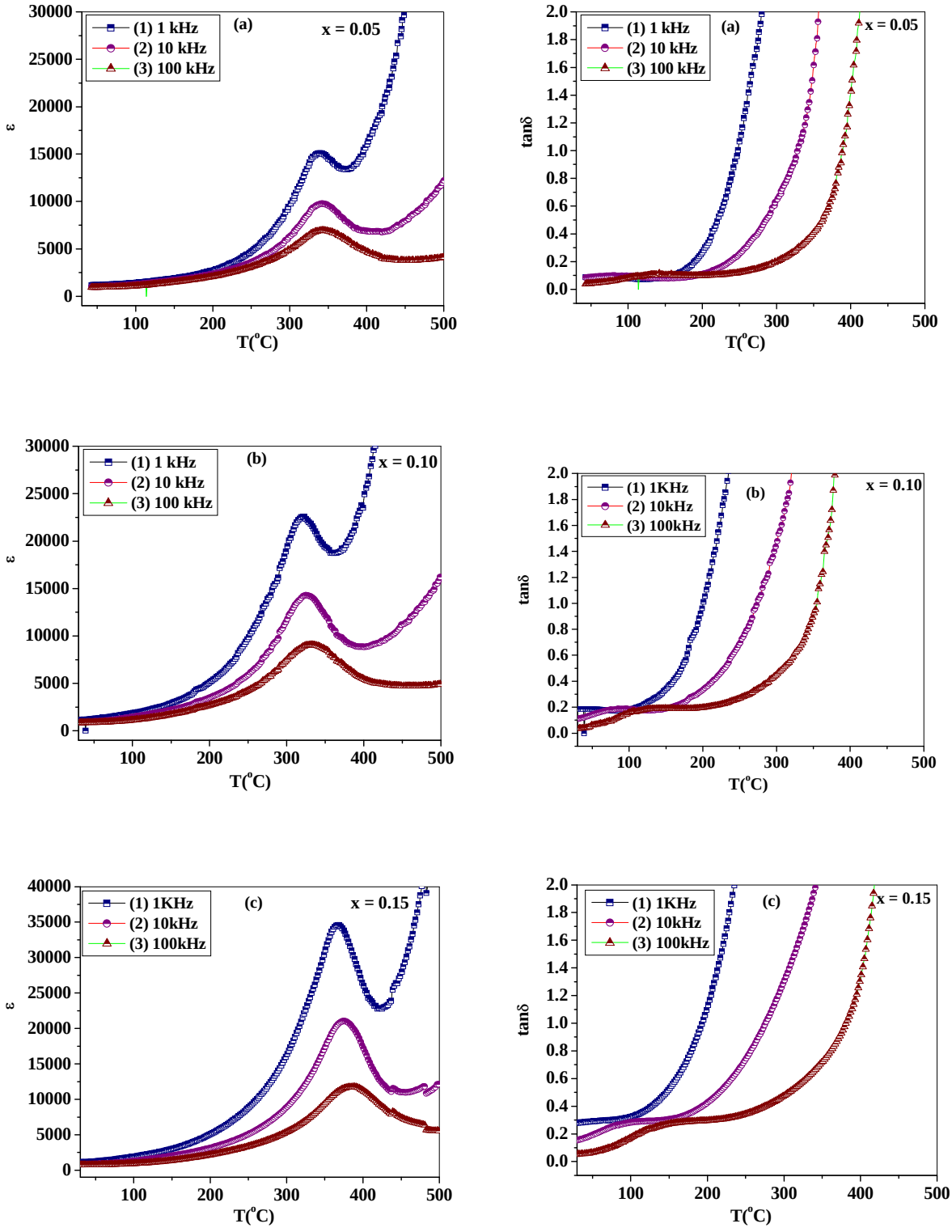

Figure 5.4 (D) Variation of ε and tanδ with temperature for **Series D** (a) x = 0.05 (b) x = 0.10 and (c) x = 0.15 at different frequencies (1 kHz, 10 kHz and 100 kHz)

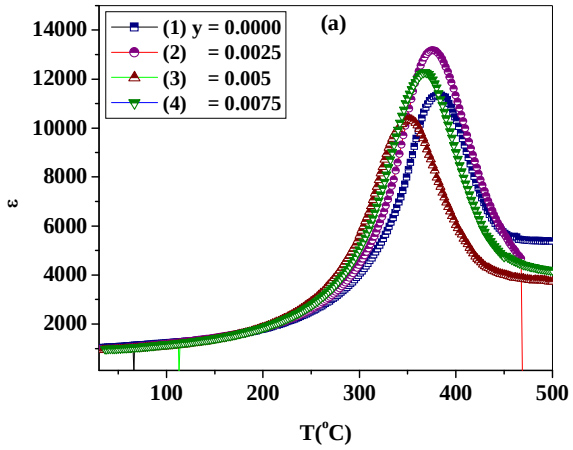
(a)
(1) y = 0.0000
(2) = 0.0025
(3) = 0.005
(4) = 0.0075
ε
T(°C)

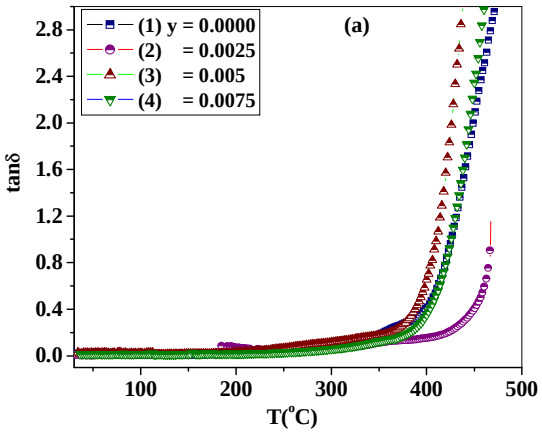
(a)
(1) y = 0.0000
(2) = 0.0025
(3) = 0.005
(4) = 0.0075
tanδ
T(°C)

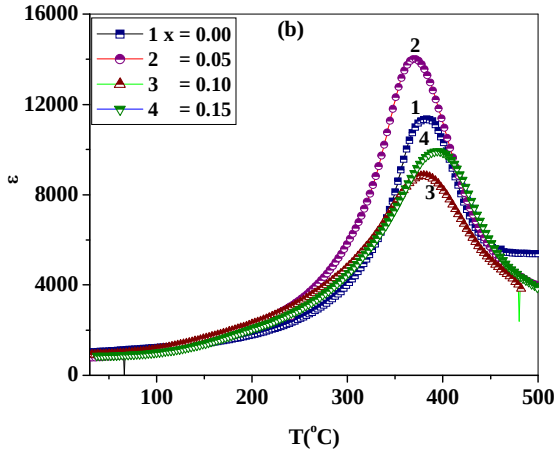
(b)
1 x = 0.00
2 = 0.05
3 = 0.10
4 = 0.15
ε
T(°C)

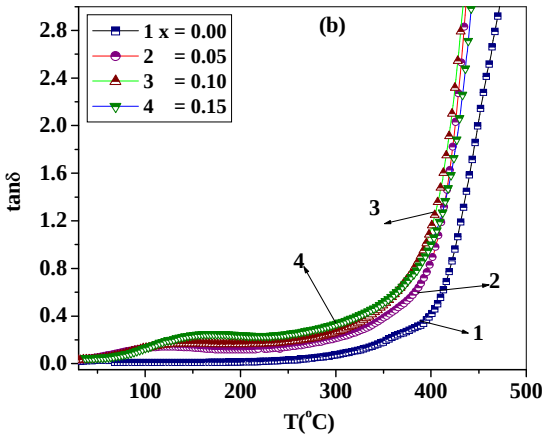
(b)
1 x = 0.00
2 = 0.05
3 = 0.10
4 = 0.15
tanδ
T(°C)

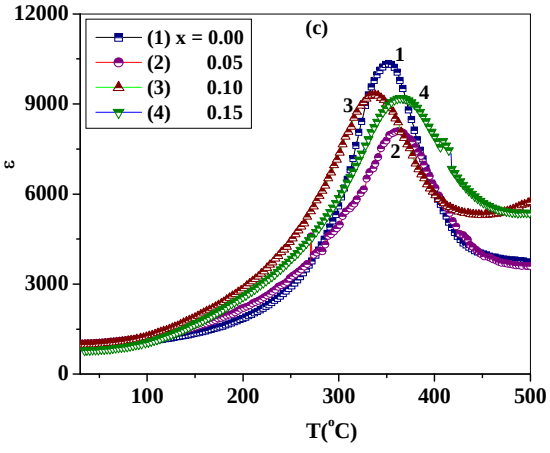
(c)
(1) x = 0.00
(2) 0.05
(3) 0.10
(4) 0.15
ε
T(°C)

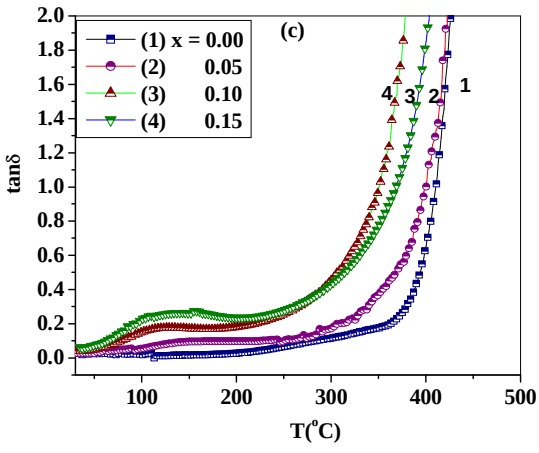
(c)
(1) x = 0.00
(2) 0.05
(3) 0.10
(4) 0.15
tanδ
T(°C)

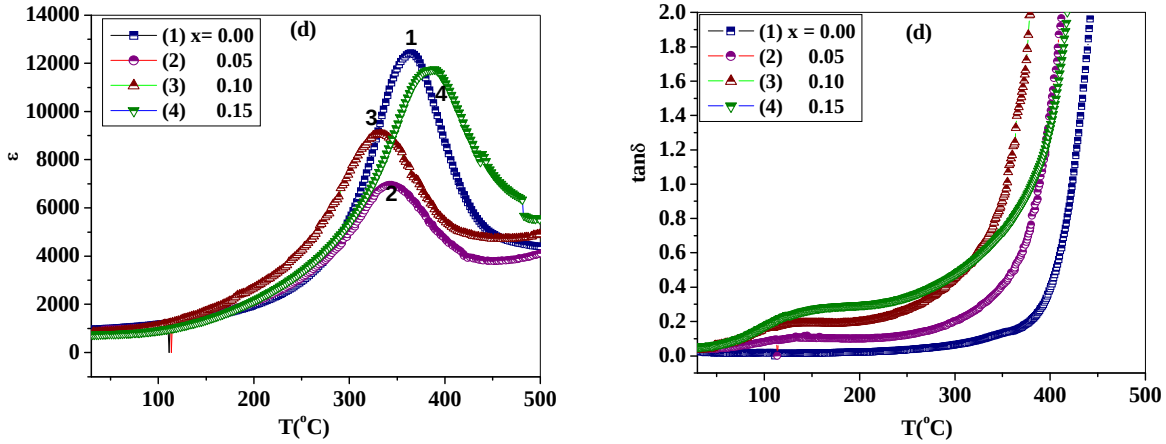

Figure 5.5 Comparative study of (a) dielectric constant (ε) and (b) dielectric loss (tanδ) measured at 100 kHz for (a) Series A (b) Series B (c) Series C and (d) Series D.

Table 5.2 Variation of dielectric parameters (ε_{RT}, T_c (°C), ε_{max}, $\tan\delta_{RT}$, $\tan\delta_{max}$) measured at 100 kHz for (x) $Co_{0.8}Ni_{0.2}Fe_2O_4$ - (1-x) $Pb_{1-3y/2}La_yZr_{0.55}Ti_{0.45}O_3$ for all values of x of all values of y.

Series A (x = 0.00)					
Parameter / y	**ε_{RT}**	**T_c (°C)**	**ε_{max}**	**$\tan\delta_{RT}$**	**$\tan\delta_{max}$**
0.0000	1028	385	11342	0.019	0.30
0.0025	965	376	13376	0.009	0.134
0.0050	927	352	10342	0.027	0.178
0.0075	985	364	12420	0.002	0.151
Series B (y = 0.0025)					
x	**ε_{RT}**	**T_c (°C)**	**ε_{max}**	**$\tan\delta_{RT}$**	**$\tan\delta_{max}$**
0.00	965	376	13376	0.009	0.134
0.05	774	370	14010	0.029	0.49
0.10	915	380	8845	0.031	0.76
0.15	900	394	9930	0.043	0.90

Series C (y = 0.005)					
0.00	927	352	10342	0.027	0.178
0.05	906	327	7950	0.038	0.382
0.10	976	337	9305	0.040	0.781
0.15	782	365	9199	0.060	0.948
Series D (y = 0.0075)					
0.00	985	364	12420	0.002	0.151
0.05	942	343	6946	0.03	0.364
0.10	855	332	9061	0.04	0.672
0.15	760	388	11762	0.06	1.09

5.2.4 Ferroelectric Properties:

The ferroelectric nature of samples (PLZT and CNFO-PLZT) was studied by the P-E Hysteresis loops. Figure 5.6 (a) shows the P-E hysteresis loops at room temperature for La doped PZT samples (Series -A) and Figure 5.6 (b-d) shows the hysteresis loops for Series B, Series C, and Series D (i.e., Composites samples), respectively, recorded at 50 Hz frequency. The values of ferroelectric parameters such as coercive field (E_c), remnant polarization (P_r) and saturation polarization (P_s) were determined from the P-E Loops for all samples (Series A- D) and are given in Table 5.3.

It is observed from Series A (PLZT), the values of remnant and saturation polarizations (P_r and P_s) are found to increase with increase in La content in PZT. This may be due to the softening effect of La substitution at Pb^{2+} site. Also La substitution makes domain switching because La ion substitute Pb site at A-site and the presence of multiple ions (Pb^{2+} and La^{3+}) results in higher multi domain polarization resulting into increase in P_r and P_s. These results are well reported in literature [28-34]. It is reported in literature that donor substituent (La^{3+} or Sm^{3+}) result in decrease in coercive field (E_c). In the present case, Increase in coercive field (E_c) with increase in La substitution (x) is seen. This can be attributed due to the decrease in grain size with La substitution [35].

For composite samples of Series B, C and D, the P-E hysteresis loops were also recorded at room temperature. As seen from the figure that P-E Hysteresis loops of composite samples are not well saturated like pure ferroelectrics. That may be due to the presence of ferrite phase

(CNFO) which acts as non-ferroelectric in the composite samples. The values of ferroelectric parameters are listed in Table 5.3. For all series of composite samples, the P-E hysteresis loop for x= 0.15 shows lossy loop (which are shown in inset of the figures). This may be due to the presence of higher amount of ferrite content. As ferrite have higher conductivity as compared to ferroelectrics resulting into leakage of charges giving rise to higher value of saturation polarization in composite samples. The values of ferroelectric parameters are not symmetric about their original points (i.e, P_r and E_c values at positive and negative quadrants are not same). This phenomenon may arise from the internal electric field that is caused by short- distance, off center, inherent movement of bound traces of electrons [36]

In all composite Series (Series B, C and D), the values of remnant and saturation polarizations (P_r and P_s) decreases with addition of small amount of ferrite content (x = 0.05) and then increases with further increase in ferrite content (x = 0.10 and x = 0.15). The increase in polarization is due to higher value of tanδ which creates the space charge across the ferroelectric phase which dilutes the ferroelectric properties [37]. P-E loop area of composites increases with increase in ferrite content which is due to decreasing the resistivity of composite samples. Similar behavior has also been reported in literature [38, 39]. It is observed that coercive field is found to increase with increase in ferrite content. This is observed due to hindered and pinned domain wall motion of ferroelectric regions due to the existence of ferrite phase [40].

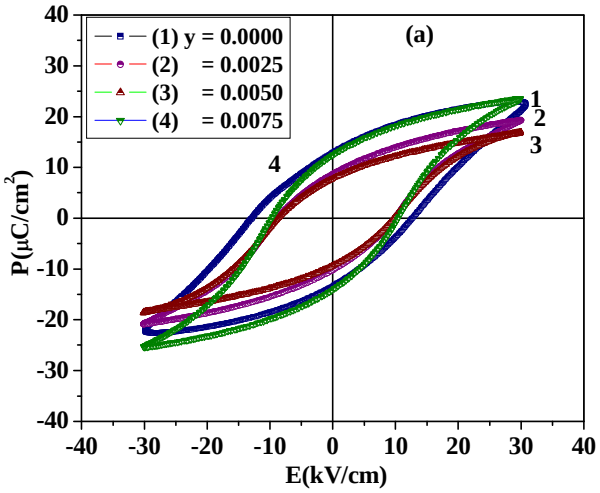

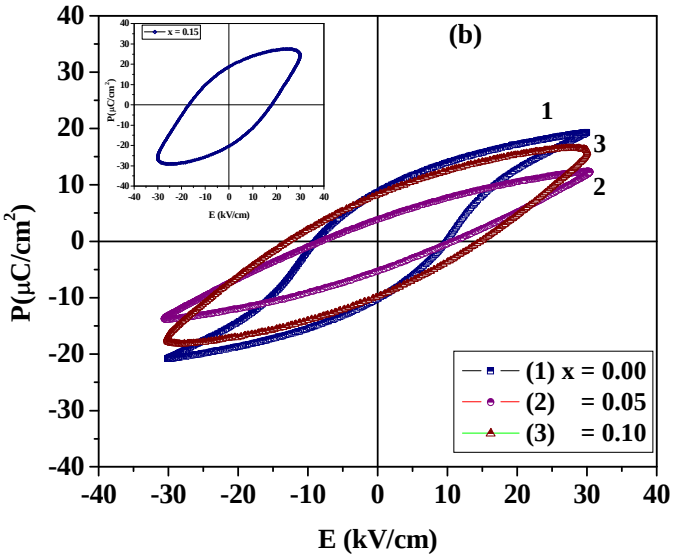
(b)
1
2
3
(1) x = 0.00
(2) = 0.05
(3) = 0.10
P(μC/cm²)
E (kV/cm)
x = 0.15

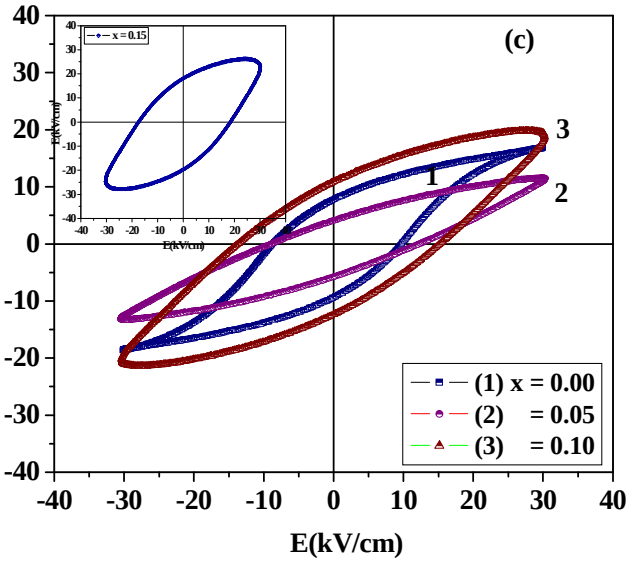
(c)
1
2
3
(1) x = 0.00
(2) = 0.05
(3) = 0.10
E(kV/cm)
x = 0.15

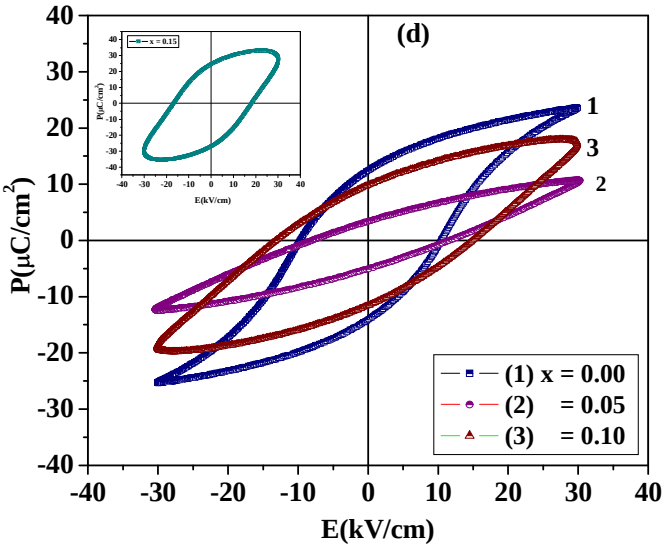

Figure 5.6 (a-d) P-E Hysteresis loops for all Series (a) Series A (b) Series B (c) Series C and (d) Series D

5.2.5 Piezoelectric Properties

The piezoelectric coefficients (d_{33}) for all samples (ferroelectrics as well as composites) are measured and are listed in Table 5.3. For measurement of piezoelectric charge coefficient, all samples are electrically poled with DC electric field of 15 kV for 1 hour in silicon oil bath at 100^{o}C-120^{o}C. It is observed that with increase in La substitution (y) in PZT (in series A), increase in charge coefficient (d_{33}) from ~110pC/N to120pC/N is observed. This increase in d_{33} may be due to increase in domain wall contribution with substitution of La. Piezoelectric coefficients are composition dependent because composition affects the dielectric permittivity, spontaneous polarization etc [41]. In series B, the gradual decrease in value of d_{33} is observed with increase in ferrite content. The high value of d_{33} for x = 0.05 in all series is due to smaller amount of ferrite. The d_{33} values observed for all samples of series B and series C are in the range of 96-54 pC/N, 111-86 pC/N. The values of d_{33} for series D is 116 pC/N for x = 0.05 and decreases for x = 0.10 and increases for x= 0.15.

Table 5.3 Ferroelectric Parameters (P_r, E_c and P_s) at 30 kV and piezoelectric charge coefficient for (x) $Co_{0.8}Ni_{0.2}Fe_2O_4$ - (1-x) $Pb_{1-3y/2}La_yZr_{0.55}Ti_{0.45}O_3$ for all values of x of all values of y

Series A (x = 0.00)					
Parameters / y	**P_r (μC/cm^2)**	**P_s (μC/cm^2)**	**E_c (kV/cm)**	**P_r/ P_s**	**d_{33} (pC/N)**
0.0000	13.26	22.78	12.80	0.582	130
0.0025	8.11	16.20	8.83	0.501	110
0.005	8.75	17.84	9.37	0.489	113
0.0075	13.33	24.56	10.61	0.542	120
Series B (y = 0.0025)					
x	**P_r (μC/cm^2)**	**P_s (μC/cm^2)**	**E_c (kV/cm)**	**P_r/ P_s**	**d_{33} (pC/N)**
0.00	8.11	16.20	8.83	0.50	110
0.05	2.56	9.19	6.76	0.278	96
0.10	5.35	11.89	15.56	0.449	72
0.15	Lossy	Lossy	Lossy	-	54
Series C (y = 0.005)					
0.00	8.725	17.841	9.37	0.489	113
0.05	4.925	12.532	10.65	0.329	111
0.10	11.63	20.734	14.77	0.561	86
0.15	Lossy	Lossy	Lossy	-	65
Series D (y = 0.0075)					
0.00	13.33	24.55	10.15	0.543	120
0.05	4.24	11.7	9.895	0.363	116
0.10	10.65	19.00	13.96	0.561	56
0.15	Lossy	Lossy	Lossy	-	80

5.2.6 Magnetic Properties: M-H Hysteresis loops

The magnetic nature of composites is studied by M-H hysteresis loops. The M-H Hysteresis loops at room temperature for series B, C, and D with varying ferrite content are shown in Figure 5.7 (a-c), respectively; with inset showing M-H loop for pure CNFO. All samples show ferromagnetic behavior which confirms the existence of magnetic ordering in the composite system. Magnetic parameters such as the values of remnant magnetization (M_r), coercive field (H_c) and saturation magnetization (M_s) were determined from M-H hysteresis loops and are given in Table in 5.4. All M-H loops are well saturated. With increase in ferrite content, the magnetic field at which saturation is obtained, increases. The observed values for remnant magnetization (M_r) and saturation magnetization (M_s) are found to increase with increase in ferrite content. This is due to the magnetic nature of ferrite and number of domain contributing to magnetization resulting into increase in magnetizations. The values of magnetizations (M_r and M_s) and coercive field in composite samples are smaller than that for pure CNFO (Saturation magnetization (M_s- 49.45 emu/g) and Coercive field (H_c – 724Oe)). This is observed due to presence of PLZT (ferroelectric phase) in the composite which act as non magnetic phase, resulting in reduction of magnetic component [42]. The ferroelectric grains of PLZT separate the magnetic grains of CNFO phase resulting into weakening of the exchange coupling between them [43].

Table 5.4 Magnetic Parameters (M_r, M_s and H_c) and magnetoelectric coupling coefficient (α) for (x) $Co_{0.8}Ni_{0.2}Fe_2O_4$ - (1-x) $Pb_{1-3y/2}La_yZr_{0.55}Ti_{0.45}O_3$ for all values of x of all values of y

Series B (y = 0.0025)				
Parameters / **x**	**M_r (emu/g)**	**M_s (emu/g)**	**H_c (Oe)**	**α(mV/cm.Oe)**
0.05	0.58	2.47	312	1.2
0.10	1.14	5.02	349	1.0
0.15	1.79	7.85	421	-
1.00	13.08	49.45	724	-
Series C (y = 0.005)				
0.05	0.47	2.26	267	0.18
0.10	1.24	5.48	347	-
0.15	1.98	8.33	374	-
1.00	13.08	49.45	724	
Series D (y = 0.0075)				
0.05	0.49	2.40	246	0.5
0.10	0.95	5.30	268	-
0.15	1.44	8.19	303	0.15
1.00	13.08	49.45	724	-

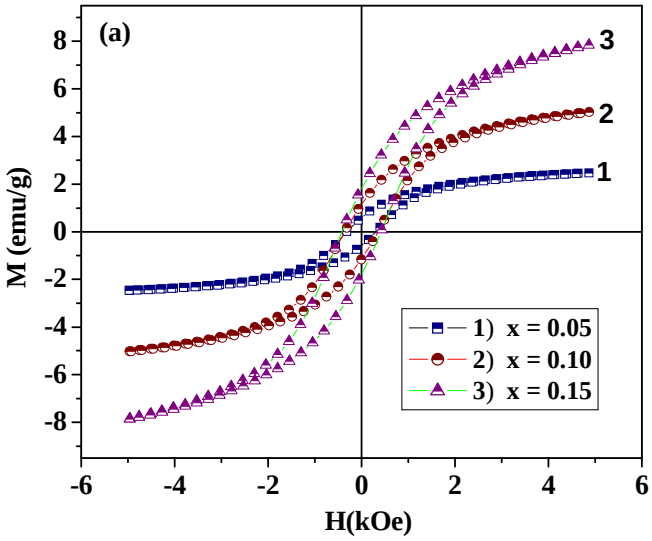

Figure 5.7 (a) M-H Hysteresis loops of **Series B**

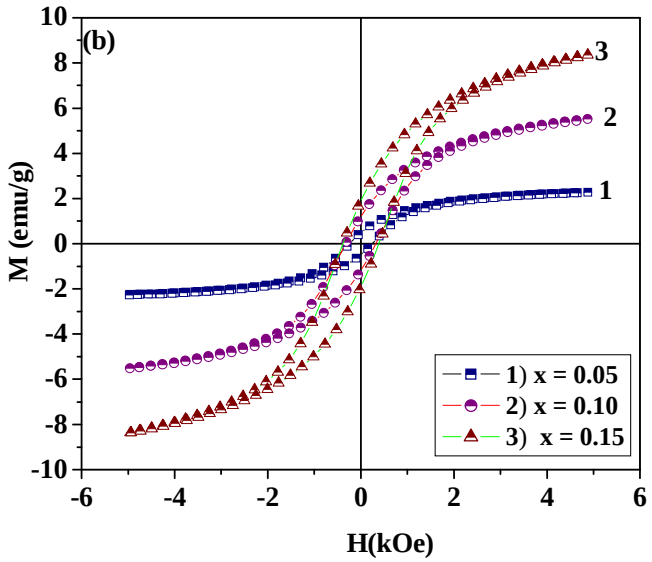

Figure 5.7 (b) M-H Hysteresis loops of **Series C**

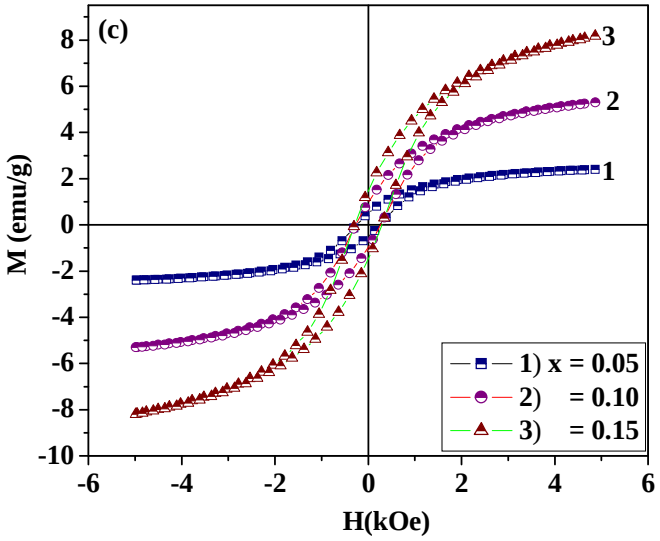

Figure 5.7 (c) M-H Hysteresis loops of **Series D**

5.2.7 Magnetoelectric measurement

For magnetoelectric measurement, composite samples were electrically poled at 15 kV/cm for 1 hour. Effect of La substitution on magnetoelectric coupling coefficient is also studied here. The logic behind doping La in PZT is to increase the resistivity of ferroelectric and their piezoelectric coefficient which helps to increase the ME coefficient. The variation of ME coupling coefficient (α) as a function of DC magnetic field in the presence of applied ac magnetic field of 1 Oe at 1 kHz frequency for all samples of series B, C and D is shown in Figure 5.8 (a-c). Initially ME coupling coefficient (α) increases with increase in magnetic field, reaches to maximum value and the start decreasing with further increase in magnetic field. The initial increase in the ME output is due to the increase in magnetostriction induced strain in CNFO phase. The decrease in α with increase in DC magnetic field is due to the fact that the magnetostriction coefficient of ferrite phase reaches its saturation value at certain values of magnetic field as already discussed in previous chapter.

The value of ME coefficient for series B, Series C and series D are given in Table 5.4. From this it is observed that the maximum value of Magnetoelectric coefficient is obtained for x = 0.05 of y = 0.0025 and its value is 1.2 mV/cm.Oe. The value of ME coefficient decreases with increase in ferrite content for x= 0.10 of same series. With further increase of La in PZT phase,

ME coefficient decreases. This may be due that La ion may diffuse in ferrite phase. The value of ME coefficient for x = 0.05 of y = 0.075 is higher as compared to value for x = 0.05 of y = 0.005. This can be related to piezoelectric charge coefficient. Explanation is already given in chapter 4.

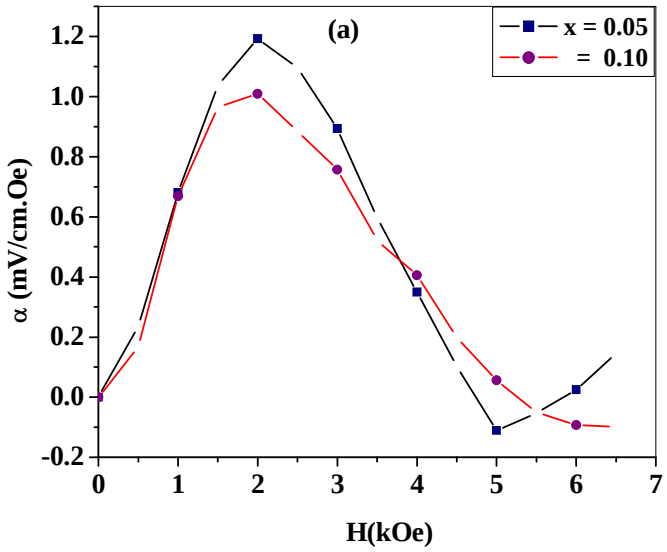

Figure 5.8 (a) Variation of magnetoelectric coupling coefficient (α) with DC magnetic field for x = 0.05, x = 0.10 of **Series B**

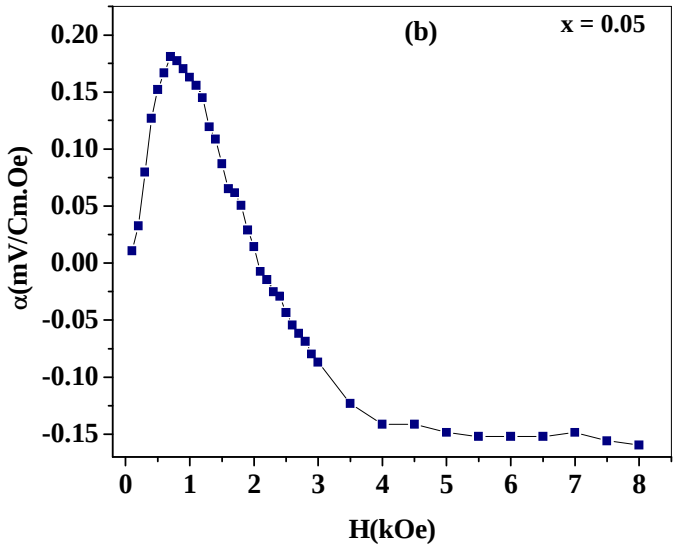

Figure 5.8 (b) Variation of magnetoelectric coupling coefficient (α) with DC magnetic field for x = 0.05 of **Series C**

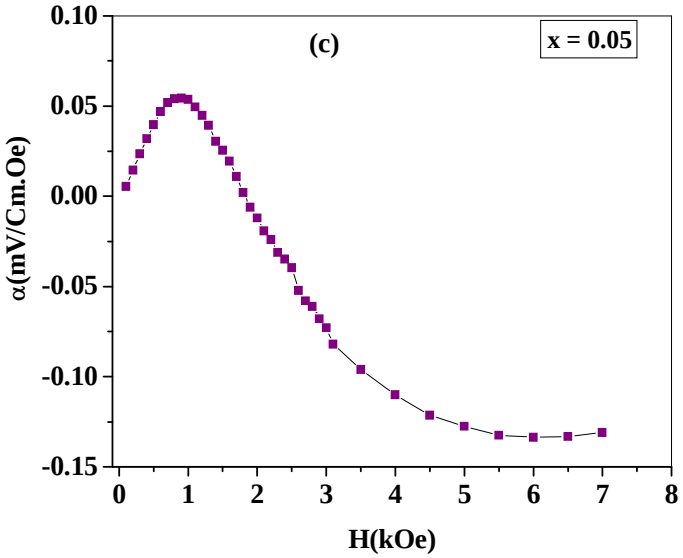

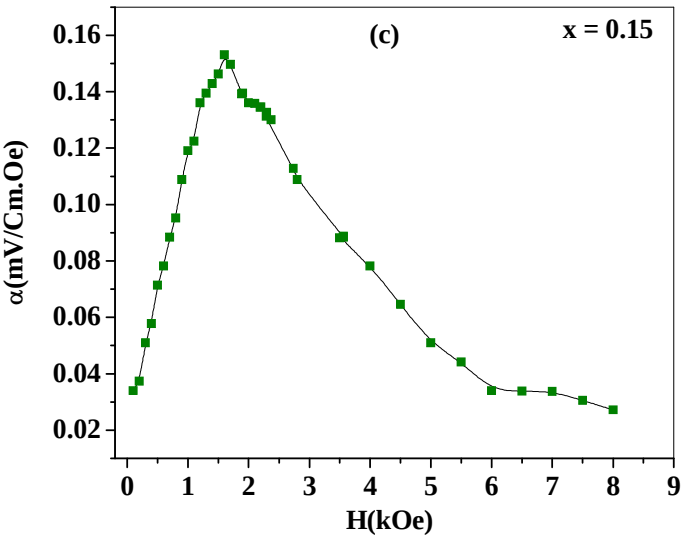

Figure 5.8 (c) Variation of magnetoelectric coupling coefficient (α) with DC magnetic field for (i) x = 0.05 (ii) x = 0.15 of **Series D**

References:

1. A. S. Fawzi, A. D. Sheikh and V. L. Mathe, Physica B., **405** (2010) 340.

2. W. Robner, Ph.D. Thesis, University of Erlangen, Erlangen, Germany (1985).

3. K. Carl and K. H. Hardtl, Ber. Dtsch. Keram. Ges., **47** (1970) 687.

4. Chandra Prakash and O.P. Thakur, Mater. Lett., **57** (2003) 2310.

5. R. Sharma, P. Pahuja and R. P. Tandon, Ceram. Int., **40** (2014) 9027.

6. M. Zivkovic, D. Stojanovic, C. R. Foschini, V. Paunovic and D. Mancic, Sci. Sinter., **35** (2003) 133.

7. S. B. Narang and D. Kaur, Ferroelectrics Lett., **36** (2009) 20.

8. J. Y. Zhai, N. Cai, L. Liu, Y. H. Lin and C. W. Nan, Mater. Sci. Eng. B., **99** (2003) 329.

9. D. R. Patil and B. K. Chougule, J. Alloys Compd., **470** (2009) 531.

10. K. W. Wagner, Ann. Phys. **40** (1993) 818.

11. C. G. Koop's Phys. Rev. B. **83** (1951) 121.

12. J. C. Maxwell, Electricity and Magnetism, Oxfrod University Press, London, (1993) 828.

13. A. M. Abdeen, O. M. Hemeda, E. E. Assem and M. M. El-Sehly, J. Magn. Magn. Mater., **238** (2002) 75.

14. C. W. Beier, M. A. Cuevas and R. L. Brutchey, J. Mater. Chem., **20** (2010) 5074.

15. G. H. Haertling, J. Am. Ceram. Soc., **82** (1999) 797.

16. X. Feng and X. Yao, J. Appl. Phys., **92** (2002) 2709.

17. L. Mitoseriu and V. Buscaglia, Phase Transitions, **79** (2006) 1.

18. K. Okazaki, Ceram. Bull., **63** (1984) 1150.

19. S. Singh, O.P. Thakur and Chandra Prakash, Def. Sci. J.**, 55** (2005) 349.

20. Xunhu Dai, Z. Xu, Jie-Fang Li, and Dwight Viehland, J. Mater. Res., **11** (1996) 618.

21. A. P. Barranco, J. D. S. Guerra, R. L. Noda and E.B. Araujo, J. Phys. D: Appl. Phys., **41** (2008) 215503.

22. R. Rani, J. K. Juneja, K. K. Raina and Chandra Prakash, J. Ceram. Process. Res., **13** (2012) 76.

23. K. K. Patankar, S. A. Patil, K. V. Sivakumar, Y. D. Kolekar and M. B. Kothale, Mater. Chem. Phys., **65** (2000) 97.

24. K. K. Patankar, V. L. Mathe, A. N. Patil, Y. D. Kolekar and P. B. Joshi, J. Electroceram., **6** (2001) 115.

25. A. Gupta and R. Chatterjee, J. Euro. Ceram. Soc., **33** (2013) 1017.

26. Y. Wang, W. Rao, M. Wang, G. Li, Y. Li, J. Gao, W. Zhou and J. Yu, J. Mater. Sci: Mater Electron., **23** (2012) 1064.

27. A. Sharma, R. K. Kotnala and N. S. Negi, J. Alloys Compd., **582** (2013) 628.

28. S. R. Shannigrahi, R. N. P. Choudhary and H. N. Acharaya, J. Mater. Sci., **35** (2000) 1737.

29. H. Ouchi, J. Am. Ceram. Soc., **51** (1968) 169.

30. M. D. Durruthy-Rodríguez, L. D. Pérez-Fernández, A. P. Barranco and F. C. Pinar, Appl. Phys. A., **95** (2009) 423.

31. L. E. Cross, Ferroelectrics, **76** (1987) 241.

32. S. Li, J. A. Eastman, R. E. Newnham and L. E. Cross, Phys. Rev. B., **55** (1997) 12067.

33. R. Yimnirun, S. Ananta and P. Loaratanakul, Mater. Sci. Eng. B., **112** (2004) 79.

34. S. L. Swartz, T. R. Shrout, W. A. Schulze and L. E. Cross, J. Am. Ceram. Soc., **67** (1984) 311.

35. P. Kumar, P. Singh, J. K. Juneja, K. K. Raina, R.P. Pant, Chandra Prakash and S. Singh, J. Alloys Compd., **601** (2014) 207.

36. A. S. Fawzi, A. D. Sheikh and V. L. Mathe., Mater. Res. Bull., **45** (2010) 1000.

37. N. S. Negi and A. C. Restogi, Integr. Ferroelectr., **121** (2010) 36.

38. Y. Wang, W. Rao, M. Wang, G. Li, Y. Li, J. Gao, W. Zhou and J. Yu, J. Mater. Sci: Mater Electron., **23** (2012) 1064.

39. A. Sharma, R. K. Kotnala and N. S. Negi, J. Alloys Compd., **582** (2013) 628.

40. Z. Yu, C. Ang and J. Mater. Sci.: Mater. Electron., **13** (2002) 193.

41. M. J. Haun, E. Furman, S. J. Jang and L. E. Cross, IEEE Trans. UFFC, **36** (1989) 393.

42. P. A. Jadhav, M. B. Shelar and B. K. Chougule, J. Alloys Compd., **479** (2009) 385.

43. P. Pahuja, R. Sharma, Chandra Prakash and R. P. Tandon, Ceram. Int., **39** (2013) 9439.

Chapter – 6

Summary and Recommendations for future work

Chapter – VI

Summary and Recommendations for Future Work

This chapter summarizes the conclusions drawn from the present work and highlights the most significant results. The marked effect of Ni substitution in ferrite phase and La substitution in ferroelectric phase on various properties of modified PZT - CFO composites is concluded. This chapter also includes some suggestions related to future investigations for basic and applied research point of view.

The present work focuses on the synthesis and characterization of modified PZT-CFO composites. The samples were synthesized by conventional solid state reaction method. The modification was carried out by substituting Ni^{2+} in ferrite phase (CFO) and La^{3+} in ferroelectric (PZT) phase. This substitution was undertaken in a view to know the suitability of the substituting elements for the enhancement of magnetoelectric properties. The substitution of Ni and La was expected to give rise to improved magnetoelectric properties.

6.1 Summary of the Results:

The important outcomes of the work are summarized here:

- Individual phases $PbZr_{0.55}Ti_{0.45}O_3$ (PZT) and $CoFe_2O_4$ (CFO) were synthesized by solid state reaction method. XRD diffraction patterns of individual phases confirm their phase formation. Composites having composition (x) $CoFe_2O_4$ - (1-x) $PbZr_{0.55}Ti_{0.45}O_3$, x = 0.05, 0.10 and 0.15 (by weight) were synthesized by mixing of these individual phases. Optimization of sintering temperature was done on the sample (0.05) $CoFe_2O_4$ - (0.95) $PbZr_{0.55}Ti_{0.45}O_3$. For optimization, the sample was sintered at three different temperature 1150^{o}C, 1200^{o}C and 1250^{o}C for 4 hours. X-ray patterns, relative density, dielectric properties (dielectric constant with temperature and tangent loss with temperature), ferroelectric P-E hysteresis loops were studied for all samples. Optimum results were observed for sample sintered at 1150^{o}C for 4 hours. So, all samples were conventionally sintered at optimum temperature 1150^{o}C for 4 hours. XRD diffraction patterns of composite sample confirm the coexistence of both cubic spinel and tetragonal phase respectively. Relative density was found to decrease with increase in ferrite content. Larger grain size of ferroelectric phase and smaller grain size of ferrite phase was observed by SEM analysis. SEM analysis of composite samples confirms the presence of both the phases. Grains of both phases could not be distinguished because of smaller content of ferrite. Room temperature dielectric constant decreases with increase in frequencies and also decreases with increase in ferrite content. Similar behavior has been observed for tangent loss. Increase in P_r and P_s with increase in ferrite content is also observed. Increase in M_r and M_s with ferrite content suggests that composites obey the rule of mixture.

Maximum value of magnetoelectric coupling coefficient of 298(μv/cm.Oe) was observed for (0.05) $CoFe_2O_4$ – (0.95) $PbZr_{0.55}Ti_{0.45}O_3$.

- Samples with composition (x) $Co_{0.8}Ni_{0.2}Fe_2O_4$ - (1-x) $PbZr_{0.55}Ti_{0.45}O_3$ were synthesized by solid state reaction method to study the effect of Ni substitution in ferrite phase on various properties of composites. Phase formation of both the phases was confirmed by X-Ray analysis. Room temperature dielectric constant is found to decrease with increase in ferrite content. Relaxation peak at 100^oC – 200 ^oC are observed in variation in tangent loss with temperature. These peak shifts towards the higher temperature with increase in frequency. Increase in ferroelectric parameters such as P_r, P_s and E_c with increase in ferrite content are observed which is due to space charge effect with substitution of ferrite content. Ni substitution in ferrite phase increases the resistivity and piezoelectric coefficient of composite samples which in turn affect the magnetoelectric coupling of the composite samples. Maximum value of magnetoelectric coupling coefficient of 855 (μv/cm.Oe) was observed for $0.05Co_{0.8}Ni_{0.2}Fe_2O_4$-$0.95PbZr_{0.55}Ti_{0.45}O_3$.

- Samples with composition $Pb_{1-3y/2}La_yZr_{0.55}Ti_{0.45}O_3$ with y = 0.00, 0.0025, 0.005 and 0.0075 were prepared by solid state reaction method to study the effect of La substitution in ferroelectric ceramics. Composite samples with composition (x) $Co_{0.8}Ni_{0.2}Fe_2O_4$ - (1-x) $Pb_{1-3y/2}La_yZr_{0.55}Ti_{0.45}O_3$ with y = 0.0025, 0.005 and 0.0075 were prepared to study the effect of different concentration of ferrite phase on various properties of composites. All samples were synthesized by solid state reaction method. The structural, microstructural, dielectric, ferroelectric, ferromagnetic and magnetoelectric properties were studied. Random values of lattice parameters are observed in all series due to stress induced by ferrite phase on ferroelectric phase. More dielectric dispersion is observed in composite series as compared to pure PLZT series. Curie temperature (T_c) was found to increase with increase in ferrite content in all series. For pure series, P_r and P_s are found to increase with increase in La content in PZT. While in composite samples, P-E loops are not well saturated. Increase in the value of P_r and P_s in all composite series with addition of ferrite content that may be due to increase the space charge polarization effect and tangent loss in the composite samples. La substitution in ferroelectric phase increases the piezoelectric

coefficient which increases the magnetoelectric coefficient. Magnetoelectric coupling coefficient of series B for x = 0.05 is 1.2 mV/cm.Oe observed and then decreases with increase in ferrite content. While for series C and series D, value of magnetoelectric coupling coefficient is 0.15 mV/cm.Oe and 0.05 mV/cm.Oe for x = 0.05 respectively.

- ❖ Ni Substituted composite samples and La substituted samples show improved piezoelectric and magnetoelectric properties as compared to unsubstituted PZT-CFO. Hence these modified composites can be used for memory devices, sensors, waveguides, transducers and actuators etc.

6.2 Recommendations for Future Work:

The thesis explored several aspects of ferrite –ferroelectric composite materials in modified PZT-CFO composites. As these materials show unique property i.e, magnetoelectric properties thus they have received continuous attention as potential sensors for magnetic field measurements and transducers for magnetoelectric conversion and actuators. These composites are of interest for a variety of device applications including electrically controlled electro-optic or piezoelectric devices, actuators and memory devices. Accordingly, it is quite interesting to explore the ways and means to improve the various properties in our future research work,

Following are the few suggestions for future extension of this work:

1. As microwave sintering is environment friendly and fast technique as compared to conventional method. So synthesis and their characterization of PZT- CFO and modified PZT- CFO can be done by Microwave sintering technique. This sintering technique may lead to the improvement in properties of the composites.
2. In the present wok, PZT-CFO composites were studied with particular ratio. With change in ratio of Zr/Ti in PZT and Ni in CFO and other substituent's may improve the properties of composites.
3. Solid state reaction method was adopted for synthesis of present composites. Different techniques such as sol-gel, co-precipitation method can be adopted for the synthesis. These techniques may offer improved properties.
4. Laminated composites and thin films of these composite samples may also be studied.

****